

Design and Implementation of Mechanical Metamaterials

by

Brittany C. Essink

A dissertation submitted in partial fulfillment
of the requirements for the degree of
Doctor of Philosophy
(Aerospace Engineering)
in the University of Michigan
2020

Doctoral Committee:

Professor Daniel J. Inman, Chair
Professor Henry Sodano
Associate Professor Veera Sundararaghavan
Professor Kon-Well Wang

Brittany C. Essink

essinkb@umich.edu

ORCID iD: 0000-0001-7043-9404

© Brittany C. Essink 2020

This thesis is dedicated to my parents.

ACKNOWLEDGMENTS

There are many people I would like to thank for their help during this process. Specifically, I would like to thank Fabian Chacon, Kaelan Hansson, Jared Mermelstein, and my parents; Dianne and Glen Essink for being there for me when I needed them the most. Thanks to all my other friends and family members for supporting me throughout this whole journey.

I would also like to thank past and previous members of the AIMS/CIMMS lab for their advice, guidance, and jokes. This non-exhaustive list includes Jared Hobeck, Alexander Pankonien, Cassio Faria, Katie Reichl, Lawren Gamble, Andrew Lee, Krystal Acosta, Lori Groo, Christina Harvey, Kevin Vaughn, and Piper Siegcrest.

Many additional thanks to Dr. Daniel Inman who made this entire dream possible as well as to my committee members: Dr. Henry Sodano, Dr. Kon-Well Wang, and Dr. Veera Sundararaghavan.

Additional thanks go to those who assisted in testing and fabrication along the way. Thanks to Terry Larrow for his machining help and wonderful ice cream parties. Thank you to Robert Haynes, Todd Henry, and Mulugeta Haile at the Army Research Lab on the Aberdeen Proving Grounds for helping us test and validate our mechanical metamaterial on the 6DOF test system located at their facilities.

Special thanks to my cat Yuki who has been with me throughout this journey and still refuses to learn to read.

TABLE OF CONTENTS

DEDICATION	ii
ACKNOWLEDGEMENTS	iii
LIST OF FIGURES	vi
LIST OF TABLES	viii
ABSTRACT	ix
CHAPTER	
I. Introduction	1
1.1 Metamaterials and Origin of Metastructures	1
1.2 Vibration Control using Mechanical Metamaterials	2
1.2.1 Passive Control	2
1.2.2 Active Control	6
1.3 Motivation and Scope	8
1.4 Outline of Dissertation	9
II. Passive Control of Mechanical Metamaterials	11
2.1 Overview	11
2.2 Mechanical Metamaterial for Transverse Excitation	12
2.2.1 Linear Zigzag Shaped Absorber	12
2.2.2 Experimental Analysis	17
2.2.3 Metastructure with Zigzag Absorber Inserts	18
2.3 Mechanical Metamaterial for Multi Axis Excitation	28
2.3.1 Initial Design	28
2.3.2 Experimental Testing of the Model	29
2.3.3 Model Updating	35
2.4 Structure Design Considerations and Limitations	46
2.5 Summary	48

III.	Damping vs. Absorption in Mechanical Metamaterials	49
3.1	Overview	49
3.2	Motivating Experiment	50
3.3	Modal Parameter Consideration	53
3.3.1	Receptance and Dynamic Stiffness	53
3.3.2	Vincent Plots	55
3.4	2-DOF Structure	55
3.4.1	Case 1: Optimal Absorber Damping	58
3.4.2	Case 2: Optimal Absorber Stiffness	58
3.4.3	Primary Structure with Negligible Internal Damping, $\zeta_1 = 0$	58
3.4.4	Primary Structure with Internal Damping, $\zeta_1 \neq 0$	59
3.5	Multi Degree of Freedom Excitation	61
3.5.1	Vibration Reduction Through Damping	62
3.5.2	Vibration Reduction Through Absorber Tuning	62
3.6	Summary	70
IV.	Active Control of Mechanical Metamaterials	72
4.1	Overview	72
4.2	Piezoelectric Equations	73
4.3	Modeling Single Absorber with Piezo Actuators	77
4.4	State Space Formulation	80
4.5	Pole Placement Control	81
4.5.1	Absorber Control	82
4.5.2	Full Metastructure Model	83
4.6	Application to Multi Axis Mechanical Metamaterial	84
4.7	Summary	88
V.	Conclusions and Future Work	90
5.1	Dissertation Summary	90
5.1.1	Chapter II	90
5.1.2	Chapter III	91
5.1.3	Chapter IV	93
5.2	Key Contributions of the Dissertation	94
5.3	Recommendations for Future Work	96
	BIBLIOGRAPHY	98

LIST OF FIGURES

FIGURE

1.1	Frequency bandgap caused by distributed vibration absorbers	3
1.2	Alternative vibration absorber geometries. From left to right: zigzag, orthogonal spiral, elephant.	4
1.3	Previous multi dimensional vibration mitigation design [1]	6
2.1	Applied forces on zigzag beam	13
2.2	Global displacement of an 8 <i>a</i> -beam zigzag structure	16
2.3	Water-jet cut experimental zigzag beams	18
2.4	Views of the <i>c</i> channel beam cutouts cutouts and tabs for absorber mounting	21
2.5	Variation of structural properties as a function of beam length for the <i>c</i> channel	23
2.6	Views of <i>c</i> channel metastructure with zigzag absorber design	24
2.7	Comparison of analytical and finite element frequency response function for main beam	26
2.8	Frequency response of <i>c</i> channel beam with and without absorbers	27
2.9	Schematic of multi axis mechanical metamaterial	29
2.10	Isometric view of multi axis mechanical metamaterial	30
2.11	Absorber and metastructure schematic	30
2.12	Absorber bending direction. Contours show a qualitative absorber displacement.	31
2.13	Experimental setup for multi axis mechanical metamaterial	33
2.14	Longitudinal tip displacement for free and blocked configurations	33
2.15	Transverse tip displacement for free and blocked configurations	34
2.16	Torsional tip displacement for free and blocked configurations	35
2.17	Comparison of modeling and experimental tip displacement under excitation in the longitudinal direction	45
2.18	Comparison of modeling and experimental tip displacement under excitation in the transverse direction	45
3.1	Periodic chiral lattice (top) and solid structure (bottom)	50
3.2	Experimental hammer setup for impact testing	51
3.3	Experimental impact data for lattice and solid metastructures	52
3.4	Two degree of freedom lumped mass system with sinusoidal force excitation a) absorber damping only b) damping on both masses	57
3.5	Minimum H_∞ norm vs. forced frequency ratio for $\zeta_1 = 0$	59
3.6	Amplitude as a function of varied absorber damping ratio and natural frequency ratio	60

3.7	Minimum H_∞ norm vs. forced frequency ratio for a) $\zeta_1 = 0$, b) $\zeta_1 = 0.05$, c) $\zeta_1 = 0.1$	60
3.8	Minimum H_∞ norm vs. forced frequency ratio for a) $\zeta_1 = 0.7$, b) $\zeta_1 = 1.5$, c) $\zeta_1 = 3$	61
3.9	Comparing vibration reduction through damping - longitudinal excitation	63
3.10	Dynamic stiffness of longitudinal excitation	64
3.11	Longitudinal Vincent plots for frequencies below (left) and above (right) natural frequency of base structure	65
3.12	Longitudinal Vincent plots showing zoomed in plot around the design point for frequencies above the natural frequency (right).	66
3.13	Updated longitudinal model based on objective parameters	67
3.14	Dynamic stiffness of transverse excitation	68
3.15	Transverse Vincent plots for frequencies below (left) and above (right) natural frequency of base structure	69
3.16	Updated transverse model based on objective parameters	69
4.1	Schematic of piezoelectric bimorph	75
4.2	Schematic of piezoelectric attached to absorber beam for active control	77
4.3	Natural frequency of absorber with open and closed loop control	85
4.4	Frequency response of longitudinally excited system	86
4.5	Absorber array number vs. maximum stress in absorber piezoelectric	87

LIST OF TABLES

TABLE

2.1	Summary of results comparing model prediction to experimental measurements for zigzag absorber	18
2.2	Constants used in design simulation	25
2.3	Summary of results comparing analytical model prediction to finite element predictions for metastructure and absorbers	26
2.4	Dimensions and properties used in models and experiment	31
2.5	Measured bandwidths and peak creation for the mechanical metamaterial beam	36
2.6	Finite element frequencies compared to experimental data for multi axis metastructure	36
2.7	Summary of results comparing analytical model prediction to finite element predictions for absorber fundamental frequencies	38
2.8	Equivalent mass and stiffness terms for absorber excitation directions	38
2.9	Summary of results comparing analytical model predictions to finite element predictions and experimental results for full multi axis beam	46
3.1	Peak separation of original design vs. optimal designs for different excitation directions	70
4.1	Three dimensional material properties for PZT-5A	76

ABSTRACT

The use of mechanical metamaterials, or metastructures, for vibration suppression has recently emerged as a viable approach to creating vibrationally resilient systems. Previous designs have proven to be effective at attenuating vibrations, however additional concerns arise with the use of these devices. Although many metastructures predict an improved performance, many have not been experimentally validated due to the infeasibility of creating their complex geometries before the advent of additive manufacturing.

Additionally, the existing research has only considered designs excited in one or two directions. This research successfully designs and fabricates the first multi axis mechanical metamaterial capable of attenuating vibration under excitation in the longitudinal, transverse, and torsional directions. This multi axis metastructure is experimentally validated against FEM and analytical models.

The majority of these metastructure devices are additively manufactured from polymers having a high amount of inherent material damping. Metastructure systems are often created for a specific use case and the geometries are optimized with a chosen material without considering the tradeoffs between optimizing the design and the effect of material damping. This work analyzes cases and frequency ranges of interest where using a highly damped material will outperform an optimized geometry and is the first to determine a dividing line between material damping and vibration absorption in mechanical metamaterial design. Considering both two degree of freedom and multi axis degree of freedom excitation structures, frequency responses suggest that for a system where a specific excitation frequency is to be avoided, it is more beneficial from a displacement reduction standpoint to tune absorbers to this frequency instead of adding system damping. Alternatively, if the system excitation is varying or broadband, increased damping provides a lower global displacement over a broader frequency range suggesting that for this excitation scenario, increasing material damping outperforms absorber tuning. By using the criteria provided in this thesis, a decision can be made on the most effective system design given known excitation constraints. These criteria can help determine whether it is necessary to undergo costly geometric optimization processes.

The peak separation capabilities of the multi axis mechanical metamaterial are considered for augmentation through a control system located on the distributed absorber system. An electromechanical model of including a piezoelectric bimorph to sense and actuate the absorber system is derived. A pole placement control system is introduced to adjust the natural frequencies of the absorbers. While a control system is not recommended to be used in this design case due to the high stresses in the piezoelectric material during excitation, a base method for active control of the absorbers of a metastructure with regards to peak separation is created. Additional insight on control use in mechanical metamaterials is discussed, including recommendations on when an active control system should be considered.

CHAPTER I

Introduction

1.1 Metamaterials and Origin of Metastructures

Metamaterials are engineered materials, made of conventional mediums such as metal and plastic, that are designed to have properties not found in naturally occurring materials [2]. Metamaterials originate from the electromagnetic materials field where, in 1967, Victor Veselago proposed a theoretical material that had negative permittivity and permeability which opposed wave propagation in materials found in nature [3, 4]. Over three decades passed before Veselago's theory could be experimentally validated, however this was achieved in 2000 by Smith et al. [5]. Expanding from its beginnings in electromagnetics, metamaterials now are an interdisciplinary subject spanning fields including antenna engineering, materials science, optics, and nanoscale structures [6]. Recently, metamaterials have expanded to include acoustic waves using the bulk modulus and density as the analogs of permittivity and permeability in electromagnetic metamaterials [7]. Metamaterials often use Bragg scattering and destructive wave interference of periodic arrays of scatterers to create band gaps at specific frequencies. To effectively use Bragg scattering, the period length of the material must be close to the wavelength of the incident wave. This limits the effectiveness at obtaining low frequency bandgaps to large structures [8].

The first metamaterial that could create a bandgap at a frequency lower than the Bragg frequency used lead spheres as local resonators to suppress acoustic waves [9]. The local resonator system was shown to be the same mechanism used in traditional vibration suppression [10, 11, 12].

Metamaterials that use local resonators are referred to as elastic or mechanical metamaterials [13]. These particular mechanical metamaterials, the focus of this work, are often referred to as metastructures and they use distributed arrays of vibration absorbers for vibration attenuation [14, 15].

1.2 Vibration Control using Mechanical Metamaterials

Although the primary purpose of most beams is to support a static load, many times these structures are subjected to dynamic loading. These dynamic loads can increase the total load seen by the beam and subject the material to fatigue failure. Furthermore, at specific frequencies, the vibrations can cause resonance conditions in the structure. This occurs when the excitation frequency on the structure is equal to the natural frequency of the structure causing the system to vibrate at a higher amplitude [16]. Under some conditions, catastrophic failure of a structure can occur if the structural resonance frequency matches that of the driving frequency. For this reason, resonance avoidance is an important part of structural design.

Methods of suppressing and canceling vibration have been widely investigated by scientists and engineers alike. Most of these suppression methods can be either classified as active or passive vibration systems. Active systems require energy input into the system and control of an actuator to suppress the vibrations whereas passive systems will operate without any additional energy input or control system.

1.2.1 Passive Control

Similar to the creation of a frequency bandgap in electromagnetic research (where electromagnetic waves are blocked at specific frequency bands), the distributed vibration absorbers in a mechanical structure also create a frequency bandgap where vibration wave propagation is suppressed [17]. When looking at the frequency response function, the bandgap can also be referred to as the peak separation due to the peaks on the plots showing where the natural frequencies of the system are. Figure 1.1 visually demonstrates the concept of a vibration peak separation band.

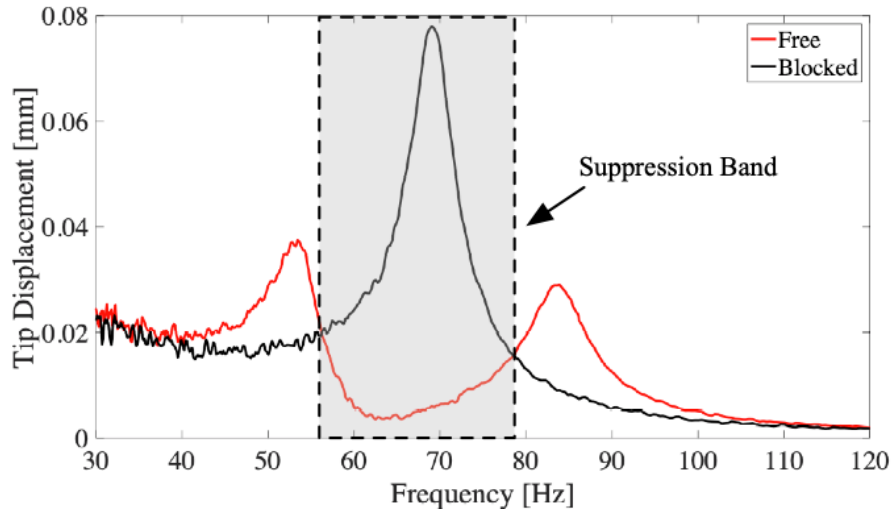


Figure 1.1: Frequency bandgap caused by distributed vibration absorbers

The more basic system to study this phenomenon is the one degree of freedom lumped mass and linear spring attached to a main mechanical system. Historically, one of the most investigated vibration systems is this system with added damping called a tuned mass damper, or TMD. This simple one degree of freedom system can be added to an existing structure and tuned through the structural and forcing parameters to suppress the vibration of the host structure. After determining the TMD was effective at modal suppression of the main structure, Den Hartog then derived the analytical formula for optimization of damper and absorber system [18]. Other papers also studied this system and numerical optimizations were determined to obtain the minimum main structure amplitude as well as the minimum total amplitude of the main structure over all of the excitation frequencies considered in the model [19, 20]. Many TMD researchers refer to the peak amplitude of the frequency response as the H_∞ norm and the total amplitude over all the excitation frequencies as the H_2 norm [21, 22].

The first researchers to suppress a single mode of vibration using an array of tuned mass dampers attached to a main system were Igusa and Xu [23, 24]. Further work was carried out by Yamaguchi where the parameters of the multiple tuned mass absorbers were varied and optimized to find that an optimal array of tuned mass dampers is more effective than a single optimally tuned mass damper because they can be tuned to attenuate vibration at multiple modes[25]. Most modern

passive control methods use these arrays of 1D absorbers attached to the structure of interest.

1.2.1.1 Alternative Vibration Absorber Geometries

For the creation of an experimental structure, the absorbers must have distributed geometries to match the natural frequencies of the main system. A limiting factor of absorber design is the geometric requirements of the natural frequency of the absorbers. This is paralleled in the energy harvesting community where the harvester is designed to match the natural frequency of the structure it is attached to and often also has geometric constraints. A traditionally chosen geometry is a cantilever beam which has a natural frequency inversely proportional to their length. Integrating absorbers into a full structural system becomes difficult because a larger system has lower natural frequencies than achievable with a regular cantilever. To remedy this issue, often a tip mass is added to the absorbers to lower their natural frequencies. This is effective in many situations, especially for the case of longitudinally excited systems where the fundamental natural frequency is higher than the other directions. Transversely excited beams, however, usually have a much lower fundamental frequency, and for this reason, alternate designs have been explored.

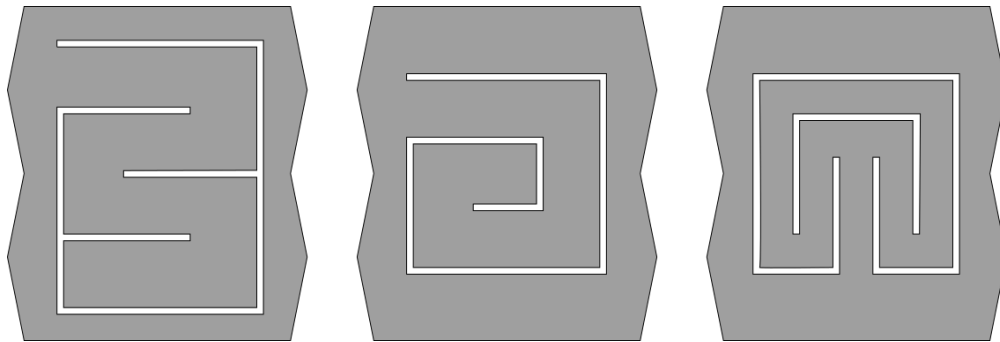


Figure 1.2: Alternative vibration absorber geometries. From left to right: zigzag, orthogonal spiral, elephant.

Zigzag absorber designs were thoroughly investigated for an energy harvesting system in a compact design space [26, 27]. Highly tunable structures achieved natural frequencies of close to 70 Hz, which is the utility frequency, or the standard power transmission on the electrical grid. An energy harvester operating at the utility frequency can easily be integrated into a power system.

Additional designs for attaining the desired absorber natural frequencies have been studied by the energy harvesting community. Orthogonal spiral structures have been proposed and analyzed by Dos Santos et al. [28] where they were able to achieve similar low natural frequencies as the zigzag.

Other designs have also been explored, including the introduction of an "elephant" two-dimensional device where the first mode shape was of a similar natural frequency, but the main concern of the paper was the second bending mode shape and how the interaction with first mode shape was able to lower the second natural frequency [29]. An overview of the previously mentioned absorber shapes is pictured in Figure 1.2.

1.2.1.2 Multi-dimensional Vibration Mitigation

Previous work in the metastructure field used distributed absorber designs for axial vibration suppression. Hobeck et al. [1] investigated preliminary modeling and experiments for the passive axial metastructure system while Drouard [30] as well as Reichl [31] delved into both passive and active axial suppression including tuning the dampers separately for varying suppression effects. Oftentimes, vibrations are restricted to unidirectional excitation which is achievable in a lab setting but is not often the type of excitation experienced by a structure in the field. The work of Drouard et al. [30] added suppression of torsional vibration to the original axial design for a 2D structure. Figure 1.3 shows the design for axial excitation created by Hobeck et al. [1].

In real world applications, a load bearing spar experiences vibration in all directions, however this spar will likely resonate at different amplitudes and frequencies. The different directions have usually constrained mechanical metamaterials design to addressing only one or two directions of excitation. For a practical application however, a generalized absorber system must be developed that can mitigate resonances in all three directions. This can improve the performance and longevity of bridge trusses, aircraft structural components, and radio transmission equipment [32].

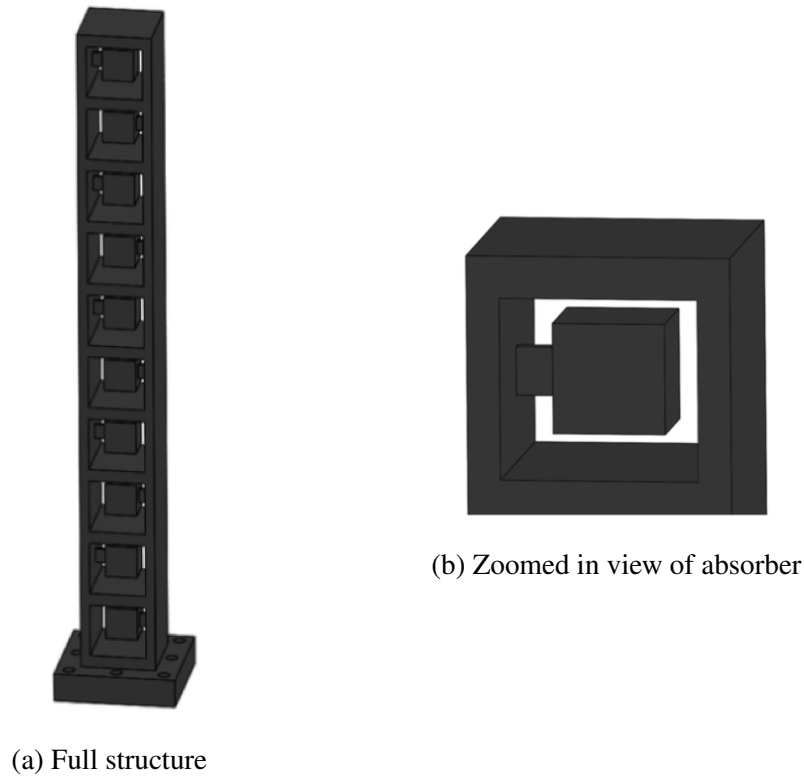


Figure 1.3: Previous multi dimensional vibration mitigation design [1]

1.2.2 Active Control

Oftentimes structures are designed for specific operating conditions, however, they are implemented in situations that have unanticipated conditions. In these cases, the options are to design for the most common operating scenarios and accept suboptimal operations in the other conditions, or to add a control system to the structure to adjust the system response.

Most previous literature in active controls has focused on reducing the displacement of the structure [33, 34, 35]. Mechanical metamaterial control however focuses on increasing the frequency bandgap of the structure. For the last decade, this type of control has been implemented into mechanical metamaterials using shunt damping [36, 37]. Only recently has active feedback control been introduced to metastructure systems [38, 39, 40]. This research focuses on modeling the addition of piezoelectric actuators and an active control system to an absorber array to maximize the peak separation between main beam natural frequencies. Separating the peaks away from an undesirable frequency will reduce the loading amplitude on the beam at that frequency. This

is necessary if the external excitation matches the natural frequency of the blocked beam system. Furthermore, if the beam is subjected to a broadband excitation, the split peaks may lower the overall loads the beam is subjected to.

Piezoelectric materials are often used be modeled as sensors and actuators in control system design due to their wide availability and their relatively straightforward implementation. Using these devices as sensors and actuators takes advantage of the piezoelectric effect, where an applied voltage to a piezoelectric material produces a strain, and conversely, a strain produces a voltage [41].

The control method generated in this work is derived using pole placement techniques. Pole placement permits a straightforward application and can provide a direct theoretical prediction of peak separation control for this multi axis mechanical metamaterial. Using a pole placement control system on the absorbers allows one to directly choose the eigenvalues, and therefore the natural frequencies, of the absorbers which can then be combined into the full metastructure model [42].

1.2.2.1 Additive Manufacturing

The creation of mechanical metamaterials using additive manufacturing provides multiple benefits over traditional machining. Using traditional machining to manufacture a mechanical metamaterial system with complex geometries would require the main structures to be fabricated separately and the absorbers attached later. With additive manufacturing techniques, the absorbers and main beam can be created as a single structure making rapid prototyping more cost-effective and efficient [43].

Additional damping can easily be incorporated directly during printing using materials with high viscoelastic properties. Advances in metal additive manufacturing printers could enable the incorporation of absorbers into commonly seen structures in the aerospace and automotive industries. This enables noise and fatigue reduction in critical load bearing applications.

1.3 Motivation and Scope

From the discovery of the benefit of using multiple tuned mass absorbers to attenuate vibration modes of a main structure, there has been a rush to model and optimize generalized structural designs. Experimental realization of these designs for integration with existing structures has been difficult to implement due to their geometric complexity which made them difficult or time consuming to create. Now that additive manufacturing has enabled quick and straight-forward construction of these designs, one can begin experimentally testing these previously theoretical designs. The current work aims to design, fabricate, and experimentally test a mechanical meta-material system that could be implemented into an existing structure.

While additive manufacturing has opened new doors to creating mechanical metamaterials, there are still other issues to consider in their design. Many additive manufacturing printers use materials that are rubber like and contain inherent material damping. The issue with this is there exists a dividing line between vibration damping and vibration absorption in metastructure design. Material damping will dominate the geometric optimization that was done in the previous modeling phase, especially in complex geometries.

More specifically, depending on the excitation scenario for these metastructures, it may be more expedient from a time and a vibration attenuation standpoint to choose a material that has higher material damping rather than spend the time to optimize the geometries of these structures. Because the origins of these absorber arrays were rooted in the novelty of the multiple tuned mass damper designs, the consideration of damping vs. absorption was not accounted for. This research seeks to determine the dividing line for these designs and make recommendations on whether it is more practical to optimize the metastructure geometry or whether more material damping should be added instead.

Current designs for 3D mechanical metamaterials either mean they exist in a three-dimensional space or they are excited in the X, Y, and Z directions [44]. The proposed structure for this thesis seeks to create a mechanical metamaterial capable of vibration attenuation in longitudinal, transverse, and torsional excitation directions.

While much of the focus for controls on existing metastructures is on decreasing the global vibration amplitude of the main beam, this research seeks to increase the peak separation created in the frequency response of the structure through both passive design and active controls.

1.4 Outline of Dissertation

This dissertation is divided into five chapters. Chapter I has explained the historical background of vibration absorbers and damping as well as the recent development of metamaterials and mechanical metamaterials. It further provided information on practical use cases of these structures as well as new advances and future improvements in the field. Lastly, a discussion of past and previous challenges in design and implementation was given.

Chapter II discusses the validity of using these structures in designs by providing a theoretical and experimental framework for an absorber system with low material damping in order to demonstrate the value of this type of device without assistance from external damping methods. A zigzag absorber is chosen for the absorber system for the wide design space they provide. Experimental and analytical models are presented for the absorbers themselves and the full implementation of the metastructure is compared with an analytical model and a numerical finite element simulation. A multi axis mechanical metamaterial capable of attenuating vibrations when excited in longitudinal, transverse, and torsional directions is created and experimental, analytical, and numerical results are presented for this structure. A discussion of model updating as well as basic design updates is also included.

Chapter III further delves into the concept of structure design and geometric optimization compared to the addition of highly damped absorbers. First, an experimental background is introduced that demonstrates the further necessity to explore this topic. Inspection of a two degree of freedom, and the previously introduced multi axis mechanical metamaterial are provided in the context of damping vs. vibration absorption and a framework and recommendations for design are included.

Chapter IV considers a control system in the frequency domain used to increase the peak sep-

aration of the multi axis mechanical metamaterial. Previous peak separation designs created in Chapter III are used to determine the desired absorber poles for the active control of the absorbers in the multi axis metastructure and the full state space model is used to find the frequency response of the main beam in the longitudinal direction. The maximum stress in the piezoelectric material on the absorbers is calculated to determine the feasibility of retroactively implementing controls in the existing design, and further discussion is included for general metastructure control implementation considerations.

Finally, Chapter V summarizes the results of this dissertation, complete with details about their furthered and continued impact as well as a discussion about their contributions to the existing fields of knowledge. A discussion of further work using this dissertation as a starting point is included.

CHAPTER II

Passive Control of Mechanical Metamaterials

2.1 Overview

This chapter has two main objectives. First, presenting a passive vibration control concept of a mechanical metamaterial made from a material with low material damping to demonstrate the validity of the metastructure concept without additional influence of material properties. The second goal is to create a metastructure capable of vibration absorption under excitation from multiple degrees of freedom.

The absorber geometries of the first system were based on a previous zigzag design that allows for a larger range of achievable natural frequencies while still maintaining a compact footprint. An analytical zigzag model and experimental validation were presented and incorporated into a full metastructure analytical model with finite element validation. Inserting these zigzag absorbers in a metastructure creates bandgaps in the frequency response that can help avoid undesired frequencies if the absorbers are tuned correctly.

The second metastructure design incorporates absorption for excitation in multiple degrees of freedom. The trends in the numerical model are experimentally validated and an analytical model is created to aid in the design of these multi axis mechanical metamaterials thereby creating the first multi axis metastructure capable of attenuating vibrations in longitudinal, transverse, and torsional excitation.

The multi axis mechanical metamaterial is comprised of a main structure with cross section

cutouts where tuned absorber arrays are attached. These absorber arrays create a bandgap in the frequency response. Altering the absorber mass and geometry can lead to an increase in the bandgap in different excitation directions.

Because the multi axis metastructure as well as an increasing number of mechanical metamaterials are created using additive manufacturing, a discussion of the current additive manufacturing limitations is included and an investigation into important design parameters is presented.

2.2 Mechanical Metamaterial for Transverse Excitation

Mechanical metastructures with low material damping demonstrate the value of the metastructure concept without the added influence of material damping.

Tuning absorbers to match the natural frequency of the main beam particularly in the transverse direction has a unique set of challenges. The transverse natural frequency is lower than that of the other directions and using a cantilever beam design for the absorber system can be difficult to frequency match - particularly in a limited geometric space. Because the frequency of a cantilever beam is inversely proportional to its length, lowering the natural frequency of the absorbers to match the main beam means either increasing the length of the absorber beam or adding a large tip mass. Both solutions can encounter issues fitting in the geometric design space or in being able to support the structural weight.

Zigzag shaped beams have been shown to have natural frequencies orders of magnitudes lower than traditional cantilever beam geometries of the same size. The use of highly tunable zigzag absorbers permits the use of metastructures in a wide variety of applications and excitation scenarios.

2.2.1 Linear Zigzag Shaped Absorber

Based on the design of zigzag absorbers from Karami [26], these structures function similarly to cantilever beam absorbers. However, due to their zigzag shape, the absorbers can achieve a lower natural frequency than a traditional cantilever beam in the same geometric footprint.

Initial modeling of the zigzag structure was calculated in Essink et al. [27] and is conducted by first modeling the zigzag as a distributed system of connected of cantilever beams. These beams are assumed to have small linear deflections. A diagram of the dimensions and applied forces is shown in Figure 2.1.

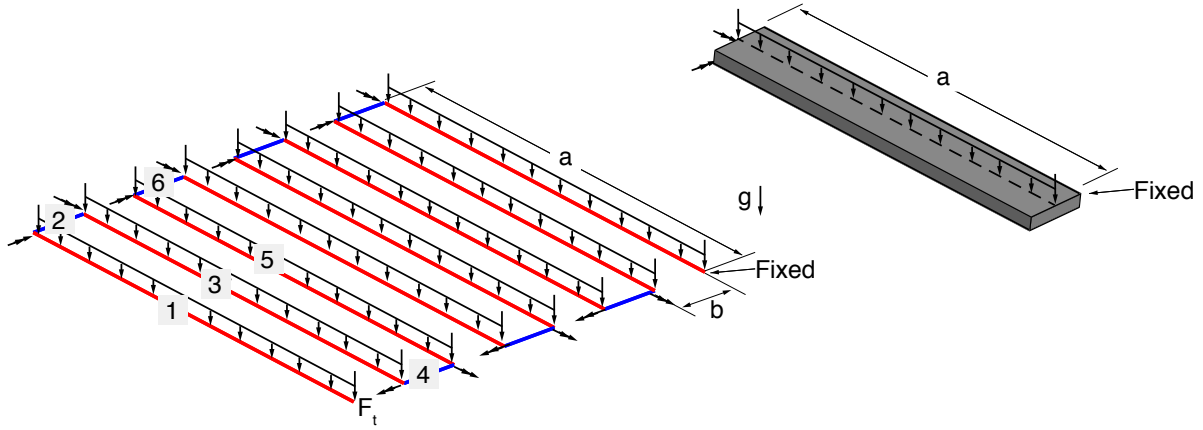


Figure 2.1: Applied forces on zigzag beam

2.2.1.1 Local Deflection

The deflections of the full structure are calculated first from local deflections. The load, moment, and torque on the tip of each beam were calculated. The solution technique involves recursively solving for each cross member of the zigzag using the loads of the member closer to the tip. The bending equation for a single member is [27]

$$\psi = \frac{Px^2}{6EI}(3l - x) + \frac{Wx^2}{24EI}(x^2 - 4lx + 6l^2) + \frac{Mx^2}{2EI} \quad (2.1)$$

where ψ_p , ψ_w , and ψ_m are transverse deflections of a cantilever beam caused by a tip load P , distributed load W , and a tip moment M . The length coordinate of the beam is given denoted by x , the total beam length by l , and the bending stiffness by EI . The torsion equation for each beam segment can be written as

$$\beta = \frac{Tx}{GJ} \quad (2.2)$$

where β is the torsion angle in radians, T is the applied tip torque, and GJ is the torsional stiffness.

Starting from the tip, by substituting in the loads of the next cross member closer to the tip, expressions for the bending and torsional deflections were developed such that the deflection and angle of all beam members could be calculated given the desired dimensions, material properties, and number of beam segments to include. The general form of the bending and torsional equations can be written as

$$\psi_i = \frac{P_i r_i^2}{6EI} [3r_i(l) - x] + \frac{W r_i^2}{24EI} [r_i^2 - 4r_i(l)r_i + 6r_i(l)^2] + \frac{M_i r_i^2}{2EI} \quad \text{for } i = 1, 2, 3, \dots, N \quad (2.3)$$

$$\beta_i = \frac{T_i r_i}{GJ} \quad \text{for } i = 1, 2, 3, \dots, N \quad (2.4)$$

$$P_i = F_t + F_c(i-1) + \frac{W}{2}(i-1)(a+b) \quad \text{for } i = 1, 3, 5, \dots$$

$$P_i = F_t + F_c(i-1) + \frac{Wi}{2}(a+b) - Wb \quad \text{for } i = 2, 4, 6, \dots \quad (2.5)$$

$$M_i = \frac{Wa}{4}(1-i)(a+b) + \frac{F_c a}{2}(1-i) \quad \text{for } i = 1, 5, 9, \dots$$

$$M_i = -F_t a + \frac{1}{4}(1-i)W a^2 + \frac{1}{4}(3-i)W ab + \frac{1}{2}(3-i)F_c a \quad \text{for } i = 3, 7, 11, \dots$$

$$M_i = \frac{1}{2}(i-2)F_t b + \left(\frac{i^2}{8} - \frac{i}{4}\right)W ab + \frac{1}{2}\left(\frac{i^2}{4} - i + 1\right)W b^2 + \left(\frac{i^2}{4} - i + 1\right)F_c b \quad \text{for } i = 2, 4, 6, \dots \quad (2.6)$$

$$\begin{aligned}
T_i &= F_t a + \frac{i}{4}(i-2)Wab + \frac{1}{2}(i-2)F_c a \quad \text{for } i = 2, 6, 10, \dots \\
T_i &+ \frac{i}{4}Wa(a+b) + \frac{i}{2}F_c a \quad \text{for } i = 4, 8, 12, \dots \\
T_i &= \frac{1}{2}(i-1)F_t b + \frac{1}{4}(i-1)^2 F_c b + \frac{1}{8}(i^2-1)Wab \\
&+ \frac{1}{4} \left[\frac{1}{2}(i^2+1) - i \right] Wb^2 \quad \text{for } i = 1, 3, 5, \dots
\end{aligned} \tag{2.7}$$

where F_c and F_t are point loads due to gravity, g on the masses M_c and M_t . W is the distributed load due to gravity on the beam mass and i is an integer indicating the beam member number starting from the free beam. The long beams in the zigzag are represented by the a coordinate and referred to as "a-beams" and the short beams by b and referred to as "b-beams" which are depicted in Figure 2.1.

These loads can be defined as

$$F_c = M_c g \tag{2.8}$$

$$F_t = (M_t + M_c)g \tag{2.9}$$

$$W = mg \tag{2.10}$$

where m is the linear mass density of the beam segments.

2.2.1.2 Global Deflection

After finding expressions for the local bending and torsion, global displacements can be calculated by beginning from the clamped end using the recursive formula for global displacement of each beam member.

$$\begin{aligned}
z_1(\psi, \beta) &= \psi_1 \\
z_2(\psi, \beta) &= z_1(a) + \psi_2 + \beta_1(a)r_2 \\
z_3(\psi, \beta) &= z_2(b) + \psi_3 + \left[\left. \frac{dz_1}{d\bar{a}} \right|_a + \beta_2(b) \right] r_3 \\
&\vdots \\
z_j(\psi, \beta) &= z_{j-1}(l) + \psi_j + \left[\left. \frac{dz_{j-2}}{dr_{j-2}} \right|_l + \beta_{j-1}(l) \right] r_j
\end{aligned} \tag{2.11}$$

where z is the global deflection of the beam member, the subscript j is an integer value denoting the beam member starting from the clamped beam and r_j is the local length coordinate of the j^{th} beam member.

Upon implementation of Equation (2.11), the normalized global displacement of an 8 a -beam zigzag structure was calculated and is shown in Figure 2.2. This deflection was used as an estimate for the fundamental mode shape of the structure and subsequently, the fundamental frequency of the structure.

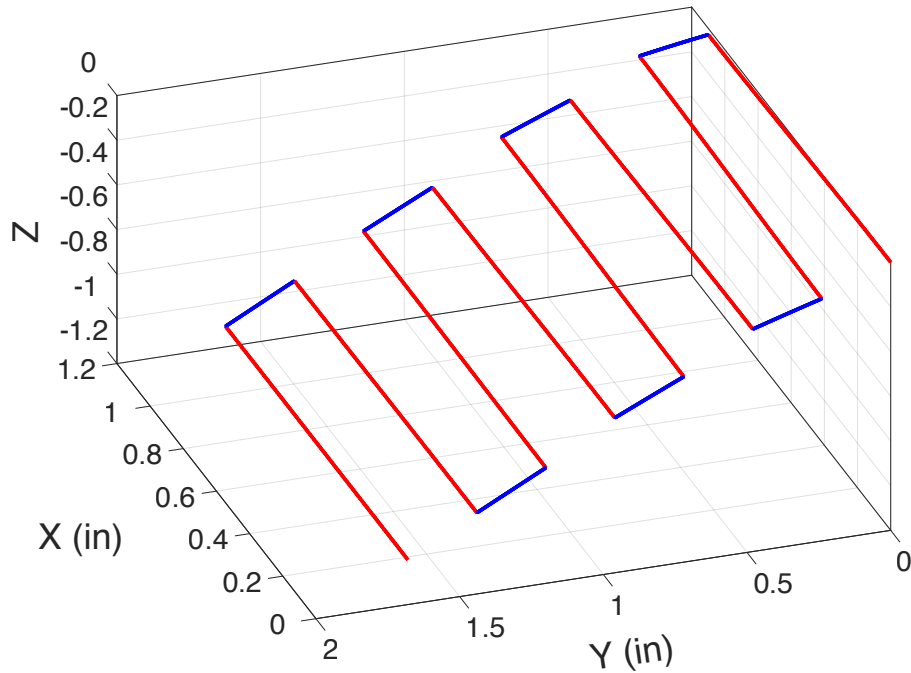


Figure 2.2: Global displacement of an 8 a -beam zigzag structure

After finding both local and global deflections, the equivalent mass and stiffness for the zigzag beam can be calculated and the first natural frequency of the zigzag can be estimated using Rayleigh's quotient. The equivalent lumped mass and stiffness are used to simplify the dynamics of the zigzag absorbers for integration in the full model of the metastructure.

Rayleigh's quotient is given as

$$\omega_0^2 = \frac{k_{eq} z_{1l}^2}{m_{eq} z_{1l}^2} = \frac{\sum_{n=1}^N \int_0^{l_n} \left[EI \left(\frac{d^2 z_n}{du_n^2} \right)^2 + GJ \theta_n^2 \right] du_n}{\sum_{n=1}^N \left[m \int_0^{l_n} z_n^2 du_n + (M_c + \delta_{n1} M_t) z_n^2(l) \right]} \quad (2.12)$$

where ω_0 is the angular frequency in radians per second, k_{eq} is the equivalent lumped stiffness, m_{eq} is the equivalent lumped mass, z_{1l} is the global deflection of the first beam segment evaluated at the beam tip, N is the number of beam segments, l is the length of the segment, EI is the bending stiffness, GJ is the torsional stiffness, z is the global deflection, θ is the twist angle, m is the linear mass density, M_t is the tip mass applied to the n^{th} beam of the tip of the free end, M_c is the incremental mass applied to all beams, and δ_{n1} is the Kroneker delta. The incremental mass is used to account for the mass removed from the end of each beam when the 2D beam surfaces were formulated into an equivalent 1D line representation.

2.2.2 Experimental Analysis

Zigzag beams with members of 4, 5, 6, and 8 a -beam members were cut out of thin plates of 6061-T6 aluminum using a high-pressure CNC waterjet and can be seen in Figure 2.3. Natural frequencies of the zigzag structures were measured and compared to model predictions to validate the model and are listed in Table 2.1 where the N_a column indicates the number of segments of length a . For a number of a -beam members larger than 5, the method has less than 2% error. The largest error between the model and the experiment is 7.44% therefore validating the analytical model of the zigzag absorbers.

The error in the system increases for a smaller number of a -beams. One possible cause for the error is that the model assumes a rigid clamp with no slope at the base. The experimental clamp

is not perfectly rigid, and this can cause a decrease in stiffness which will have a higher influence on the zigzags with less a -beams, leading to a lower natural frequency as seen in the experiment when compared with the model.

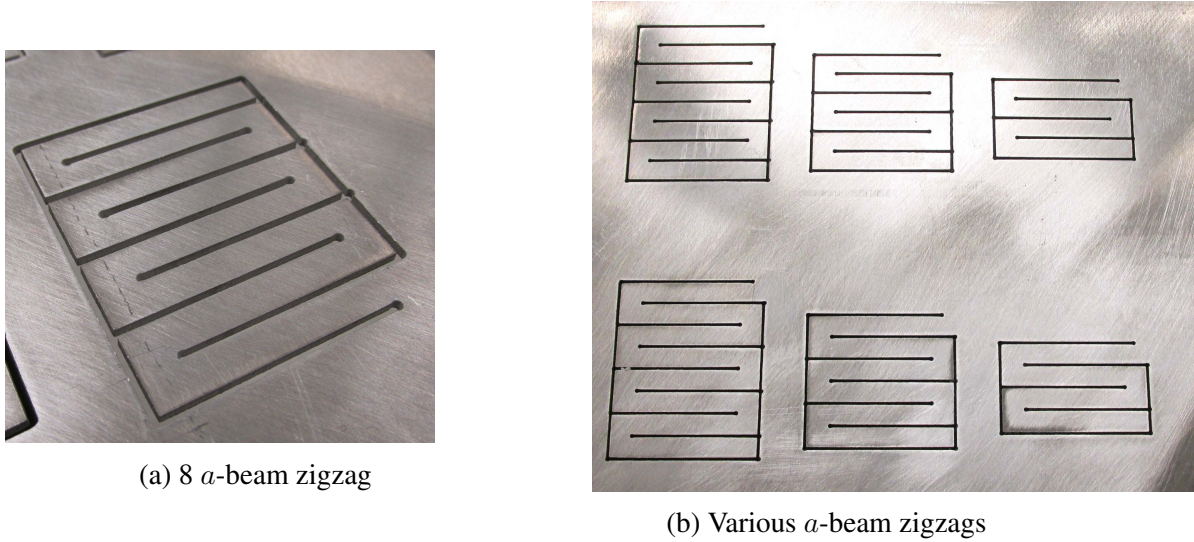


Figure 2.3: Water-jet cut experimental zigzag beams

Table 2.1: Summary of results comparing model prediction to experimental measurements for zigzag absorber

N_a	Experimental Fundamental Frequency (Hz)				Exp. Average (Hz)	Model (Hz)	% Error
	Sample #1	Sample #2	Sample #3	Sample #4			
8	77.9	78.2	78.2	78.6	78.2	77.5	0.84%
6	131.2	129.0	-	130.3	130.1	129.0	0.9%
5	177.7	-	-	-	177.7	174.4	1.90%
4	230.9	230.6	228.8	224.8	228.8	247.2	7.44%

2.2.3 Metastructure with Zigzag Absorber Inserts

Inserting these zigzag absorbers in a metastructure creates bandgaps in the frequency response that can help avoid undesired frequencies if the absorbers are tuned correctly. Choosing zigzag shaped

absorbers increases the achievable natural frequencies without adding a large amount of additional size or mass to the structure.

Using the equivalent mass and stiffness of the zigzag structure allows a full metastructure beam to be modeled as a base beam with a set of attached single degree of freedom oscillators. By using the lumped values instead of the full absorber dynamics, the complexities of the vibrating absorber dynamics are reduced to a single degree of freedom system. The overall dynamics of the combined beam and absorber structure are still captured when using the reduced absorber model by including the coupling between the absorbers and the main beam. Modeling the full system in this manner reduces complexity and computation time while still reproducing the coupled system behavior.

The Rayleigh-Ritz formulation can be used to model the entire structure starting with the kinetic and potential energy equations

$$T = \frac{1}{2} \int_0^L \rho A \dot{w}^2 dx + \frac{1}{2} \sum_{j=1}^{N_\beta} M_j^\beta \dot{y}_j^2 \quad (2.13)$$

$$U = \frac{1}{2} \int_0^L EI w''^2 dx + \frac{1}{2} \sum_{j=1}^{N_\beta} k_j [w(\beta_j) - y_j]^2 \quad (2.14)$$

where ρ is the material density, A is the cross sectional area of the main structure which is allowed to vary along the length, EI is the bending stiffness which is also allowed to vary along the length, w is the transverse beam deflection, y is the absorber deflection, L is the beam length, and β is the x-axis locations of the absorber system. M is the absorber mass, k is the absorber stiffness, N_β is the number of absorbers.

The beam deflection is assumed to be a finite convergent series

$$w = \sum_{r=1}^{N_w} W_r d_r \quad (2.15)$$

where W_r is the equation for the mode shape of a cantilever beam, d_r is a weighting term associated with each shape function, and N_w is the number of modes under consideration. Full mass and

coupled stiffness matrices can be created by taking a partial derivative with respect to d and y and collecting coefficients.

$$\mathbf{M} = \begin{bmatrix} \mathbf{M}^\alpha & \mathbf{0} \\ \mathbf{0} & \mathbf{M}^\beta \end{bmatrix} \quad (2.16)$$

where \mathbf{M} is the sub-matrix of beam deflections and \mathbf{M}^β is the sub-matrix of the absorbers at the β locations along the length of the beam. The sub-matrices can be defined as:

$$\mathbf{M}^\alpha = M_{rs}^\alpha = \left[\int_0^L m W_r W_s dx + \sum_{i=1}^{N_a} M_i^\beta W_r(\beta_i) W_s(\beta_i) \beta_i \right]_{N_w \times N_w} \quad (2.17)$$

$$\mathbf{M}^\beta = \text{diag} \left[M_1^\beta \quad M_2^\beta \quad \dots \quad M_{N_\beta}^\beta \right]_{N_\beta \times N_\beta} \quad (2.18)$$

Similarly, for the stiffness

$$\mathbf{K} = \begin{bmatrix} \mathbf{K}^\alpha & \mathbf{K}^{\alpha\beta} \\ [\mathbf{K}^{\alpha\beta}]^T & \mathbf{K}^\beta \end{bmatrix} \quad (2.19)$$

$$\mathbf{K}^\alpha = K_{rs}^\alpha = \left[\int_0^L EI W_r'' W_s'' dx + \sum_{j=1}^{N_\beta} k_j^\beta W_r(\beta_j) W_s(\beta_j) \right]_{N_w \times N_w} \quad (2.20)$$

$$\mathbf{K}^\beta = \text{diag} \left[k_1^\beta \quad k_2^\beta \quad \dots \quad k_{N_\beta}^\beta \right]_{N_\beta \times N_\beta} \quad (2.21)$$

$$\mathbf{K}^{\alpha\beta} = K_{rj}^{\alpha\beta} = [-k_j W_r(\beta_j)]_{N_w \times N_\beta} \quad (2.22)$$

where both \mathbf{M} and \mathbf{K} are square matrices with rows and columns of dimensions of $N_w + N_\beta$. Using the mass and stiffness matrices, the structural eigenvalue problem can be solved using

$$(\mathbf{K} - \lambda\mathbf{M})[\mathbf{d}] = \mathbf{0} \quad (2.23)$$

where the natural frequencies, ω_r are calculated using the relation $\omega_r^2 = \lambda_r$. The mode shapes and shape functions can be determined from the eigenvectors of the system, \mathbf{d} .

In order to have a beam with an effective mass comparable to the absorber system, a c channel shaped beam was considered as the host beam. This ensures that the host structure is stiff, but still lightweight. For each location of the absorber, voids in the c channel are made to fit the geometry profile of the zigzag. This adds to a changing mass and stiffness of the beam as a function of the length.

Additional mounting tabs for the zigzags are also considered in the cutouts, leading to three different cross sections of the structure. These different cross sections are the solid c channel, the cutout, and the cutout with a tab. These cross sections are presented in Figure 2.4. Using the parallel axis theorem to find the neutral axis of each cross section, the moments of inertia for each cross section can be calculated to find the changing mass and stiffness for each section. Using the Heaviside function, the mass and stiffness of the beam can be defined as a discontinuous function of the beam length.

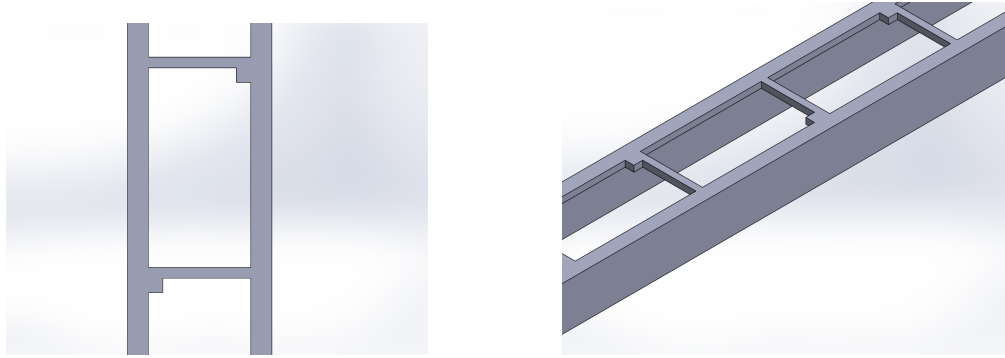


Figure 2.4: Views of the c channel beam cutouts and tabs for absorber mounting

For example, one can consider a single void in the structure and assume the density and Young's modulus of the structure to be uniform. The mass and stiffness functions are calculated for each cross section along the beam length axis and added summed to find the mass and stiffness as a

function of the beam length.

$$m(x) = \rho \{A_{aa} [H(x_1) - H(x - x_1)] + A_{bb} [H(x - x_1) - H(x - x_2)] + A_{cc} [H(x - x_2) - H(x - x_3)]\} \quad (2.24)$$

$$EI(x) = E \{I_{aa} [H(x_1) - H(x - x_1)] + I_{bb} [H(x - x_1) - H(x - x_2)] + I_{cc} [H(x - x_2) - H(x - x_3)]\} \quad (2.25)$$

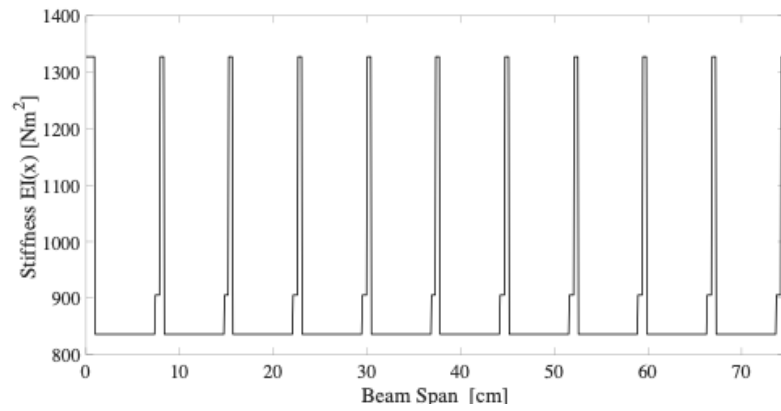
where H is the Heaviside step function.

Returning to the full beam, using the material properties and geometries, the mass and stiffness functions can be created for the beam. Figure 2.5 shows a plot of the variation of the c channel stiffness and mass as a function of beam length.

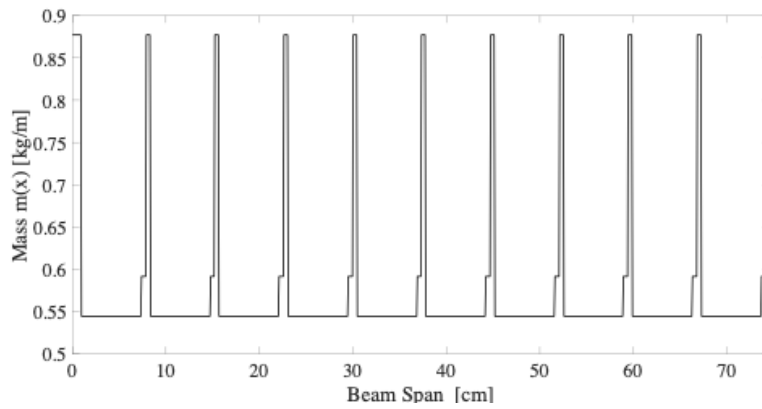
2.2.3.1 Model Verification

The analytical model for each component was created in MATLAB and validated using the commercial finite element software ANSYS. The zigzags, the solid c channel, the c channel with cutouts, and the full channel with absorbers were all modeled and validated. A full view of the c channel cutout with attached absorbers is shown in Figure 2.6. Table 2.3 lists both the analytical and finite element frequencies with their percent error. As shown in the table, the highest error is in the zigzag absorbers themselves which have an error of 5.49%. Figure 2.7 shows the frequency response for both the finite element and the analytical model using the design constants listed in Table 2.2.

Figure 2.8 shows the frequency response for the c channel beam both with and without absorbers. It is clear from the frequency response data that the addition of the absorbers can create a bandgap at the frequency of the c channel without absorbers. The results from this model demonstrate the value of the metastructure without assistance from external damping methods.

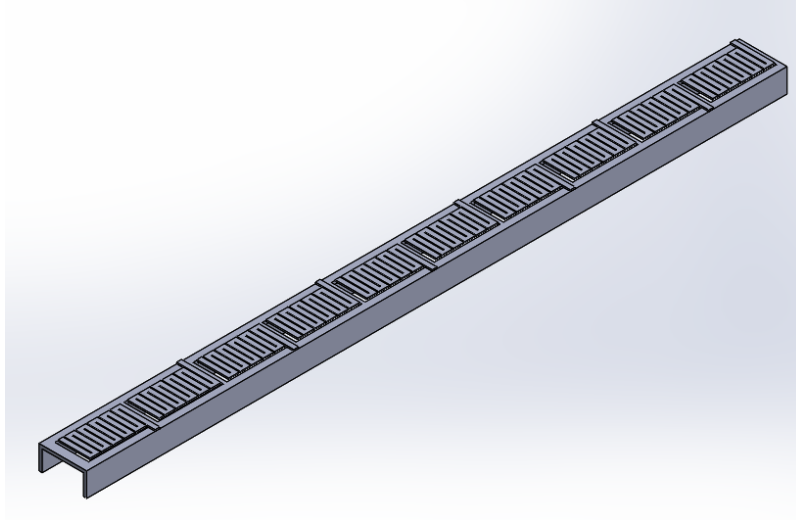


(a) Stiffness as a function of length

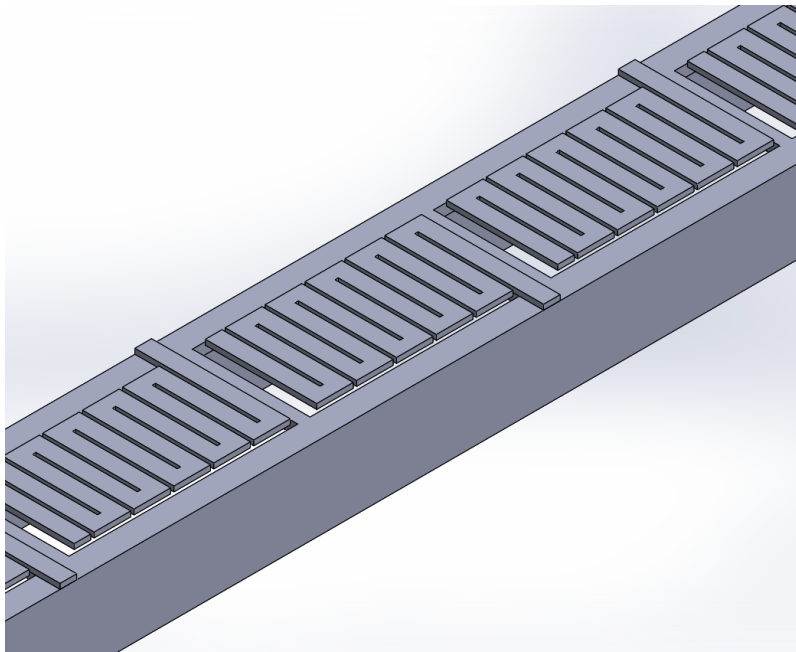


(b) Mass as a function of length

Figure 2.5: Variation of structural properties as a function of beam length for the c channel



(a) Fully integrated metastructure with absorbers



(b) Zoomed in view of the c channel metastructure

Figure 2.6: Views of c channel metastructure with zigzag absorber design

Table 2.2: Constants used in design simulation

Material Property	Symbol	Value	Units
Young's Modulus	E	69.00	GPa
Density	ρ	2700	kg/m ³
Shear Modulus	G	25.90	GPa
Channel Dimensions			
Length	L	74.61	cm
Base Width	O_1	5.080	cm
Leg Length	O_3	2.540	cm
Thickness	O_4	3.429	mm
Cutout Dimensions			
Length	O_5	6.922	cm
Width	O_6	3.594	cm
Spacing (x-direction)	δ_h	4.445	cm
Zigzag Dimension	Symbol	Value	Units
a -Beam Length	a	2.794	cm
a -Beam Width	w_a	5.080	mm
b -Beam Length	b	6.096	mm
b -Beam Width	w_b	4.064	mm
Thickness	h	1.588	mm
Number of a -Beams	N_a	11	-
Equivalent Mass	m_{eq}	8.022	gm
Equivalent Stiffness	k_{eq}	843.3	N/m

Table 2.3: Summary of results comparing analytical model prediction to finite element predictions for metastructure and absorbers

Structure	Analytical Frequency (Hz)	FEM Frequency (Hz)	Error (%)
Solid Channel	39.40	40.68	3.15%
Cut Channel (no inserts)	39.13	38.94	0.49%
Cut Channel (with inserts)	34.17	34.48	0.90%
Zigzag Absorber	51.60	54.60	5.49%

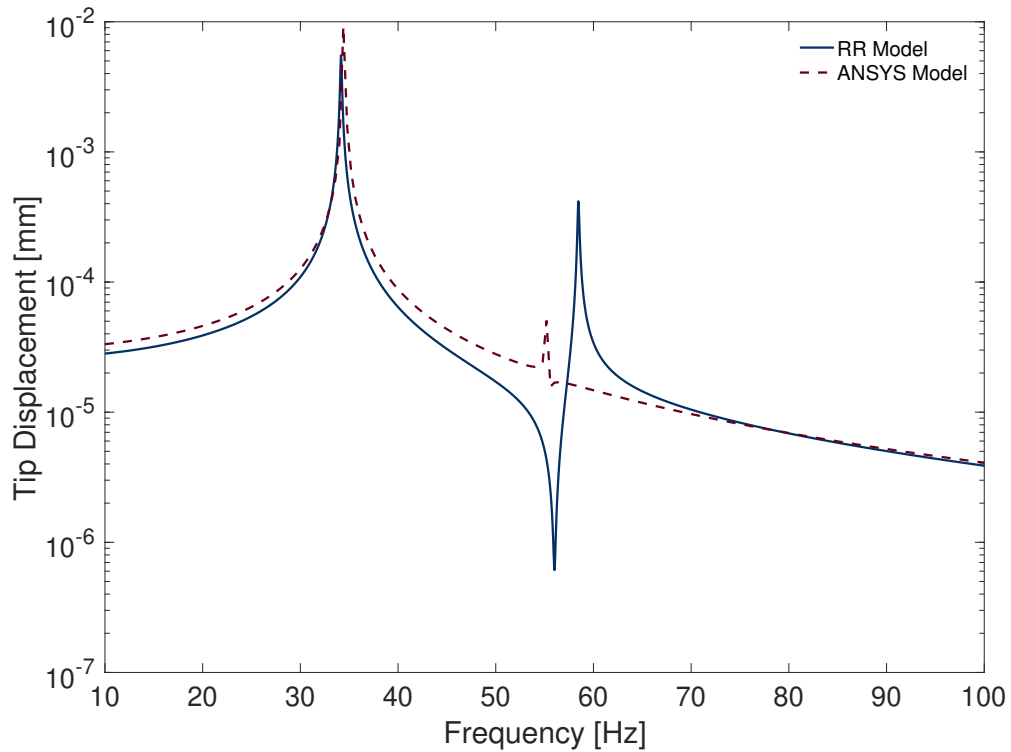


Figure 2.7: Comparison of analytical and finite element frequency response function for main beam

Additionally, the use of a zigzag absorber in the system demonstrates the ability to match the natural frequency of the main beam in the transverse direction which can often be difficult in a small design space. Because the frequency of a cantilever beam is inversely proportional to the length, as the main structure increases in length, the transverse natural frequency decreases. When using a cantilever beam design, the absorbers must also increase in length to account for the decrease in natural frequency. This can often be difficult in a limited design space. The use of highly tunable zigzag absorbers permits the use of metastructures in a wide variety of applications and excitation scenarios.

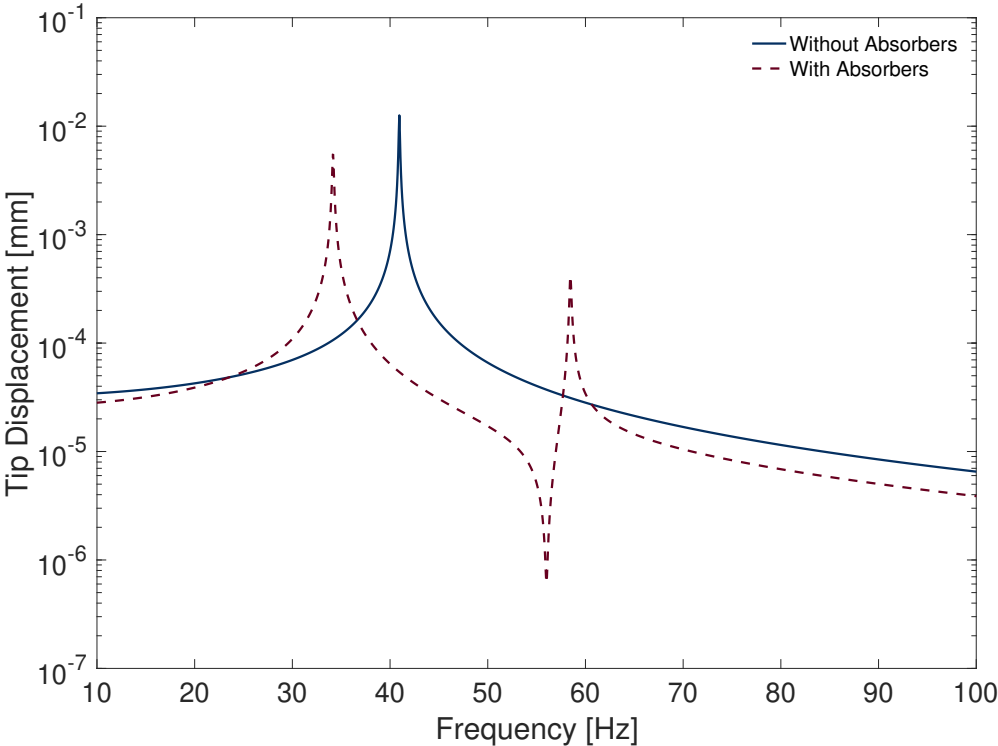


Figure 2.8: Frequency response of c channel beam with and without absorbers

2.3 Mechanical Metamaterial for Multi Axis Excitation

2.3.1 Initial Design

In real world applications, a load bearing spar experiences vibration in all directions, however the vibrations in each direction resonate at different amplitudes and frequencies. These difficulties have usually led research in mechanical metamaterials design to address only one or two directions of excitation. For a practical application, however, a generalized absorber system must be developed that can mitigate resonances in longitudinal, transverse and torsional excitation.

We begin creating this multi axis mechanical metamaterial by first creating a model of the structure. The initial finite element model of the structure was created using the commercial software ANSYS. There were two main components considered in the design of the structural model. First was the determination of the natural frequencies of the entire structure with the absorbers blocked from moving. This created a mass conserved structure that mimics a traditional beam with no attached vibration absorbers. The second part of the design was completed by modeling the individual absorbers and tuning them to vibrate at the first natural frequencies of each respective excitation direction for the blocked beam. By tuning the absorbers to the natural frequency of the entire assembly, it is possible to eliminate or significantly reduce vibration of the structure when the absorbers are free to vibrate. After creating the tuned absorbers, the full structure was modeled in ANSYS and tests were conducted in all three excitation directions. Using the blocked and free absorber conditions enables the comparison of the change in frequency response due to only absorber dynamics while excluding mass loading effects.

The base beam structure with no attached absorbers is shown in Figure 2.9a. It consists of a hollowed-out beam with a square cross section. There are eight cutouts in the frame with a central post to attach the absorbers. The total length of this design is 26.7 cm and the width is 4 cm. The absorber system is made of eight absorbers on each side of the structure attached in the cutouts for a total of 64 absorbers. The full structure used in ANSYS is shown in Figures 2.9b and 2.10. Figure 2.11a shows a schematic of a single absorber. Each absorber is attached to a middle rod on

the main structure as shown in the top down view of the full structure in Figure 2.11b. A table of dimensions and properties for the main beam and absorber are listed in Table 2.4. Depending on the excitation directions, bending of the absorbers in the thick or thin directions can occur. The different bending scenarios are shown in Figure 2.12 where excitation in the longitudinal direction will excite the absorbers in the thick direction as shown in Figure 2.12a, and the longitudinal and torsional excitation will cause the absorbers to vibrate in the thin direction depicted in Figure 2.12b.

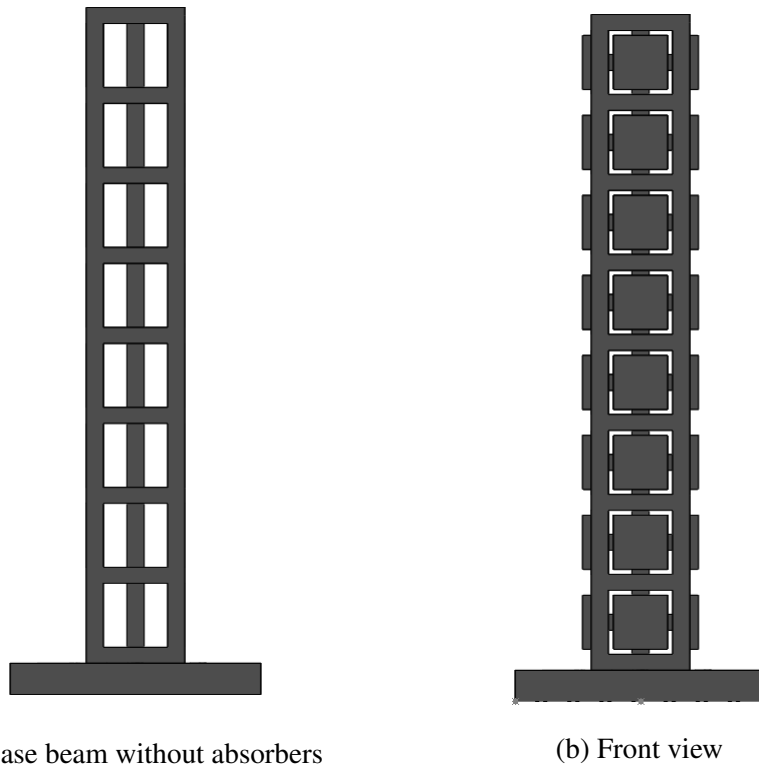


Figure 2.9: Schematic of multi axis mechanical metamaterial

2.3.2 Experimental Testing of the Model

The initial design for the multi axis mechanical metamaterial was fabricated using a Stratasys Objet Connex 500 3D printer. Both the host beam and the absorbers were printed from VeroWhite, the stiffest available material. Since the print bed of the Connex is 490 x 390 x 200 mm (with the vertical dimension being 200 mm) and the initial metastructure prototype including the mounting base had a vertical dimension of 279.2 mm, the metastructure had to be rotated to print on its side

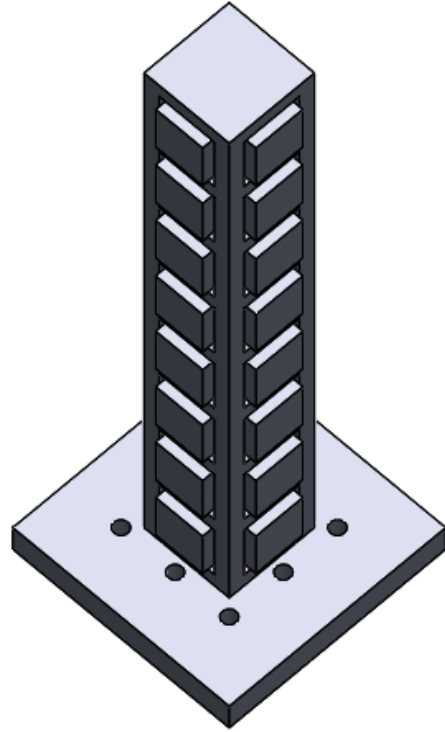


Figure 2.10: Isometric view of multi axis mechanical metamaterial

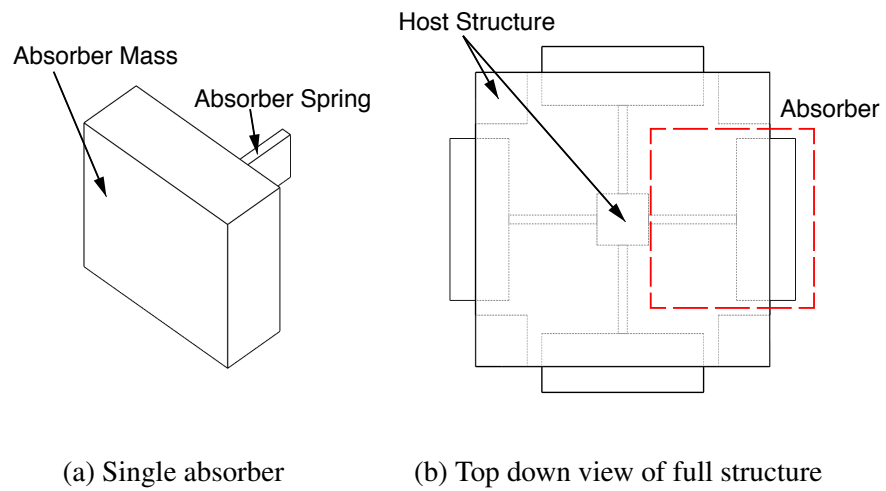


Figure 2.11: Absorber and metastructure schematic

Table 2.4: Dimensions and properties used in models and experiment

Material Property	Symbol	Value	Units
Young's Modulus	E	2.00	GPa
Density	ρ	1170	kg/m ³
Dimension	Symbol	Value	Units
Main Beam Length	L	26.7	cm
Main Beam Width	W	4.00	cm
Absorber Beam Length	l_b	12.0	mm
Absorber Beam Width	w_b	6.50	mm
Absorber Beam Thickness	h_b	1.20	mm
Mass Length	l_m	8.00	mm
Mass Width	w_m	22.0	mm
Mass Thickness	h_m	22.0	mm
Eccentricity	e	4.00	mm



Figure 2.12: Absorber bending direction. Contours show a qualitative absorber displacement.

to be completed in one piece.

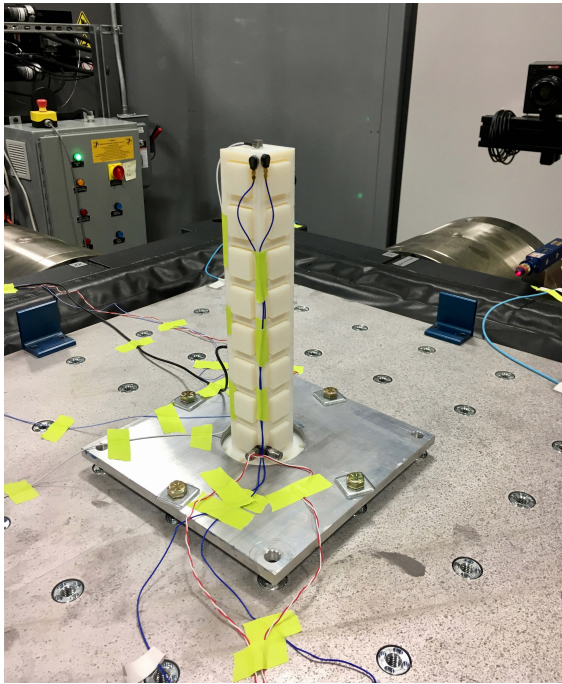
After fabrication was complete, the support material was mechanically removed from the main structure and the absorbers. The prototype was tested at the Army Research Laboratory on the Aberdeen Proving Grounds using a Team Corporation Tensor 18kN 6-DOF shaker table.

The 6DOF system has 12 electrodynamic shakers for multi-axis testing. Each shaker can be controlled individually for a wide range of testing scenarios. Excitation in the longitudinal direction was achieved by exciting the shakers in only the Z direction. The transverse excitation was measured by exciting the structure only in the X direction. The torsional excitation was achieved by exciting opposing Y direction shakers on each side of the table to create the twisting motion. All tests were sine sweep excitations from 20 to 1000 Hz. Figure 2.13 shows the shaker setup for both the free and blocked absorber experiments. The base of the beam was clamped to the shaker table using an accessory plate and accelerometers were attached to the beam using wax. Torsional base and tip measurements were taken using four accelerometers attached at the tip and four accelerometers at the base. Longitudinal and transverse measurements were taken using the base accelerometers and a triaxial accelerometer at the top center of the beam.

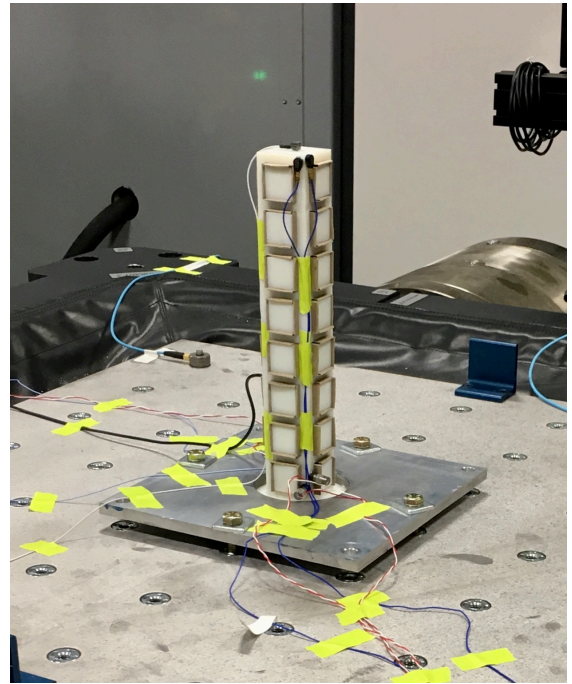
Sine sweeps were conducted both in individual X and Z directions as well as Y controlled torsion. Additional tests were run with simultaneous multi direction excitations and it was determined that there was no coupling between the excitation directions for the frequency range of interest. The displacements for each experiment were calculated from the accelerations recorded during testing.

Testing was conducted with both a free and blocked absorber configuration. Cardboard inserts were used to block the absorbers from vibrating during excitation without adding significant additional mass to the structure. To demonstrate the effect of adding absorbers, one can simply compare the frequency response of the blocked and free absorber configuration. This is a reasonable approximation since the mass is conserved.

Results of the free and blocked longitudinal sine sweeps are compared in Figure 2.14. For the blocked test of the absorber system, there is a single resonance peak at approximately 672



(a) Free absorber configuration



(b) Blocked absorber configuration

Figure 2.13: Experimental setup for multi axis mechanical metamaterial

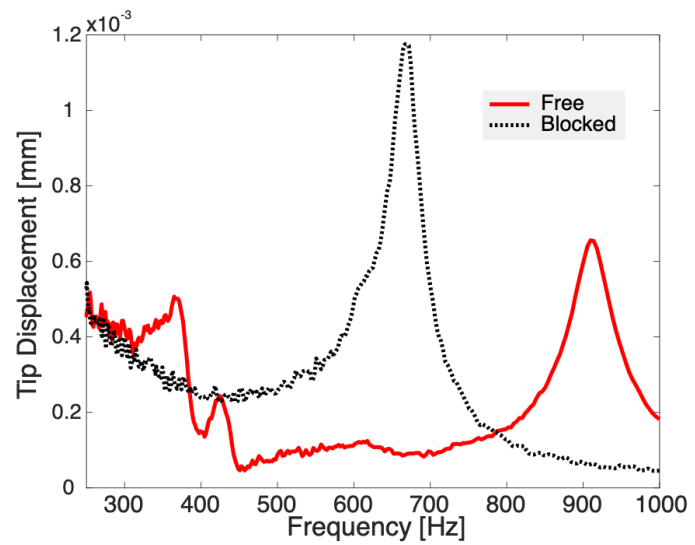
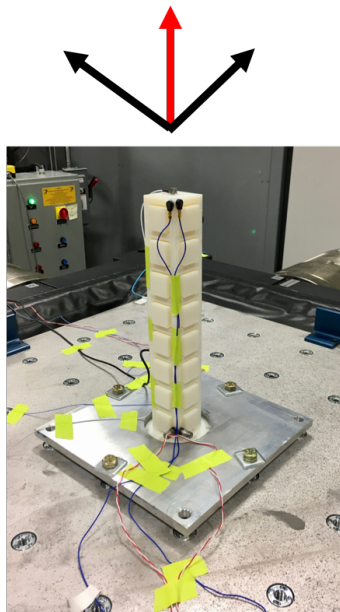


Figure 2.14: Longitudinal tip displacement for free and blocked configurations

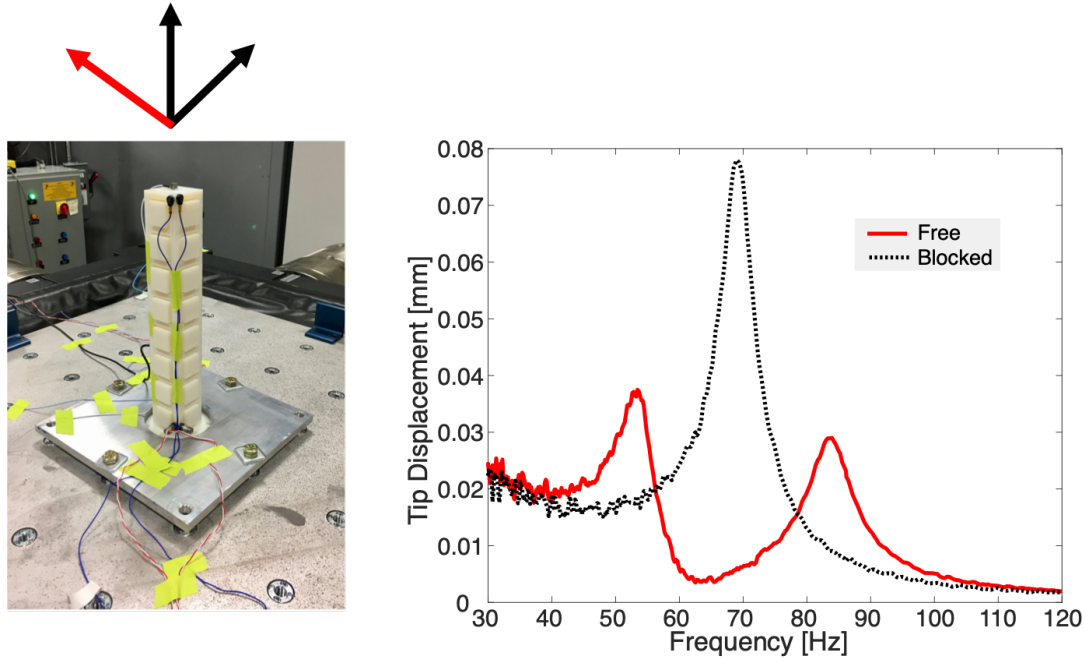


Figure 2.15: Transverse tip displacement for free and blocked configurations

Hz. When the absorbers are free to vibrate, the absorber system eliminates the vibration at and around the blocked natural frequency between 428 Hz and 786 Hz for a bandwidth of 358 Hz. Additionally, the global vibration amplitude of the free configuration is reduced compared to the blocked case. Figure 2.15 compares the free and blocked frequency responses for the structure excited in the transverse direction. The results show a similar trend to the longitudinal results, with a single resonance peak for the blocked system which is eliminated for the free absorber case. The blocked case single peak is located at approximately 69 Hz. The vibration is reduced between approximately 56 Hz and 79 Hz for a bandwidth of 23 Hz in the transverse direction. Similar to the longitudinal response, the global vibration of the structure is reduced for the free absorber case.

The torsional blocked and free response results are compared in Figure 2.16. Both the blocked and the free configurations show a single resonance peak, however the free absorbers drastically reduced vibration at the blocked resonance frequency and created a new resonant peak approximately 40 Hz higher. At the new free absorber resonance, the global displacement is lower compared to the blocked case. A summary of the experimental results is listed in Table 2.5. These promising results demonstrate that a metastructure can be effectively designed to suppress vibrations in all

three directions of excitation.

A comparison between finite element and experimental results for both blocked and free responses are listed in Table 2.6. While the trends for the expected peaks match quite well for all three excitation directions, there are some disparities between predicted and measured results, notably for the second split peaks in the free absorber system. This difference is most likely due to having chosen a single value for each of the material properties of VeroWhite. In reality, the manufacturer's website provides a range for material density and the material modulus and damping properties are frequency dependent due to the viscoelastic nature of the material [45]. With a more accurate material model, the discrepancies between predicted and experimental values are expected to decrease.

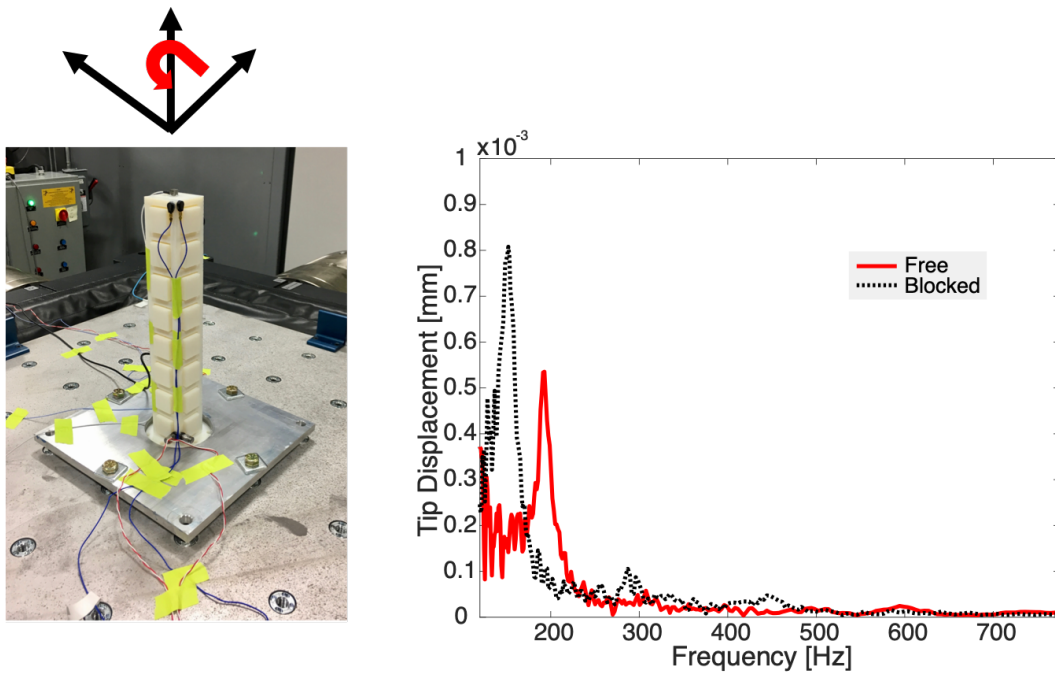


Figure 2.16: Torsional tip displacement for free and blocked configurations

2.3.3 Model Updating

Due to the large number of nodes used in the ANSYS mesh for the metastructure, it was necessary to create an analytical model to allow the acceleration of the design process and understand the

Table 2.5: Measured bandwidths and peak creation for the mechanical metamaterial beam

		Experimental Frequency [Hz]
Longitudinal	Blocked Beam Frequency	672
	Suppression Band	358
	Peak Gaps	240
Transverse	Blocked Beam Frequency	69
	Suppression Band	23
	Peak Gaps	15
Torsional	Blocked Beam Frequency	152
	New Frequency	40

Table 2.6: Finite element frequencies compared to experimental data for multi axis metastructure

Blocked Absorbers	ANSYS Model (Hz)	Experimental Data (Hz)	Error
Longitudinal	634	672	5.65%
Transverse	66	69	4.35%
Torsional	140	152	7.89%

Free Absorbers	ANSYS Model (Hz)		Experimental Data (Hz)		Error	
Longitudinal	355	805	370	914	4.05%	11.93%
Transverse	56	92	54	84	3.70%	9.52%
Torsional	192		193		0.52%	

effects of varying properties on the response of the structure. The absorbers were analytically modeled and compared to the ANSYS model for verification and the full free absorber system was analytically modeled and verified using the ANSYS model and experimental data.

Using a similar technique to the metastructure introduced in Section 2.2.3, the absorbers were modeled as distributed systems and the lumped mass and stiffnesses were used for the full Rayleigh-Ritz model of the metastructure. The absorber was modeled as a distributed cantilever beam with an attached tip mass. Coupling between the different directions was not included in the

model as it was not observed during the experimental testing.

2.3.3.1 Absorber Modeling

Each directional equation was derived using energy methods. Depending on the excitation directions, bending of the absorbers in the thick or thin directions can occur. For this reason, the natural frequencies and consequent lumped mass and stiffnesses were derived for both thick and thin bending scenarios.

Since the tip mass is large compared to the beam, the absorber energy equations include both the bending and rotational effects of the tip mass. These equations are given as:

$$T = \frac{1}{2} \int_0^{l_b} \rho A_b \dot{w}^2 dx + \frac{1}{2} M_m (w + ew')^2 + J_m w'^2 \quad (2.26)$$

$$U = \frac{1}{2} \int_0^{l_b} EI w''^2 dx \quad (2.27)$$

where w is the vertical displacement of the beam, l_b is the length of the cantilever beam, A_b is the cross sectional area of the beam, e is the eccentricity of the mass from the tip of the beam, J_m is the polar moment of inertia of the tip mass, E is the Young's modulus of the material, and I_b is the area moment of inertia of the beam.

The only difference between the vertical and horizontal excitation of the absorbers occurs in the area moment of inertia term. For vertical excitation, the equation is given as $I_b = \frac{1}{12} b_b h_b^3$ whereas the horizontal equation is $I_b = \frac{1}{12} h_b b_b^3$ where b_b is the thin dimension of the absorber beam, and h_b is the thick dimension of the absorber beam.

The area for the beam can be calculated as

$$A_b = b_b h_b \quad (2.28)$$

The polar moment of inertia is calculated for a rectangular tip mass about the end of the can-

the lever beam is given as

$$J_m = \frac{1}{12}M_m b_m^2 + \frac{1}{3}M_m l_m^2 \quad (2.29)$$

and the tip mass is found using

$$M_m = \rho b_m h_m l_m \quad (2.30)$$

Table 2.7: Summary of results comparing analytical model prediction to finite element predictions for absorber fundamental frequencies

Structure	Analytical Frequency (Hz)	FEM Frequency (Hz)	Error (%)
Thin Bending	75.01	76.91	3.65%
Thick Bending	431.81	396.6	8.88%

Lumped versions of the mass and stiffness for both absorber directions were obtained and are listed in Table 2.8.

Table 2.8: Equivalent mass and stiffness terms for absorber excitation directions

Direction	Parameter	Symbol	Value	Units
Thick Bending	Equivalent Mass	M_{eq1}	0.0991	kg
	Equivalent Stiffness	K_{eq1}	7.2916×10^5	N/m
Thin Bending	Equivalent Mass	M_{eq2}	0.0991	kg
	Equivalent Stiffness	K_{eq2}	2.4852×10^4	N/m

The value for the equivalent mass is the same for both excitation directions which follows the expectations based on the difference between the two directions only being in the potential energy term.

Using the lumped mass and stiffness terms for the absorbers, the natural frequencies of the full structure for the free absorber configuration can be obtained. Each degree of freedom is modeled

by using the energy equations and an assumed mode shape. The beam without absorbers is modeled initially and the absorbers are added into the model as four lumped masses at each absorber attachment location. Each absorber is the same equivalent mass and stiffness and therefore has the same natural frequency.

2.3.3.2 Free Configuration Mechanical Metamaterial Modeling

For each excitation direction, the model begins with the energy equations to get the full mass and stiffness matrices. Using the mass and stiffness matrices, the structural eigenvalue problem can be solved

$$(\mathbf{K} - \lambda\mathbf{M})[\mathbf{d}] = \mathbf{0} \quad (2.31)$$

where the natural frequencies, ω_r are calculated using the relation $\omega_r^2 = \lambda_r$. The mode shapes and shape functions can be determined from the eigenvectors of the system, \mathbf{d} .

Longitudinal Direction The energy equations for the entire system in the longitudinal direction are

$$T = \frac{1}{2} \int_0^L \rho A \dot{u}^2 dx + \frac{1}{2} \sum_{j=1}^N 4M_{eq1} \dot{u}(x_j)^2 \quad (2.32)$$

$$U = \frac{1}{2} \int_0^L EA u'^2 dx + \frac{1}{2} \sum_{j=1}^N 4K_{eq1} u(x_j)^2 \quad (2.33)$$

where ρ is the density, M_{eq1} is the equivalent absorber mass in the thick direction, E is the Young's modulus, K_{eq1} is the equivalent absorber stiffness in the thick direction, A is the cross sectional area of the beam, x_j is the location of the absorber along the length of the beam and u is the displacement in the longitudinal direction. The equivalent masses are multiplied by four since each location has four attached absorbers.

It is assumed that the beam extension can be expressed as the following convergent finite series

$$u = \sum_{i=1}^{N_u} U_r d_r \quad (2.34)$$

From these equations, the mass and stiffness matrices for the beams can be formulated.

The full mass matrix is given by

$$\mathbf{M} = \begin{bmatrix} \mathbf{M}^\alpha & \mathbf{M}^{\alpha\beta} \\ [\mathbf{M}^{\alpha\beta}]^T & \mathbf{M}^\beta \end{bmatrix} \quad (2.35)$$

where \mathbf{M}^α is the sub-matrix of beam deflections, \mathbf{M}^β is the sub-matrix of the absorbers at the β locations of the beam, and $\mathbf{M}^{\alpha\beta}$ is the sub-matrix coupling the beam and the absorber deflections.

The sub-matrices can be defined as

$$\mathbf{M}^\alpha = M_{rs}^\alpha = \left[\int_0^L \rho A U_r U_s dx + \sum_{i=1}^{N_a} M_i^\beta U_r(\beta_i) U_s(\beta_i) \right]_{N_u \times N_u} \quad (2.36)$$

$$\mathbf{M}^\beta = \text{diag} \left[M_1^\beta \quad M_2^\beta \quad \cdots \quad M_{N_\beta}^\beta \right]_{N_\beta \times N_\beta} \quad (2.37)$$

$$\mathbf{M}^{\alpha\beta} = M_{rj}^{\alpha\beta} = [M_j U_r(\beta_j)]_{N_u \times N_\beta} \quad (2.38)$$

Similarly, for the stiffness

$$\mathbf{K} = \begin{bmatrix} \mathbf{K}^\alpha & \mathbf{0} \\ \mathbf{0} & \mathbf{K}^\beta \end{bmatrix} \quad (2.39)$$

$$\mathbf{K}^\alpha = K_{rs}^\alpha = \left[\int_0^L E A U_r' U_s' dx + \sum_{j=1}^{N_\beta} k_j^\beta U_r(\beta_j) U_s(\beta_j) \right]_{N_u \times N_u} \quad (2.40)$$

$$\mathbf{K}^\beta = \text{diag} \left[k_1^\beta \quad k_2^\beta \quad \cdots \quad k_{N_\beta}^\beta \right]_{N_\beta \times N_\beta} \quad (2.41)$$

Transverse Direction The bending direction equations are

$$T = \frac{1}{2} \int_0^L \rho A \dot{u}^2 dx + \frac{1}{2} \sum_{j=1}^N 4M_{eq2} \dot{u}(x_j)^2 \quad (2.42)$$

$$U = \frac{1}{2} \int_0^L EI w''^2 dx + \frac{1}{2} \sum_{j=1}^N 4K_{eq2} w(x_j)^2 \quad (2.43)$$

where L is the length of the beam, M_{eq2} is the equivalent absorber mass in the thin direction, K_{eq2} is the equivalent absorber stiffness in the thin direction.

It is assumed that the beam bending can be expressed as the following convergent finite series

$$w = \sum_{i=1}^{N_u} W_r d_r \quad (2.44)$$

where W_r is the equation for the mode shape of a cantilever beam, d_r is a weighting term associated with each shape function, and N_w is the number of modes under consideration. Full mass and coupled stiffness matrices can be created by taking a partial derivative with respect to d and y and collecting coefficients.

$$\mathbf{M} = \begin{bmatrix} \mathbf{M}^\alpha & \mathbf{M}^{\alpha\beta} \\ [\mathbf{M}^{\alpha\beta}]^T & \mathbf{M}^\beta \end{bmatrix} \quad (2.45)$$

where M is the sub-matrix of beam deflections and M_β is the sub-matrix of the absorbers at the β locations of the beam.

The sub-matrices can be defined as

$$\mathbf{M}^\alpha = M_{rs}^\alpha = \left[\int_0^L m W_r W_s dx + \sum_{i=1}^{N_a} M_i^\beta W_r(\beta_i) W_s(\beta_i) \beta_i \right]_{N_w \times N_w} \quad (2.46)$$

$$\mathbf{M}^\beta = \text{diag} \left[M_1^\beta \quad M_2^\beta \quad \cdots \quad M_{N_\beta}^\beta \right]_{N_\beta \times N_\beta} \quad (2.47)$$

$$\mathbf{M}^{\alpha\beta} = M_{rj}^{\alpha\beta} = [-m_j W_r(\beta_j)]_{N_w \times N_\beta} \quad (2.48)$$

Similarly, for the stiffness

$$\mathbf{K} = \begin{bmatrix} \mathbf{K}^\alpha & \mathbf{0} \\ \mathbf{0} & \mathbf{K}^\beta \end{bmatrix} \quad (2.49)$$

$$\mathbf{K}^\alpha = K_{rs}^\alpha = \left[\int_0^L EI W_r'' W_s'' dx + \sum_{j=1}^{N_\beta} k_j^\beta W_r(\beta_j) W_s(\beta_j) \right]_{N_w \times N_w} \quad (2.50)$$

$$\mathbf{K}^\beta = \text{diag} \left[k_1^\beta \quad k_2^\beta \quad \cdots \quad k_{N_\beta}^\beta \right]_{N_\beta \times N_\beta} \quad (2.51)$$

Torsional Direction The torsional equations are

$$T = \frac{1}{2} \int_0^L \rho J \dot{\Theta}^2 dx + \frac{1}{2} \sum_{j=1}^N 4M_{eq2} \dot{\Theta}(x_j)^2 \quad (2.52)$$

$$U = \frac{1}{2} \int_0^L G J \Theta'^2 dx + \frac{1}{2} \sum_{j=1}^N 4K_{eq2} \Theta(x_j)^2 \quad (2.53)$$

where G is the shear modulus of the material calculated as

$$G = \frac{E}{2(1 + \nu)} \quad (2.54)$$

θ is the angle of twist, and ν is the Poisson's ratio of the material. The equivalent mass and stiffness in the thin bending direction is also used for the torsional case due to the direction of absorber vibration under the full beam in torsion.

It is assumed that the beam twist can be expressed as the following convergent finite series

$$\theta = \sum_{i=1}^{N_u} \Theta_r d_r \quad (2.55)$$

The mass and stiffness matrices can be found from the energy equations

The sub-matrices can be defined as

$$\mathbf{M}^\alpha = M_{rs}^\alpha = \left[\int_0^L \rho J \Theta_r \Theta_s dx + \sum_{i=1}^{N_a} M_i^\alpha \Theta_r(\alpha_i) \Theta_s(\alpha_i) \right]_{N_\theta \times N_\theta} \quad (2.56)$$

$$\mathbf{M}^\beta = \text{diag} \left[M_1^\beta \quad M_2^\beta \quad \cdots \quad M_{N_\beta}^\beta \right]_{N_\beta \times N_\beta} \quad (2.57)$$

$$\mathbf{M}^{\alpha\beta} = M_{rj}^{\alpha\beta} = [M_j \Theta_r(\beta_j)]_{N_\theta \times N_\beta} \quad (2.58)$$

Similarly, for the stiffness

$$\mathbf{K} = \begin{bmatrix} \mathbf{K}^\alpha & \mathbf{0} \\ \mathbf{0} & \mathbf{K}^\beta \end{bmatrix} \quad (2.59)$$

$$\mathbf{K}^\alpha = K_{rs}^\alpha = \left[\int_0^L G J \Theta_r' \Theta_s' dx + \sum_{j=1}^{N_\beta} k_j^\beta \Theta_r(\beta_j) \Theta_s(\beta_j) \right]_{N_\theta \times N_\theta} \quad (2.60)$$

$$\mathbf{K}^\beta = \text{diag} \left[k_1^\beta \quad k_2^\beta \quad \cdots \quad k_{N_\beta}^\beta \right]_{N_\beta \times N_\beta} \quad (2.61)$$

where both \mathbf{M} and \mathbf{K} are square matrices with rows and columns of dimensions of $N_\theta + N_\beta$.

To calculate the variation of the beam properties along the length, the Heaviside function was used for each type of excitation (assuming material properties are the same for the entire beam).

The mass and stiffness equations across one representative section are

$$m(x) = \rho \{A_{solid} [H(x_1) - H(x - x_1)] + A_{hollow} [H(x - x_1) - H(x - x_2)]\} \quad (2.62)$$

$$EA(x) = E \{A_{solid} [H(x_1) - H(x - x_1)] + A_{hollow} [H(x - x_1) - H(x - x_2)]\} \quad (2.63)$$

$$EI(x) = E \{I_{solid} [H(x_1) - H(x - x_1)] + I_{hollow} [H(x - x_1) - H(x - x_2)]\} \quad (2.64)$$

$$GJ(x) = G \{J_{solid} [H(x_1) - H(x - x_1)] + J_{hollow} [H(x - x_1) - H(x - x_2)]\} \quad (2.65)$$

$$\rho J(x) = \rho \{J_{solid} [H(x_1) - H(x - x_1)] + J_{hollow} [H(x - x_1) - H(x - x_2)]\} \quad (2.66)$$

2.3.3.3 Frequency Resonse

Figures 2.17 and 2.18 display the frequency responses for the tip displacement of the main beams for the analytical and finite models for comparison with the experimental data. Results show that both the analytical and finite element models are able to capture the natural frequencies of the dynamically vibrating coupled beam absorber system in both the longitudinal and transverse directions with a maximum error of 12%. Because the finite element model is a full three-dimensional numerical simulation, the time to obtain the results is much greater than the analytical Rayleigh-Ritz model. The results from these calculations show that the Rayleigh-Ritz method is an effective

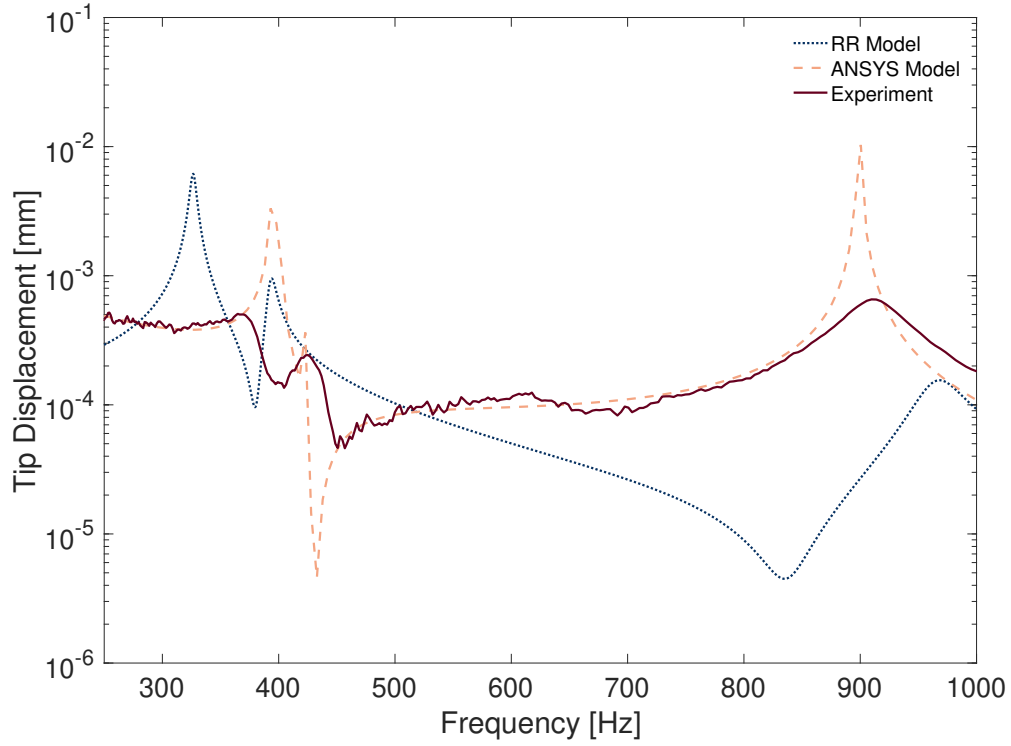


Figure 2.17: Comparison of modeling and experimental tip displacement under excitation in the longitudinal direction

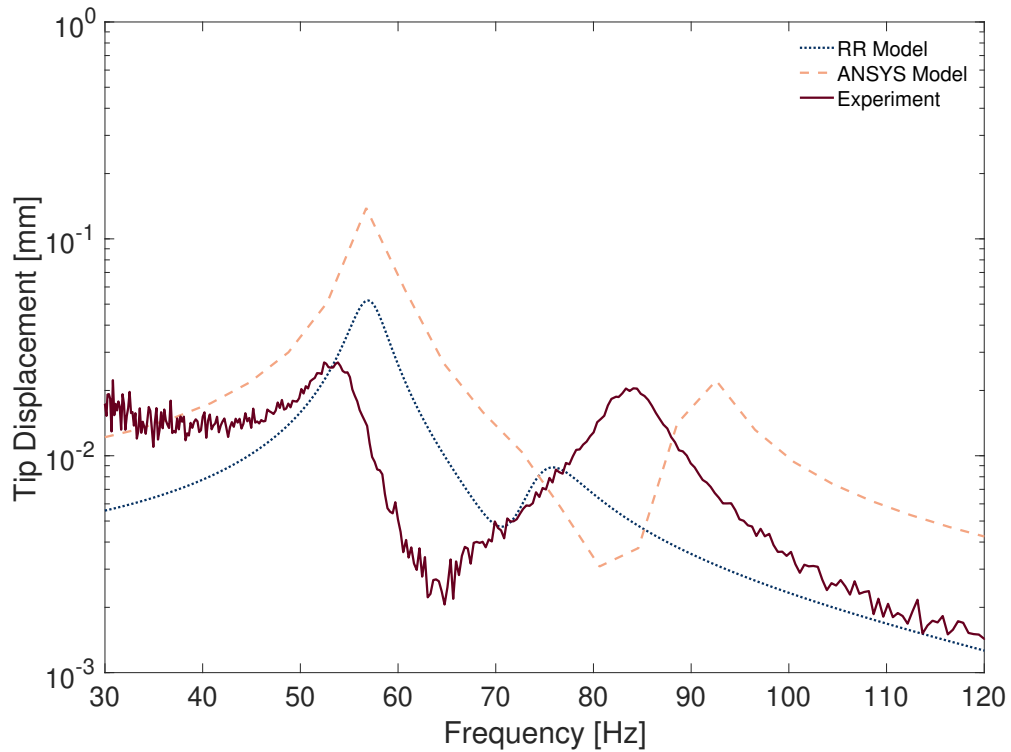


Figure 2.18: Comparison of modeling and experimental tip displacement under excitation in the transverse direction

tool for preliminary design. A summary of these results are provided in Table 2.9.

Table 2.9: Summary of results comparing analytical model predictions to finite element predictions and experimental results for full multi axis beam

Free Absorbers	Analytical Frequency (Hz)		FEM Frequency (Hz)		Experimental Frequency (Hz)		Analytical Error		FEM Error	
Longitudinal	326	966	355	805	370	914	11.90%	5.59%	4.05%	11.93%
Transverse	57	75	56	92	54	84	5.56%	10.7%	3.70%	9.52%
Torsional	150		192		193		22.3%		0.52%	

2.4 Structure Design Considerations and Limitations

The main considerations when designing a mechanical metamaterial in this configuration are the geometry of the absorbers, the geometry of the beam, and the location of the absorbers.

Changing the natural frequency of the absorber can be accomplished most effectively by altering the absorber beam length or the tip mass. The analogue of this absorber in traditional 1DOF lumped mass systems would be altering the spring or the mass of the absorber. By changing these parameters, the natural frequency of the absorber can be tuned to the frequency of the main structure and therefore the bandwidth of the overall design in the free configuration can be adjusted.

Within this absorber design space, considerations for material properties as well as main absorber geometries have to be taken into account which is further investigated in Chapter III. If the length of the absorber beam or the tip mass is increased, the overall frequency of the absorber will decrease, however the choice material for the structure will need to support the mass at the additional length. Furthermore, if the length of the beam is extended, the absorbers will be more exposed on the outside of the main structure, creating a higher likelihood of impacts or other jostling to break them.

The main structure is also open to geometrics and material changes. Changes in the overall length of the structure have a great impact on whether the absorbers can be tuned to the correct

natural frequencies, particularly in the transverse excitation direction. The frequency of a cantilever beam is inversely proportional to the length, therefore as the main structure increases in length, the transverse natural frequency decreases. In order to account for this decrease in natural frequency, the absorbers must also increase in length. Since the absorbers are much thinner and shorter than the main beam, it becomes difficult to tune the absorbers to the appropriate frequency without a large tip mass. The ability to match the absorber frequencies with the transverse natural frequency of the main structure then becomes dependent on the available space and the material properties of the absorber.

This work used additive manufacturing to create the investigated metastructure. This type of rapid prototyping provides multiple benefits over traditional machining. Using traditional machining for this system would require the main beam to be fabricated separately and the absorbers attached later. With additive manufacturing techniques, the absorbers and main beam can be created as a single structure. While this structure is printed out of a stiff polymer material, additional damping can be incorporated using materials with higher viscoelastic effects. Advances in metal additive manufacturing printers could enable the incorporation of absorbers into commonly seen structures in the aerospace and automotive industries.

While additive manufacturing technology has rapidly improved over the short time since its invention, there are currently limited materials available for printing as well as limitations on the devices print bed size. The print bed limitations introduce additional issues caused by available print direction. The structure may need to be rotated to fit within the space limitations as was the case with the multi axis mechanical metamaterial, or if the structure is too large to fit into the print bed size, it must either be fabricated separately and adhered together as in the case of the chiral lattice (shown in in Chapter III).

As mentioned in [46], homogeneity of material is proving to be an issue in current 3D printing technology. Designs have a wide range and variability of material Young's modulus as well as other parameters between printed parts and in a single printed part. Even with the help of support material to keep the printed part from deviation from the design shape, there will still be non-negligible

errors introduced in the printing process due to sagging. Variability needs to be minimized before accurate enough models can be made to implement these structures in existing designs.

2.5 Summary

This chapter presents the passive vibration control concept of a mechanical metamaterial made from a material with low material damping to demonstrate the validity of the metastructure concept without additional influence from material properties. The absorber geometries were based on a previous zigzag design that allows for a larger range of achievable natural frequencies while still maintaining a compact footprint. An analytical zigzag model and experimental validation were presented and incorporated into a full metastructure analytical model with finite element verification.

A second metastructure design was presented that incorporated absorption for excitation in multiple degrees of freedom. Experimentally validated finite element and analytical models were presented comparing the structure with blocked absorbers to free absorbers to achieve vibration reduction bandwidths of 358 Hz in the longitudinal direction, 24 Hz in the transverse direction, and a resonance creation 40 Hz higher in the torsional direction. These promising results create the first multi axis metastructure capable of reducing vibration in three excitation directions.

Because the multi axis metastructure as well as an increasing number of mechanical metamaterials are created using additive manufacturing, a discussion of the current additive manufacturing limitations is included and an investigation into the important design parameters is presented.

CHAPTER III

Damping vs. Absorption in Mechanical Metamaterials

3.1 Overview

This chapter demonstrates the need to consider both the geometry and material selection in metastructure design. Metastructure systems are often created for a specific use case and the geometries are optimized with a chosen material without considering the tradeoffs between optimizing the design and the effect of material damping. An investigation into these tradeoffs is conducted in this chapter. First, an experimental proof of concept is introduced by comparing the vibrations of two mass conserved structures - one being a mechanical metamaterial with a designed geometry and one with a solid mass in place of the geometric design. This experiment demonstrates there are cases where the material damping outperforms geometric design for reduction of broadband global vibration. Next, the dynamic stiffness, a way to separate the modal parameters and visualize their individual influence on the structural response is presented. A further visualization technique called a Vincent plot is described which shows the minimum achievable deflection of the system with variation of modal parameters. Finally, these techniques are applied to the multi axis mechanical metamaterial, and recommendations are made for further design improvements.

3.2 Motivating Experiment

A specific system where the discrepancies in the global vibration of a geometrically designed and a heavily damped structure can be seen is in a structure similar to the one first presented in a paper by Baravelli and Ruzzene [47]. This metastructure was initially designed and tuned to reduce the global vibration of the structure. A recreation of a similar periodic chiral lattice structure detailed in Inman et. al. [48] was fabricated using an aluminum frame, a 3D printed TangoPlus lattice structure, and milled steel masses. An additional structure was created using an identical aluminum frame with the same dimensions and a solid mass printed out of the same material as the lattice in the original structure. To better compare results between the two structures, the solid beam was created with the same mass as the chiral lattice structure. This was accomplished by reducing the thickness of the solid insert from the original design thickness of 19.05 mm to 13.90 mm.



Figure 3.1: Periodic chiral lattice (top) and solid structure (bottom)

The outer frames were cut from a solid plate of 6061 aluminum using a waterjet cutter. Both viscoelastic inserts were fabricated from TangoPlus using a Stratasys Objet Connex 500 3D printer. Each insert was printed in two parts to fit on the 3D printer bed. The inserts were then glued

together using Alteco Ace-D cyanoacrylate adhesive and affixed to the aluminum frame using 3M Scotch-Weld DP460 epoxy adhesive. Annular masses for the lattice insert were milled from 12L14 steel bar stock to the correct sizes to fit into the chiral nodes. Dimensions of the beams and annular masses were taken from the designs detailed in [48]. A photograph of the fabricated beams can be seen in Figure 3.1.

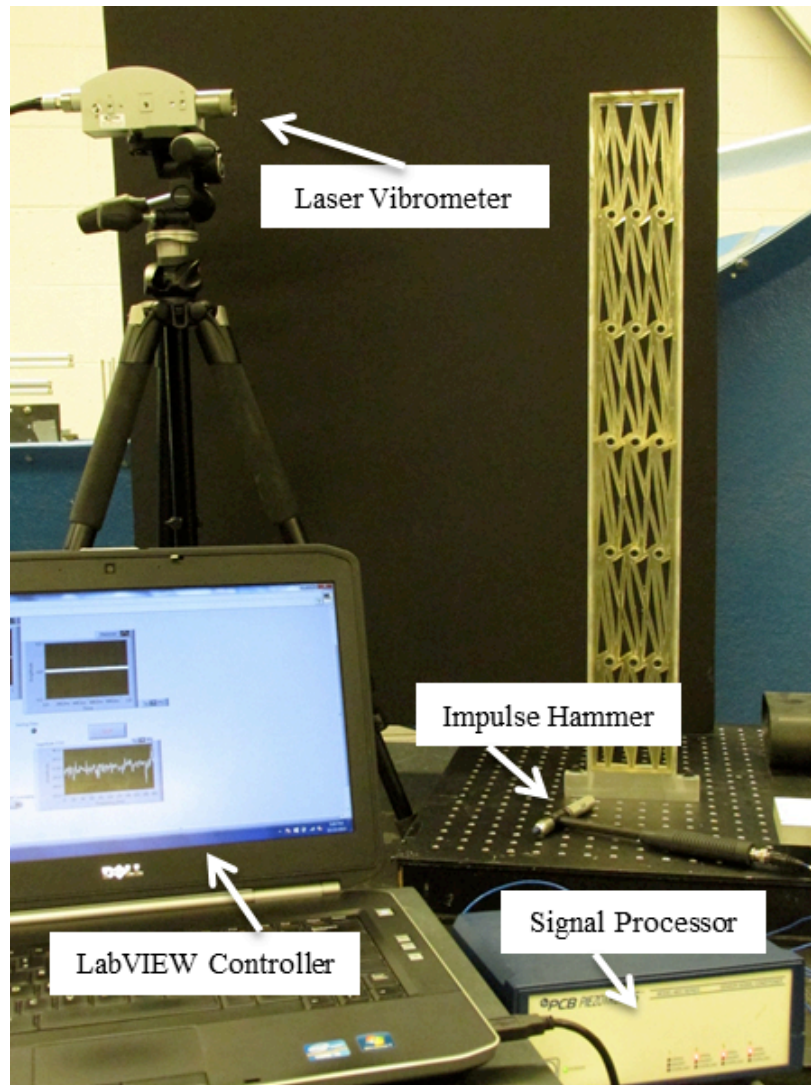


Figure 3.2: Experimental hammer setup for impact testing

The setup to determine the frequency response of the beams is shown in Figure 3.2. The base was clamped to an optical table to create fixed-free boundary conditions and both solid and lattice experiments used a PCB 086C01 impact hammer to excite the structures. Velocity data was

collected using a Polytech OFV-534 laser vibrometer and a Polytech OFV-5000 laser vibrometer controller. LabVIEW was used with National Instruments data acquisition hardware to collect and display real time data at a rate of 20 kHz on a PC laptop. The impact hammer and laser vibrometer data were saved to a file for data reduction.

Both solid and lattice frame and assembly data were obtained by impacting the frame 10.5 cm from the base. The velocity data was collected at the free end of the beam opposite the impact side. Velocity data was converted to displacement and the experimental results for both structures are plotted in Figure 3.3. While both structures can achieve small magnitude displacements, it can clearly be seen that the solid structure outperforms the chiral lattice when considering maximum magnitude. Viewing both plots together demonstrates a specific scenario in metastructure design where inherent damping in material choice overpowers the geometric design. This experiment leads to the question of whether there exists a dividing line between material choice and geometric design for metastructures.

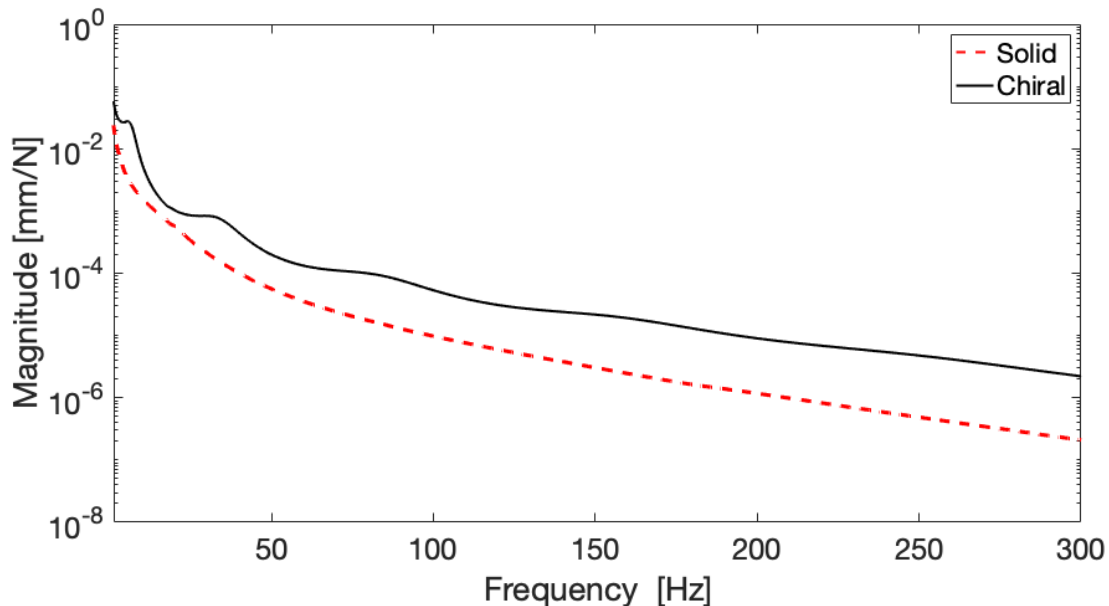


Figure 3.3: Experimental impact data for lattice and solid metastructures

3.3 Modal Parameter Consideration

As seen in the equations for both simple and complex structures - the modal parameters of mass, stiffness, and damping are interdependent. This leads to difficulties in determining which parameter has the greatest influence on the structural design. Viewing the responses in terms of dynamic stiffnesses and using Vincent plots allows further insight into the effect of the varying design parameters on the structural response.

3.3.1 Receptance and Dynamic Stiffness

A common representation of the frequency response of a system is the receptance method, defined as a complex harmonic displacement at one point due to a harmonic force at another point [49]. The equation for the harmonic receptance between two points on a structure denoted as r and s is given as [50]

$$\alpha_{rs} = \frac{X_r e^{i\omega t}}{F_s e^{i\omega t}} = \frac{X_r}{F_s} \quad (3.1)$$

where $X_r e^{i\omega t}$ is the complex steady-state response at location r with respect to $F_s e^{i\omega t}$, the harmonic exciting force at location s .

The dynamic stiffness, DS_{sr} , is the complex harmonic force at one point required to produce a harmonic displacement at another point. It is the inverse of the receptance and can be written as

$$DS_{sr} = \frac{1}{\alpha_{rs}} \quad (3.2)$$

The frequency response in the form of receptance depends on all three interconnected modal components - system mass, stiffness, and damping. This makes it difficult to easily see which parameter dominates the frequency response of the system. By plotting the dynamic stiffness, or the reciprocal of the receptance, the influence of various modal parameters can be obtained. The real component is influenced only by the mass and stiffness parameters, and the imaginary

component only depends on the damping parameter [51].

In terms of modal parameters, the receptance can be written as

$$\alpha = \frac{1}{(K_j - \omega^2 M_j + i\omega C_j)} \quad (3.3)$$

therefore, the modal dynamic stiffness, ds_j is

$$ds_j = K_j - \omega^2 M_j + i\omega C_j \quad (3.4)$$

Using the expression for harmonic displacement, the general complex receptance is written as

$$\alpha_{rs} = \sum_{j=1}^{\infty} \Phi_j(x_s) \Phi_j(x_r) \alpha_j = \sum_{j=1}^{\infty} \alpha_{j,rs} \quad (3.5)$$

where Φ_j is the mode shape of the j th mode, x_r and x_s are the position coordinates, and $\alpha_{j,rs}$ is the receptance at location r due to an input at location s for the j mode.

Based on Equation (3.1), the modal dynamic stiffness is

$$DS_{rs} = \frac{1}{\alpha_{rs}} = \frac{1}{\sum_{j=1}^{\infty} \frac{\Phi_j(x_r) \Phi_j(x_s)}{ds_j}} \quad (3.6)$$

which can also be represented as

$$\frac{1}{DS_{rs}} = \frac{\Phi_1(x_r) \Phi_1(x_s)}{ds_1} + \frac{\Phi_2(x_r) \Phi_2(x_s)}{ds_2} + \dots = \sum_{j=1}^{\infty} \frac{\Phi_j(x_r) \Phi_j(x_s)}{ds_j} \quad (3.7)$$

demonstrating that the principle of superposition can be applied to find the total dynamic stiffness of a system by summing the dynamic stiffness of its individual modal components [49].

When looking at the dynamic stiffness plots, shown for the longitudinal excitation of the multi axis mechanical metamaterial in Figure 3.10, the real part can be either positive or negative corresponding to whether the system is more influenced by the stiffness or the mass parameter. If the real part of the dynamic stiffness is positive, the system behavior is more influenced by the stiffness modal parameter. A negative real part is more affected by the changing of the mass parameter. The

imaginary part is always positive, and a larger imaginary component implies a larger displacement resistance from the damping parameter [49].

The real part of the dynamic stiffness always changes sign near or at a resonance or anti resonance frequency. In lower frequencies, the system is always positive below each resonance meaning it is most affected by changes in stiffness and damping. Above each resonance it is negative, corresponding to being more influenced by changes in mass and damping. When a structure is excited close to its natural frequency, it behaves as a pure damper and is only influenced by the damping coefficient.

3.3.2 Vincent Plots

Designing a structure with multiple dependent components has been made easier with the advances in finite element and optimization software, however, it is still beneficial to be able to quickly visualize the parameter effects in a design without running costly simulations. In 1973, A.H. Vincent found that if an auxiliary system (or absorber) is attached to a main structure, the response of the structure maps out a circle in the complex plane. The closer to the origin the displacement is, the lower the response at that frequency. These Vincent plots can then be used to visualize the effect on the receptance response caused by changing absorber parameters [52, 53].

By looking at the dynamic stiffness of the structure response, a frequency can be chosen either above or below the resonance frequency and auxiliary modal parameters can be altered to minimize the response of the full structure.

3.4 2-DOF Structure

Before looking at a more complicated system, will first consider a simple 2DOF absorber system to find general trends in the frequency response plots between mass conserved heavily damped systems and systems with stiffness tuned absorbers. These insights can be used to determine preliminary trends in the data which can then be further investigated on the previously presented

multi axis system.

This exploration will use the H_∞ criterion, also called the H_∞ norm, which in this case is the maximum amplitude magnification factor for the primary system. Since sinusoidally excited systems experience their peak amplification factor at the natural frequency of the system, lowering this value would lead to an improvement in the performance of the structure [54].

This formulation considers a lumped mass two degree of freedom system experiencing sinusoidal force excitation. Figure 3.4a shows this system with Voigt damping only on the absorber and Figure 3.4b includes damping on both masses.

The mass, stiffness, and damping coefficients of the primary system are, m_1 , k_1 , and c_1 , respectively, while the corresponding absorber coefficients are m_2 , k_2 , and c_2 .

The dimensionless amplitude of the steady state response of the primary system can be written as [54, 55]

$$H_\infty = A = \left| \frac{x_1 k_1}{f_0} \right| = \sqrt{\frac{A_1^2 + B_1^2}{C^2 + D^2}} \quad (3.8)$$

where

$$\begin{aligned} A_1 &= \beta^2 - r^2 \\ B_1 &= 2\beta r \zeta_2 \\ C &= \beta^2 - [1 + 4\beta \zeta_1 \zeta_2 + (1 + \mu)\beta^2]r^2 + r^4 \\ D &= 2r\{(\beta^2 - r^2)\zeta_1 + \beta[1 - (1 + \mu)r^2]\zeta_2\} \end{aligned} \quad (3.9)$$

The steady state response depends on five dimensionless constants

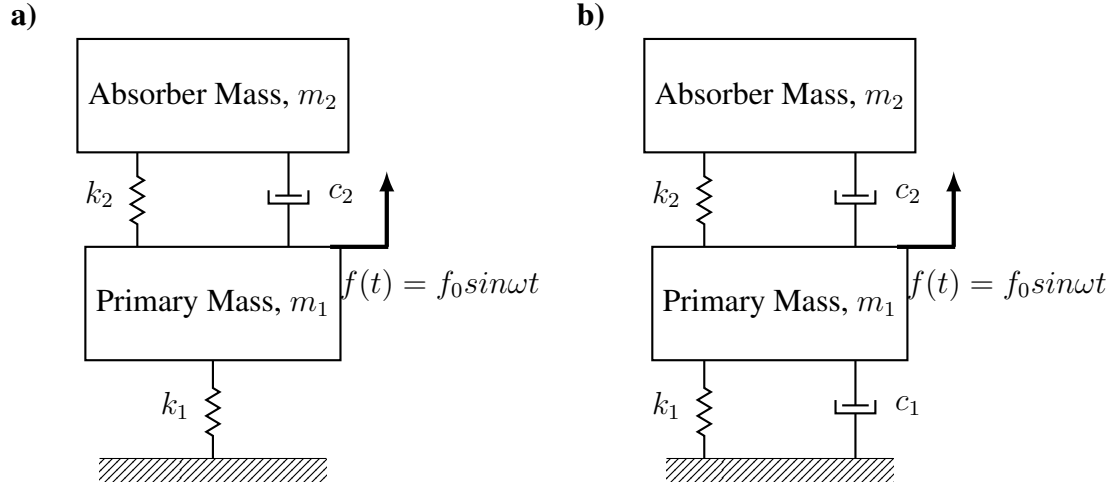


Figure 3.4: Two degree of freedom lumped mass system with sinusoidal force excitation a) absorber damping only b) damping on both masses

$$\begin{aligned}
 \mu &= \frac{m_2}{m_1} : \text{mass ratio} \\
 \beta &= \frac{\omega_2}{\omega_1} : \text{natural frequency ratio} \\
 r &= \frac{\omega}{\omega_1} : \text{forced frequency ratio} \\
 \zeta_1 &= \frac{c_1}{(2m_1\omega_1)} : \text{primary damping ratio} \\
 \zeta_2 &= \frac{c_2}{(2m_2\omega_2)} : \text{absorber damping ratio}
 \end{aligned} \tag{3.10}$$

where the natural frequencies of the primary system and the absorber are, respectively

$$\begin{aligned}
 \omega_1 &= \sqrt{\frac{k_1}{m_1}} \\
 \omega_2 &= \sqrt{\frac{k_2}{m_2}}
 \end{aligned} \tag{3.11}$$

Two cases are considered for modeling. Case 1 considers varying geometry by changing only the absorber stiffness, k_2 , and holding all other variables constant. Case 2 considers varying material damping by changing only the absorber damping coefficient, c_2 . For both cases a constant mass ratio, μ , is set at 0.25.

3.4.1 Case 1: Optimal Absorber Damping

This case uses an optimal absorber damping and varies the absorber stiffness in the form of the natural frequency ratio, β , to model a changing absorber geometry. Since the primary system natural frequency and mass ratio are constants, varying the natural frequency ratio effectively alters only k_2 . While the absorber stiffness varies, the absorber damping ratio is set to the approximate optimal value of a two degree of freedom spring mass damping system [18]

$$\zeta_{2opt} \approx \sqrt{\frac{3\mu}{8(1+\mu)}} \quad (3.12)$$

3.4.2 Case 2: Optimal Absorber Stiffness

The absorber damping ratio has been defined previously as $\zeta_2 = \frac{c_2}{(2m_2\omega_2)}$. Because the absorber mass and stiffness (and therefore the absorber natural frequency) is kept constant, varying the damping absorber ratio effectively only alters c_2 .

The constant natural frequency ratio for this case is again set to the approximate optimal value [18]

$$\beta_{opt} \approx \frac{1}{1+\mu} \quad (3.13)$$

Both cases are modeled first considering a primary damping ratio of zero as seen in Figure 3.4a. For a metal primary structure, the damping term is often neglected due to low internal damping of the material [55]. Primary structure materials with non-trivial damping are then considered.

3.4.3 Primary Structure with Negligible Internal Damping, $\zeta_1 = 0$

Figure 3.5 plots the minimum H_∞ norm vs. the forced frequency ratio for both the varied absorber stiffness and absorber damping coefficient. This minimum value H_∞ is the minimum possible primary mass vibration amplitude over the frequency range. The Case 2 system outperforms the Case 1 system for frequencies of $0.741 \leq r \leq 0.987$ which are near the natural frequency of the

main absorber system. Viewing this plot in the context of the surface plot shown in Figure 3.6, the minimum obtainable H_∞ values near the natural frequency of the main system are when the damping ratio is lower. This suggests that a tuned vibration absorber will attenuate the vibration of the main system better near the natural frequency of the main system. Altering the initial constants chosen for the model causes a shift in this performance range.

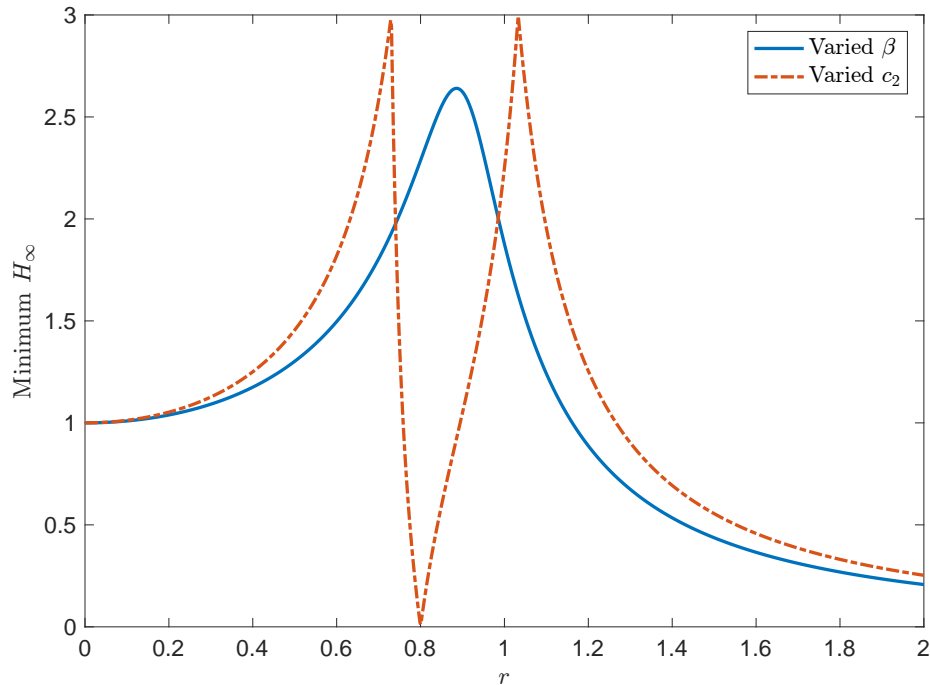


Figure 3.5: Minimum H_∞ norm vs. forced frequency ratio for $\zeta_1 = 0$

3.4.4 Primary Structure with Internal Damping, $\zeta_1 \neq 0$

For lower primary mass damping ratios, the trends are similar to the undamped primary mass with shifting intersection points between the minimum norm values for each case. Figure 3.7 shows these trends for primary damping ratios of $\zeta_1 = 0$, $\zeta_1 = 0.05$, and $\zeta_1 = 0.1$.

Figure 3.8 displays the minimum H_∞ norm vs. forced frequency ratio for higher primary system damping ratios. This plot demonstrates how large of an effect the primary damping ratio has on the vibration amplitude of the primary mass. For $\zeta_1 = 0$ and $\zeta_1 = 1$, the optimal absorber stiffness case still shows benefits compared to the optimal absorber damping case. Once the primary

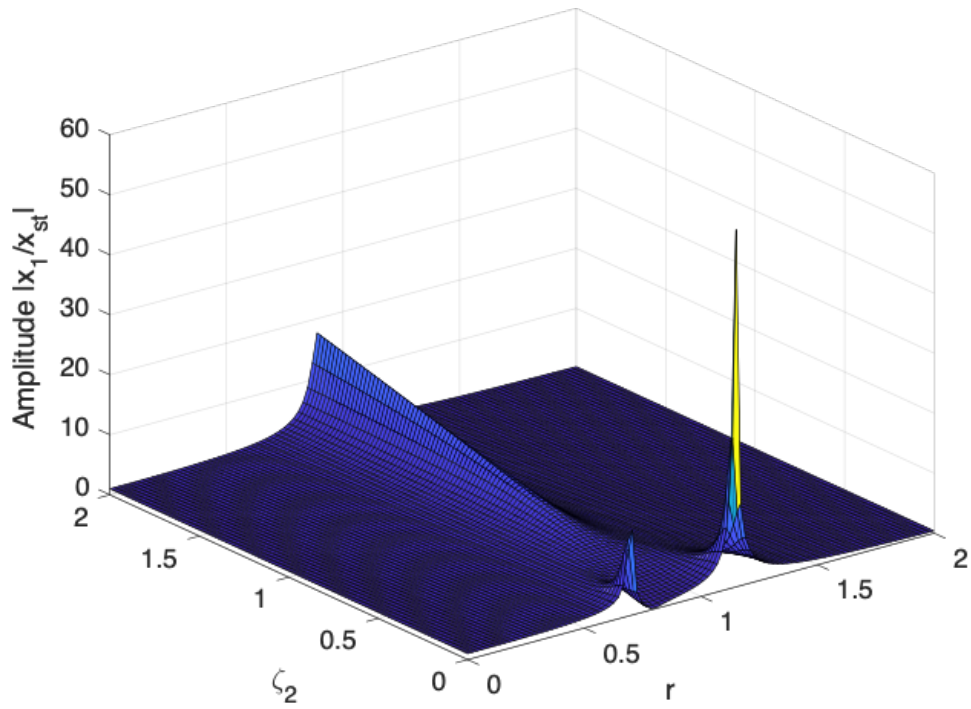


Figure 3.6: Amplitude as a function of varied absorber damping ratio and natural frequency ratio

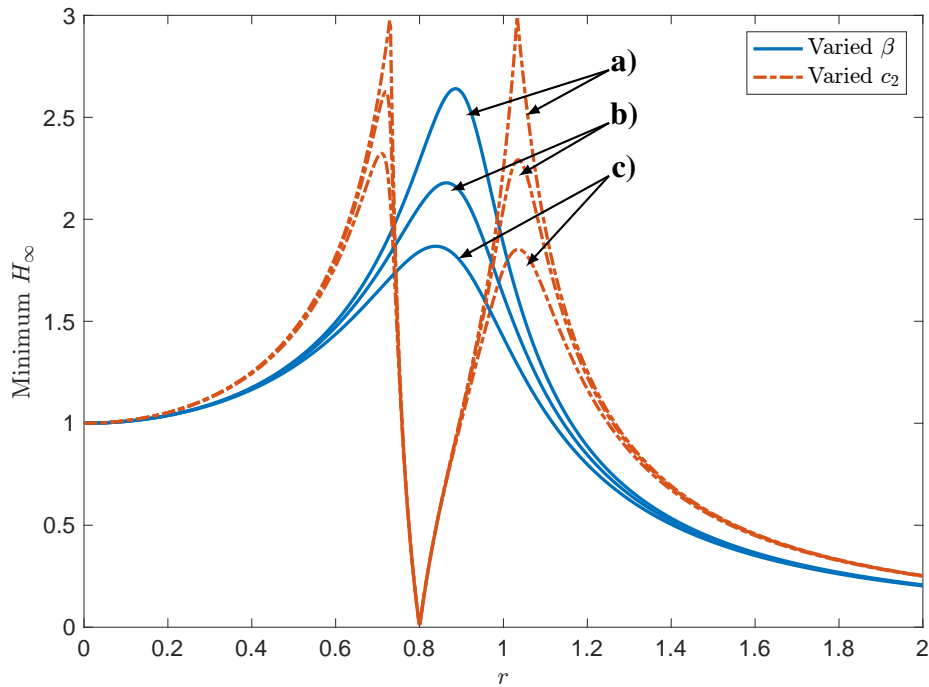


Figure 3.7: Minimum H_∞ norm vs. forced frequency ratio for a) $\zeta_1 = 0$, b) $\zeta_1 = 0.05$, c) $\zeta_1 = 0.1$

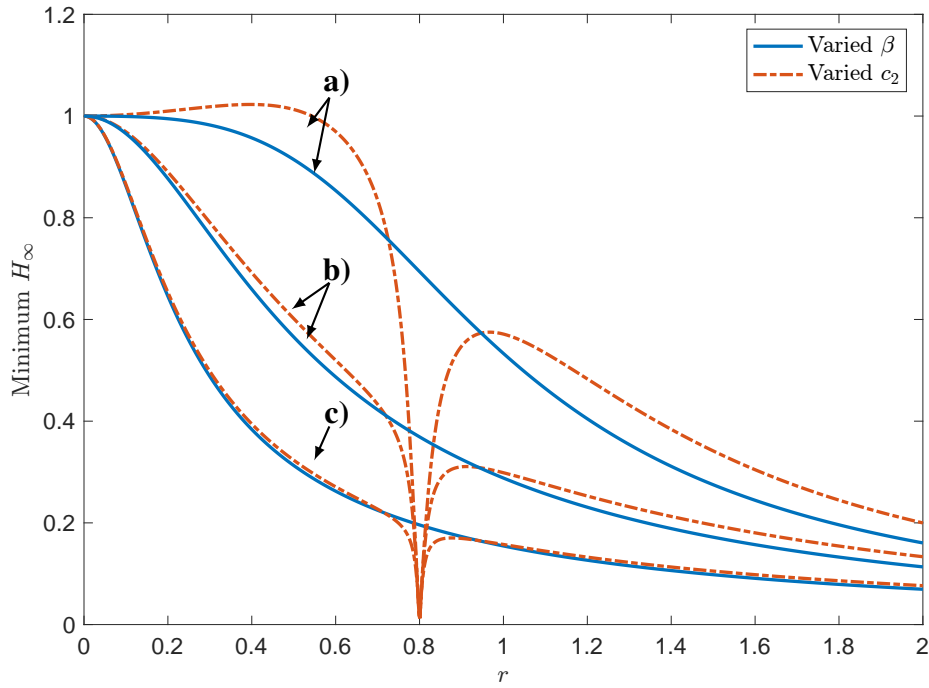


Figure 3.8: Minimum H_∞ norm vs. forced frequency ratio for a) $\zeta_1 = 0.7$, b) $\zeta_1 = 1.5$, c) $\zeta_1 = 3$

damping ratio reaches 3, however, the effect of the primary damping ratio overpowers the varying absorber parameters. If the primary structure has a high damping ratio, the minimum vibration amplitude of the primary mass becomes similar for both changing absorber geometry and material, with the change in material outperforming the change in geometry.

3.5 Multi Degree of Freedom Excitation

Expanding on the two degree of freedom system, we can look at the multi axis metastructure system to determine the effects of damping compared with the addition of absorbers. In this section, alterations to damping coefficients of both the main beam and the absorber systems are considered, and recommendations on general metastructure design are provided. Further design considerations are then introduced for a metastructure system with absorbers and potential improvements to the current multi axis metastructure design are presented.

3.5.1 Vibration Reduction Through Damping

Similar to the analysis in Section 3.4, the multi axis excitation system is considered for varied damping in both the main beam and the absorbers using the analysis presented in Chapter II. Figure 3.9 plots two results for each case to show a representative effect on the frequency response at different damping levels in both the blocked and free configuration. For this analysis, the absorbers in the free excitation are tuned to the experimental design with the total mass being conserved between both the blocked and free cases. The blocked cases demonstrate the change in frequency response when the main beam damping ratio is altered while the free cases alter the absorber damping ratio.

As seen in Figure 3.9, the maximum vibration amplitude is reduced in both the free and the blocked response when the damping ratio is increased. The increased damping ratio of the blocked response has a lower global vibration amplitude than the free response, however it is unable to achieve the reduction in the displacement seen in the response of the lower damping of the free absorbers. This is due to the superior vibration reduction of tuned absorbers in the narrow range of the tuned frequency. This suggests that for a system where the excitation frequency is known or where a specific frequency is determined undesirable, it is more beneficial from a displacement reduction standpoint to tune absorbers to this frequency instead of adding system damping.

Alternatively, if the system excitation is varying or broadband, increased damping provides a lower global displacement over a broader frequency range suggesting that for this excitation scenario, increasing material damping outperforms absorber tuning.

3.5.2 Vibration Reduction Through Absorber Tuning

When the frequency of excitation is known, or the addition of damping is infeasible, additional considerations can be made to lower the structural displacement.

The results of the transverse and longitudinal multi axis metastructure are displayed in Figure 3.10 and Figure 3.14 respectively. They both display the expected trends of the dynamic stiffness results with a positive real value below the resonance frequency indicating this region is

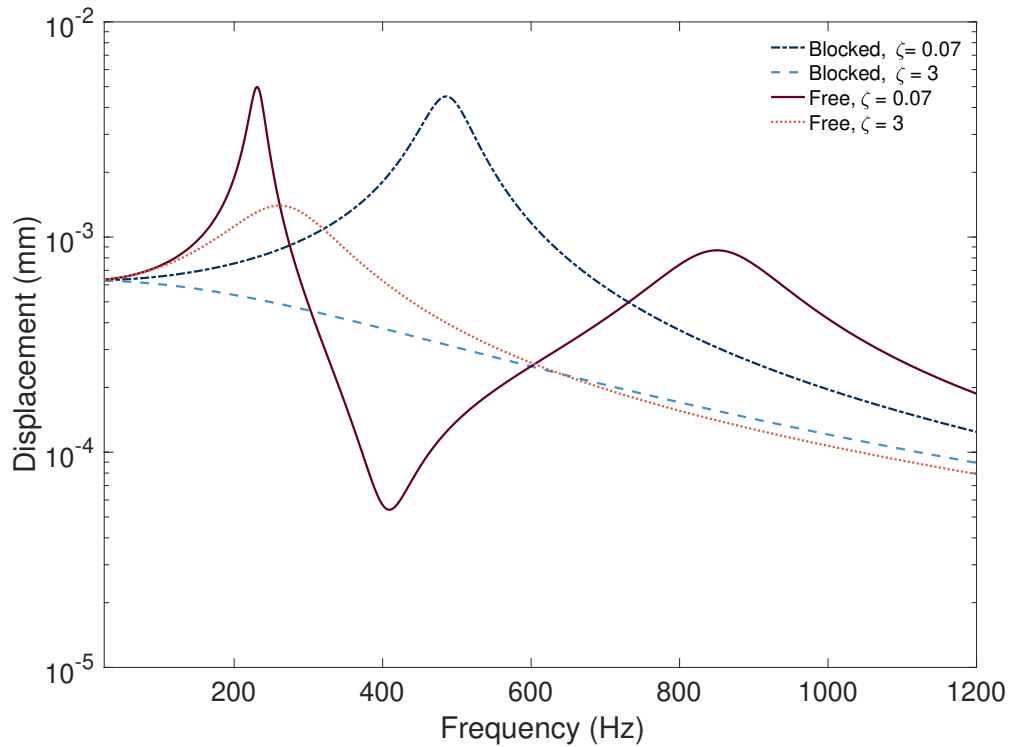


Figure 3.9: Comparing vibration reduction through damping - longitudinal excitation

controlled by stiffness and damping changes, and a negative real value above the resonance frequency meaning the response is more influenced by changes in the mass and damping values. The imaginary plots are both positive as expected and are influenced solely by damping in a region close to the resonance frequency.

Figure 3.11 and 3.15 show the Vincent plots for frequencies slightly above and below the blocked resonance frequency for each excitation direction. Each plot has the circular shape expected in Vincent plots. For the frequencies slightly below the blocked resonance, an addition of stiffness in the absorbers initially moves the plot closer to the origin while in the plots slightly above the resonance frequency, an addition of mass moves closer to the origin instead.

As can be seen in the longitudinal Vincent plot shown in Figure 3.11 and more closely in the right plot in Figure 3.12, the experimental design point is quite close to the origin already, demonstrating that this design would be effective for a minimal displacement in the longitudinal excitation direction. In Figure 3.15, the experimental design is slightly to the right of the origin showing that this is not the minimum obtainable displacement for the structure in the transverse

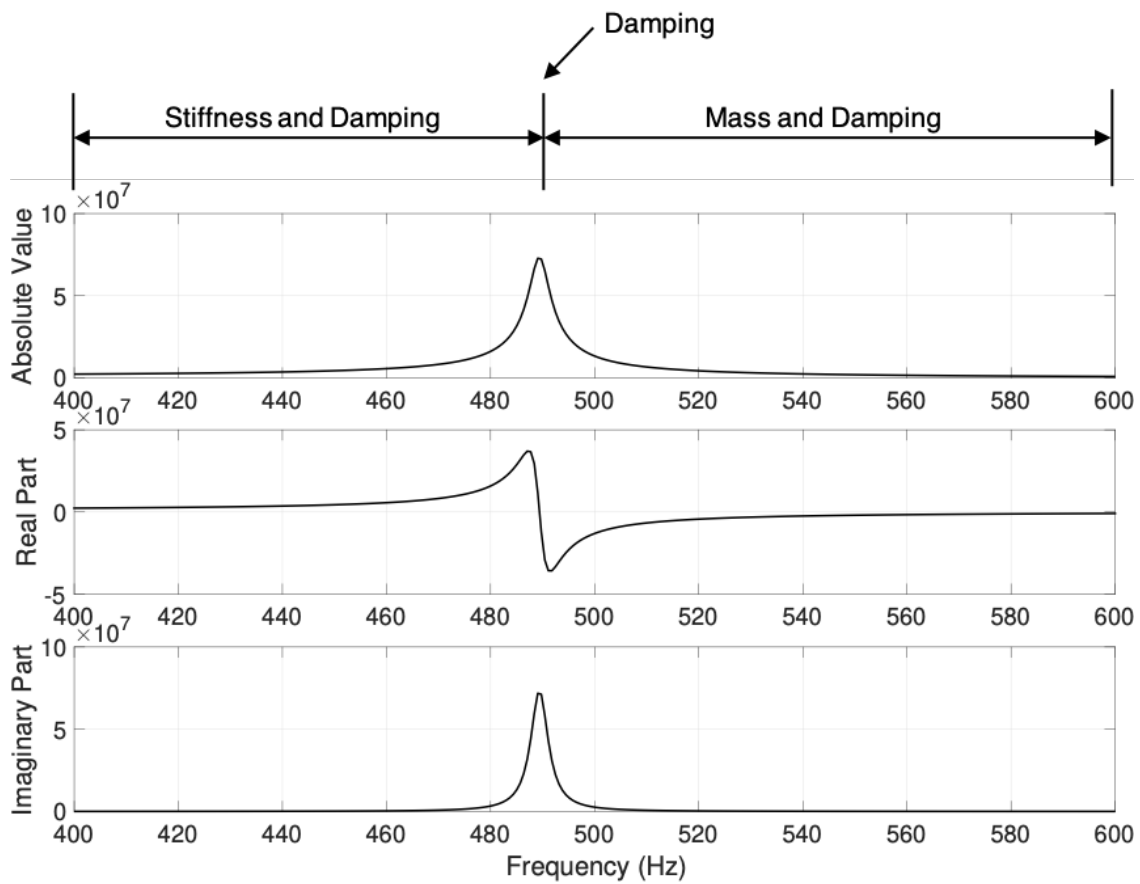


Figure 3.10: Dynamic stiffness of longitudinal excitation

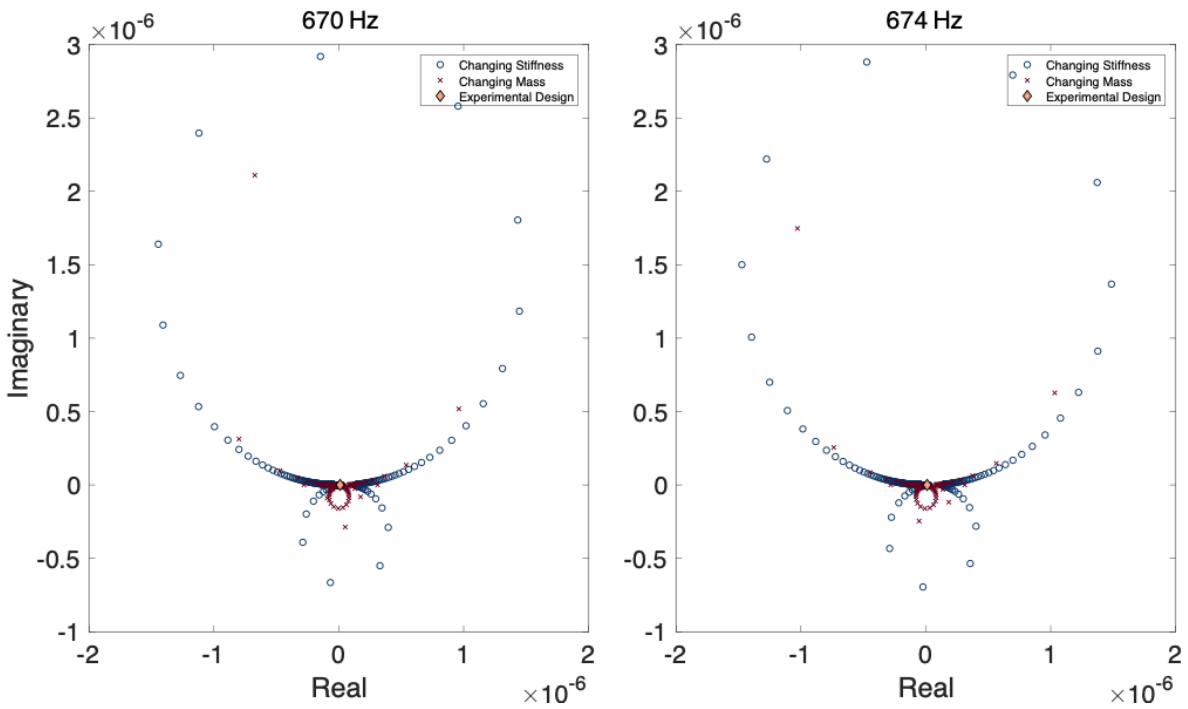


Figure 3.11: Longitudinal Vincent plots for frequencies below (left) and above (right) natural frequency of base structure

excitation direction and further changes to the absorber mass and stiffness could provide a lower response.

It is important to realize that the lowest response may not be the most important consideration in the design process of a mechanical metamaterial. Because the absorbers are often tuned to create split peaks in the system to move the resonance frequencies far away from the original natural frequency, one must also consider the new peak distance created by the absorber addition. The peak separation is governed by the mass ratio of the structure [49], [56] and therefore must be considered as an additional component to the structural design.

Figure 3.13 depicts a possible updated design for longitudinal excitation of the structure by considering the effect on the structure’s displacement with changing absorber mass and stiffness. Within each of these calculations, the peak separation is calculated and only designs with both low displacement and high peak separation are considered as design improvements. Finally, the design is further limited to results that center the peak separation within an acceptable tolerance error to

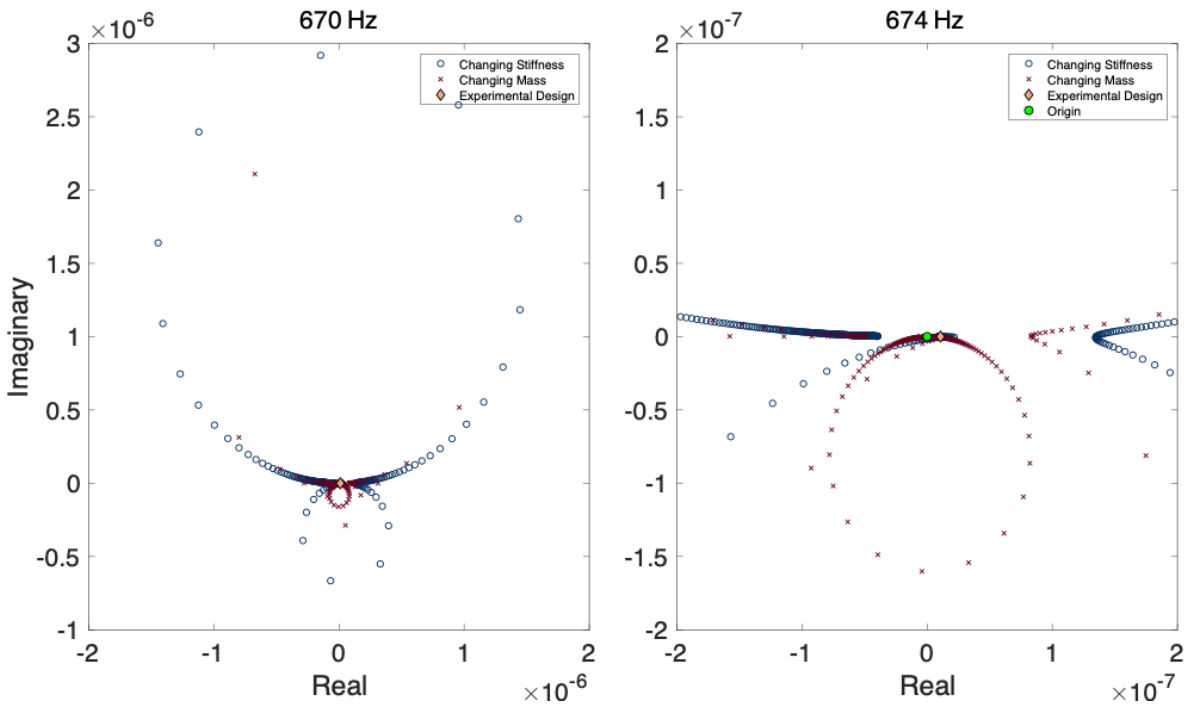


Figure 3.12: Longitudinal Vincent plots showing zoomed in plot around the design point for frequencies above the natural frequency (right).

the chosen operating frequency, in this case the blocked frequency of the structure. The plots in Figure 3.13 show that the original design is not far off from the improved design.

As with all designs there are tradeoffs between design choices and improvements in one area entail sacrifices in another. This is marginally demonstrated in the longitudinal case, but more pronounced in the transverse design as seen in the peak displacement amplitudes. To increase the bandwidth of the peaks, some gains in displacement minimization at the natural frequencies are sacrificed. Additionally, for the longitudinal case there is not a large difference in achievement between varying the stiffness or the mass absorber parameter, but the effects are more pronounced when viewed for the transverse displacement.

Based on the Vincent plots shown in Figure 3.15, the initial design has greater room for improvement for excitation in the transverse direction. On both sides of the blocked frequency, the design is further away from the origin than other possible represented designs. According to these plots, the transverse excitation response was optimized based on the same criteria as the longitu-

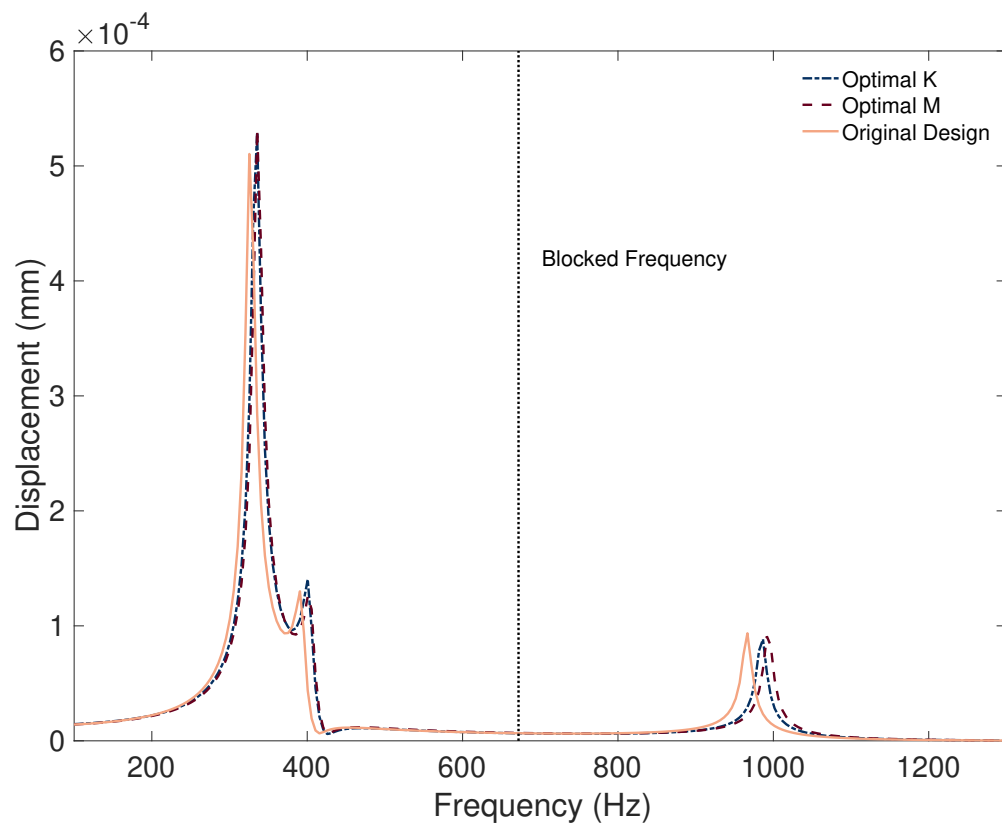


Figure 3.13: Updated longitudinal model based on objective parameters

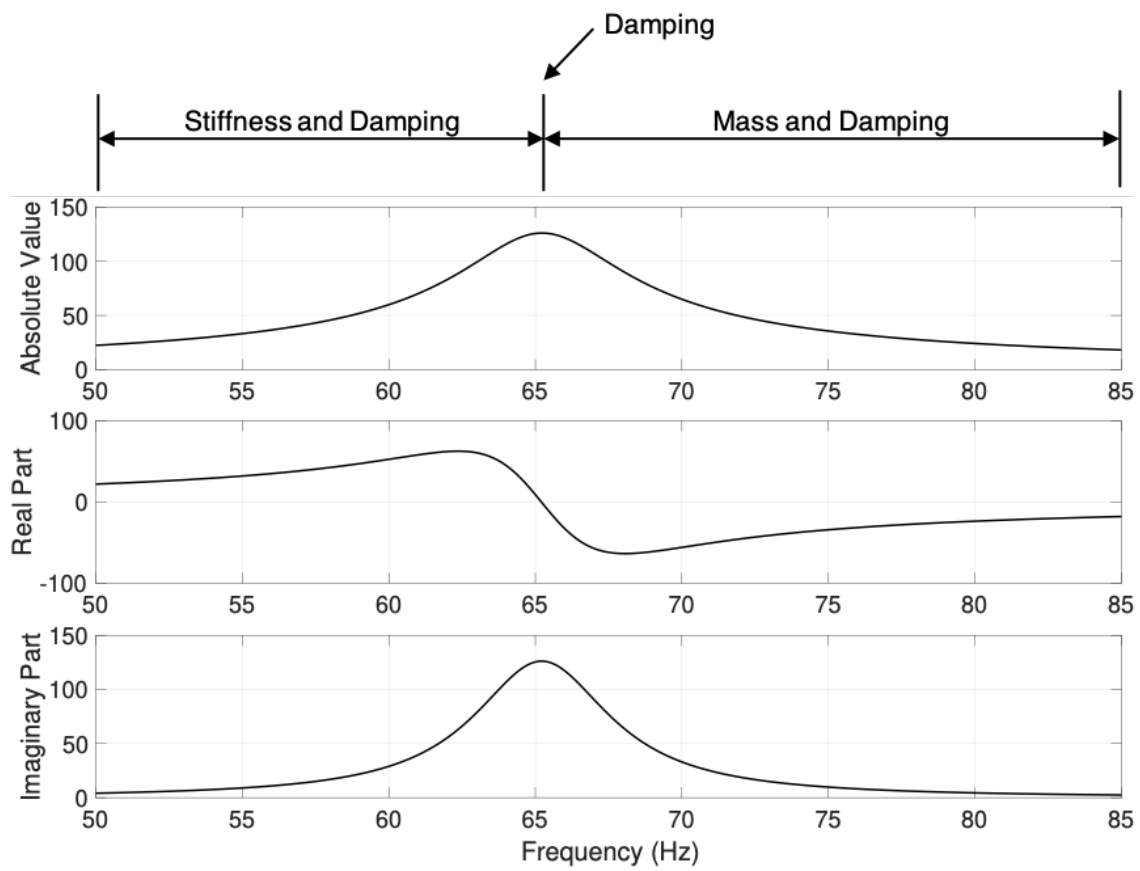


Figure 3.14: Dynamic stiffness of transverse excitation

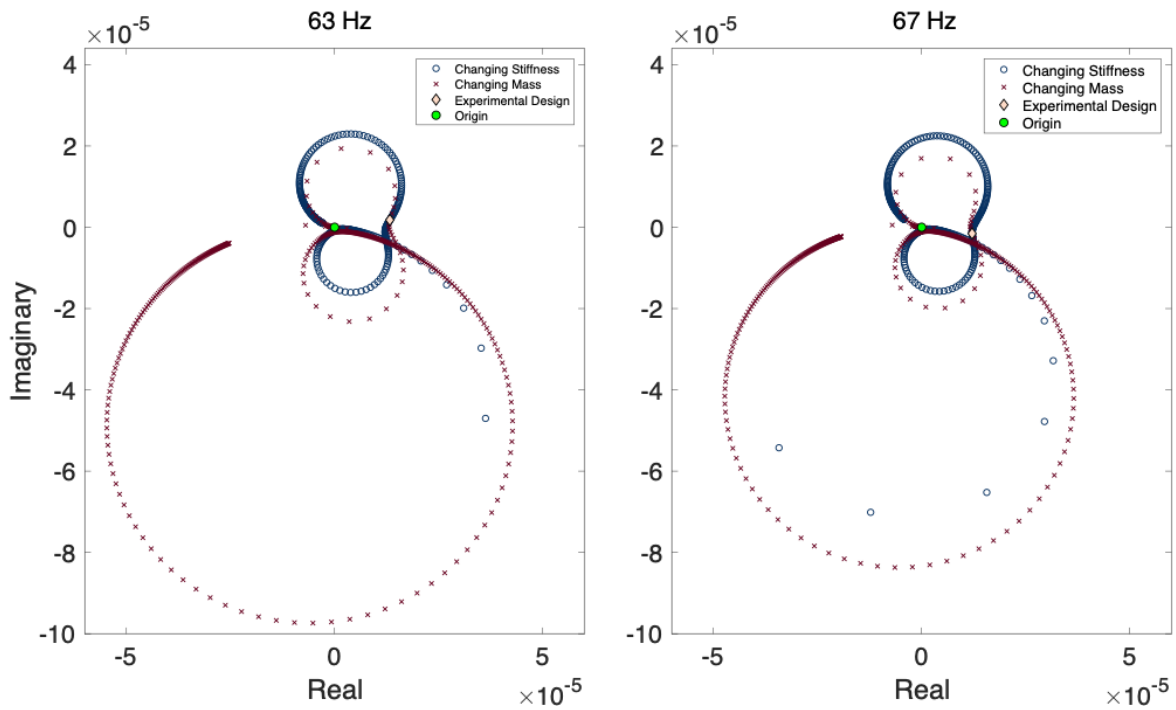


Figure 3.15: Transverse Vincent plots for frequencies below (left) and above (right) natural frequency of base structure

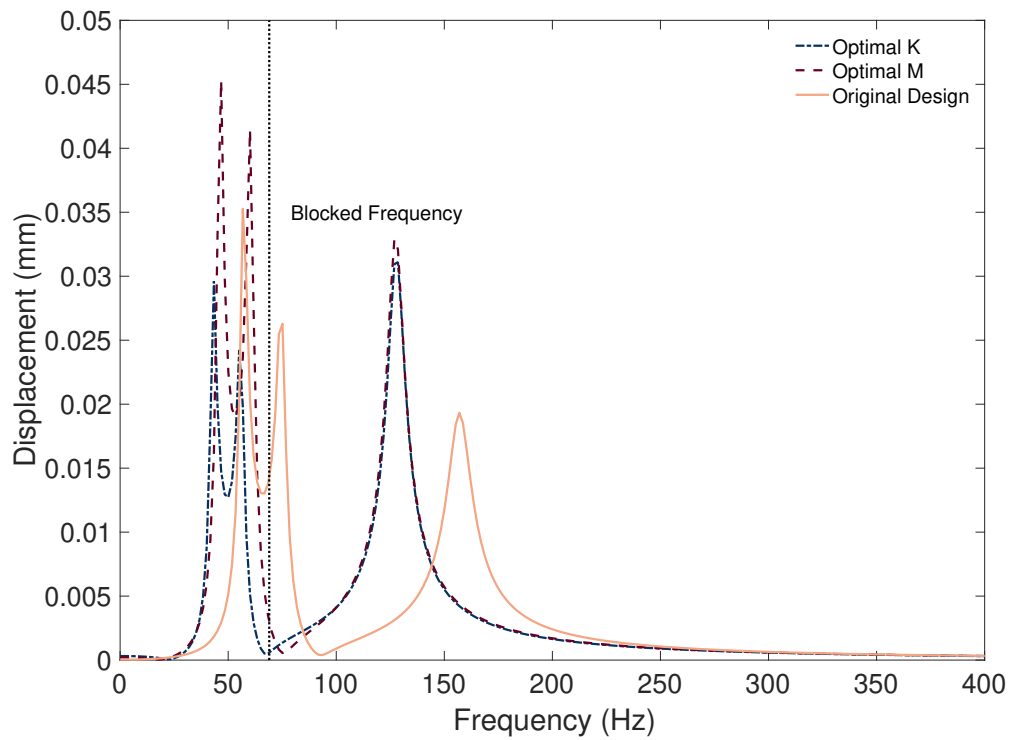


Figure 3.16: Updated transverse model based on objective parameters

dinal response and an updated design is presented in Figure 3.16. It can be seen that the original design placed the blocked peak between the first and second natural frequencies. Because the peak separation at this location is narrow, the minimum achievable displacement is higher than the one attainable by between the second and third bending frequencies as demonstrated as the updated designs shown in Figure 3.16.

It is also apparent, particularly in the optimized mass response, that with this increase in bandwidth, sacrifices are made in the displacement response at the natural frequencies. The optimal stiffness of the structure also increases the displacement of the third bending frequency; however, it lowers displacements of the first two peak frequencies when compared with the original design. A summary of the peak separations is listed in Table 3.1.

Table 3.1: Peak separation of original design vs. optimal designs for different excitation directions

Excitation Direction	Peak Separation [Hz]		
	Original Design	Optimal K	Optimal M
Longitudinal	575.9	585.9	591
Transverse	11.68	81.77	66.8

3.6 Summary

This chapter demonstrated the need to consider both the geometry and material selection in metastructure design. The initial impetus for this assertion was based on experimental comparisons between a chiral lattice metastructure and a mass conserved solid metastructure. When the frequency responses for each design were experimentally determined, the structure containing the solid material outperformed the designed metastructure when considering the global vibration attenuation. This led to the question of whether there are cases where it is worthwhile to optimize geometries or whether it is instead better to apply more material damping.

The dynamic stiffness was presented as a way to separate the modal parameters and visual-

ize their individual influence on the structural response allowing for quick determination of which modal parameter has more influence on the structural design at a given frequency. A further visualization technique called a Vincent plot was introduced which involved plotting the complex displacement response of the structure in the phase plane to show which design has the lowest displacement and how a variation in the modal parameters changes this response. The use of both of these techniques provides a method to first visualize what components will have the most effect on the structural response and then optimize the structure based on desired results.

Considering both the 2DOF and multi axis mechanical metamaterial structures, frequency responses suggest that for a system where the excitation frequency is known or when a specific frequency is to be avoided, it is more beneficial from a displacement reduction standpoint to tune absorbers to this frequency instead of adding system damping. Alternatively, if the system excitation is varying or broadband, increased damping provides a lower global displacement over a broader frequency range suggesting that for this excitation scenario, increasing material damping outperforms absorber tuning.

For the situations when vibration absorbers are desired, both the dynamic stiffness and the Vincent plots were considered for the multi axis metastructure. Design improvements were discussed and suggested for different individual excitation directions. Further restrictions to the optimization for this specific use case were implemented and both the peak separation and the blocked frequency location within said separation were considered in the design updating.

CHAPTER IV

Active Control of Mechanical Metamaterials

4.1 Overview

While the work in Chapter III involved adjusting the absorber frequencies at the original design phase, a control system on the absorbers can achieve the same results during operation. If the structure is excited at a different frequency than expected, or has a varying frequency, a control system would allow the adjustment of the absorber natural frequencies, and therefore the peak separation of the full structure. Piezoelectric patches were chosen for this model because easily attainable and have been widely characterized. This chapter begins by presenting the piezoelectric constitutive relationships and incorporating the piezoelectric material into the absorber system. Next, the absorber system is converted into a state space representation in order to implement the pole placement control system by calculating the control gains necessary for the absorber to achieve a desired natural frequency. Once completed, the adjusted absorber system can be incorporated into the full structure state space model to determine the new main beam frequency response.

Previous peak separation designs created in Chapter III are used to determine the desired absorber poles and the full state space model is used to find the frequency response of the multi axis mechanical metamaterial in the longitudinal direction. The maximum stress in the piezoelectric material on the absorbers is calculated to determine the feasibility of implementing controls in the existing design. Further discussion is included for general metastructure control implementation considerations.

4.2 Piezoelectric Equations

Piezoelectric materials exhibit electromechanical coupling, where the application of a mechanical stress creates an electrical displacement and an applied electric field produces mechanical strain in the material. This piezoelectric effect is useful for the design of devices for sensing and actuation.

In order to analyze the piezoelectric system with energy methods, it is beneficial to use the piezoelectric constitutive equations in the stress-voltage form where the independent variables are the strain and electric displacement. Beginning with the strain-charge form, the constitutive equations can be transformed to the stress-voltage form through a series of matrix manipulations.

The piezoelectric material considered in this section is considered to be a transversely isotropic material, meaning that there are two orthogonal planes of symmetry and the number of independent variables used to describe the material is reduced from 21 for a fully anisotropic material down to five [57]. Equation (4.1) presents this reduced form in the coordinate system shown in Figure 4.1.

$$\begin{Bmatrix} S_1 \\ S_2 \\ S_3 \\ S_3 \\ S_5 \\ S_6 \end{Bmatrix} = \begin{bmatrix} s_{11}^E & s_{12}^E & s_{13}^E & 0 & 0 & 0 \\ s_{12}^E & s_{11}^E & s_{13}^E & 0 & 0 & 0 \\ s_{13}^E & s_{13}^E & s_{33}^E & 0 & 0 & 0 \\ 0 & 0 & 0 & s_{55}^E & 0 & 0 \\ 0 & 0 & 0 & 0 & s_{55}^E & 0 \\ 0 & 0 & 0 & 0 & 0 & s_{66}^E \end{bmatrix} + \begin{Bmatrix} 0 & 0 & d_{31} \\ 0 & 0 & d_{31} \\ 0 & 0 & d_{33} \\ 0 & d_{15} & 0 \\ d_{15} & 0 & 0 \\ 0 & 0 & 0 \end{Bmatrix} \begin{Bmatrix} E_1 \\ E_2 \\ E_3 \end{Bmatrix} \quad (4.1)$$

$$s_{ij} = s_{ji} = 0 \quad i = 1, 2, 3 \quad j = 4, 5, 6 \quad (4.2)$$

$$s_{45} = s_{46} = s_{56} = s_{65} = 0$$

$$\begin{Bmatrix} D_1 \\ D_2 \\ D_3 \end{Bmatrix} = \begin{bmatrix} 0 & 0 & 0 & 0 & d_{15} & 0 \\ 0 & 0 & 0 & d_{15} & 0 & 0 \\ d_{31} & d_{31} & d_{33} & 0 & 0 & 0 \end{bmatrix} \begin{Bmatrix} T_1 \\ T_2 \\ T_3 \\ T_4 \\ T_5 \\ T_6 \end{Bmatrix} + \begin{bmatrix} \varepsilon_{11}^T & 0 & 0 \\ 0 & \varepsilon_{11}^T & 0 \\ 0 & 0 & \varepsilon_{33}^T \end{bmatrix} \begin{Bmatrix} E_1 \\ E_2 \\ E_3 \end{Bmatrix} \quad (4.3)$$

where s^E are the piezoelectric compliance coefficients, d are the piezoelectric coupling coefficients for the strain-charge form, and ε^T is the electric permittivity. This can be written in compact form as

$$\mathbf{S} = s^E \mathbf{T} + \mathbf{dE} \quad (4.4)$$

$$\mathbf{D} = \mathbf{d}' \mathbf{T} + \varepsilon^T \mathbf{E}$$

where \mathbf{S} are the strain components, \mathbf{T} are the stress components, \mathbf{E} are the electric field components, \mathbf{D} are the electric charge density displacement components, and prime denotes the transpose. The 1, 2, and 3 directions are the directions in which an electric field can be applied. Figure 4.1 shows a schematic of the axes of the piezoelectric actuators.

To more conveniently use energy equations with piezoelectric materials, the strain-charge form of the constitutive equations can be transformed to the stress-voltage form through a series of matrix transformations [41, 57].

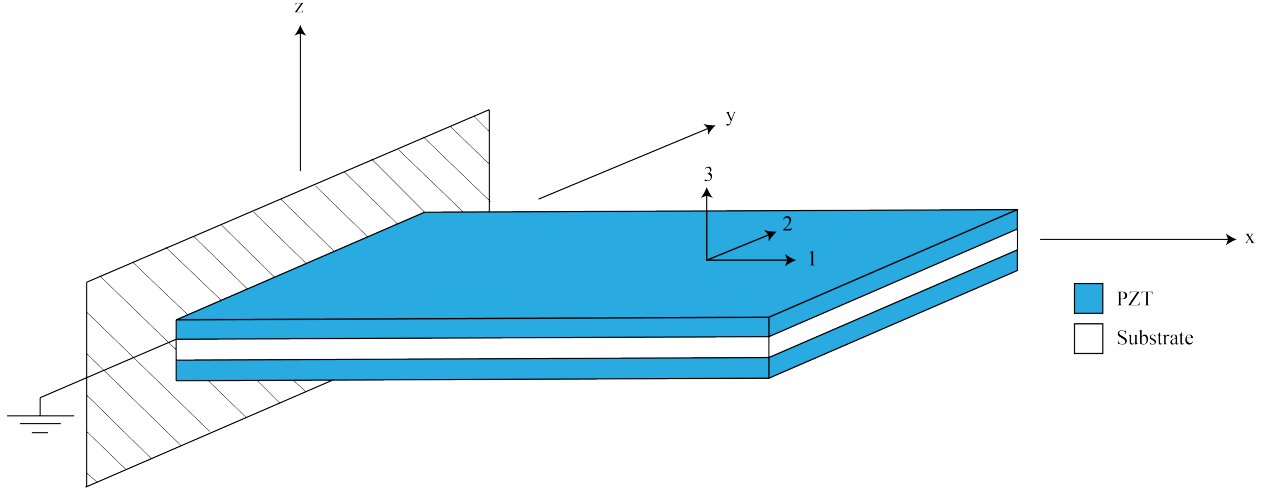


Figure 4.1: Schematic of piezoelectric bimorph

$$\mathbf{T} = c^D \mathbf{S} - \mathbf{h} \mathbf{D} \quad (4.5)$$

$$\mathbf{E} = -\mathbf{h}' \mathbf{S} + \beta^S \mathbf{D}$$

$$\mathbf{h} = c^D \mathbf{g} \quad (4.6)$$

$$\beta^S = \beta^T + \mathbf{g}' c^D \mathbf{g} \quad (4.7)$$

$$\mathbf{g} = \mathbf{d} \beta^T \quad (4.8)$$

where c^D are the stiffness coefficients under a constant electric charge, \mathbf{g} are the piezoelectric coupling coefficients for the strain-voltage form, \mathbf{h} are the piezoelectric coupling coefficients for the stress-voltage form, \mathbf{d} are the piezoelectric coupling coefficients for the strain-charge form, and β^S is the inverse of the electric permittivity under a constant strain. For this model, we will use PZT-5A due to its extensive characterization and wide availability. The material properties can be found in Table 4.1.

Table 4.1: Three dimensional material properties for PZT-5A

Property	Value
ρ_p	7750 kg/m ³
s_{11}^E	16.4 pm ² /N
s_{12}^E	-5.74 pm ² /N
s_{13}^E	-7.22 pm ² /N
s_{33}^E	18.8 pm ² /N
s_{55}^E	47.5 pm ² /N
s_{66}^E	44.3 pm ² /N
d_{31}	-171 pm/V
d_{33}	374 pm/V
d_{15}	584 pm/V
$\varepsilon_{11}^T/\varepsilon_0$	1730
$\varepsilon_{33}^T/\varepsilon_0$	1700

where the permittivity of free space is $\varepsilon_0 = 8.854$ pF/m

The alternative form of s^E can be used to find the Young's modulus Y_i and the Poisson's ratios

ν_{ij}

$$[s^E] = \begin{bmatrix} \frac{1}{Y_1^E} & -\frac{\nu_{12}}{Y_1^E} & -\frac{\nu_{13}}{Y_1^E} & 0 & 0 & 0 \\ -\frac{\nu_{12}}{Y_1^E} & \frac{1}{Y_1^E} & -\frac{\nu_{13}}{Y_1^E} & 0 & 0 & 0 \\ -\frac{\nu_{13}}{Y_1^E} & -\frac{\nu_{13}}{Y_1^E} & \frac{1}{Y_3^E} & 0 & 0 & 0 \\ 0 & 0 & 0 & \frac{1}{G_{23}^E} & 0 & 0 \\ 0 & 0 & 0 & 0 & \frac{1}{G_{13}^E} & 0 \\ 0 & 0 & 0 & 0 & 0 & \frac{1}{G_{12}^E} \end{bmatrix} \quad (4.9)$$

4.3 Modeling Single Absorber with Piezo Actuators

For this model, we begin with the Rayleigh Ritz analysis of Chapter II. Piezoelectric bimorphs are then applied to the cantilevered absorber as shown in Figure 4.2 beams and the properties will be generalized into one amplitude with a corresponding shape function as modeled in Chapter II. In this model, two charges will be added to the model - one for the upper and one for the lower piezoelectric patch.

The strain on the beams is given as

$$\mathbf{S}(\mathbf{x}) = \mathbf{B}_r(\mathbf{x})\mathbf{r} \quad (4.10)$$

The electric displacement on the piezoelectric is

$$\mathbf{D}^i(\mathbf{x}) = \mathbf{B}_q^i(\mathbf{x})\mathbf{q} \quad (4.11)$$

where i is the upper or lower piezoelectric patch.

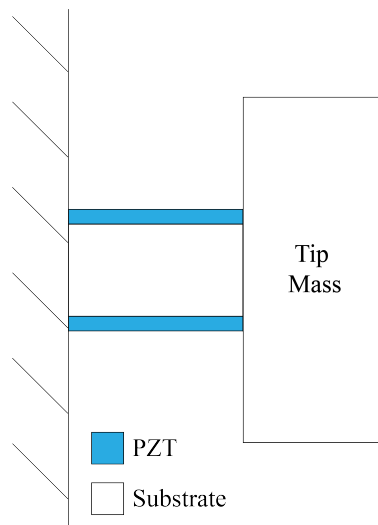


Figure 4.2: Schematic of piezoelectric attached to absorber beam for active control

The total energy can then be expressed as

$$U = \frac{1}{2} \mathbf{r}' K_s \mathbf{r} + \frac{1}{2} \mathbf{r}' K_p^D \mathbf{r} - \mathbf{r}' \Theta \mathbf{q} + \frac{1}{2} \mathbf{q}' C_p^{S-1} \mathbf{q} \quad (4.12)$$

where U is the total potential energy, \mathbf{r} is the generalized displacement matrix, K_s is the substrate stiffness (which is the same as in Chapter II), K_p^D is the piezoelectric actuator stiffness, Θ is the electromechanical coupling matrix, C_p^S is the capacitive matrix, and \mathbf{q} is the matrix of charges in each actuator.

The matrices K_p^D , Θ , and C_p^{S-1} are defined as

$$K_p^D = \int_{V_p^i} B_r(\mathbf{x})' c^D B_r(\mathbf{x}) dV_p^i \quad (4.13)$$

$$\Theta = \int_{V_p^i} B_r(\mathbf{x})' h B_q^{\text{upper}}(\mathbf{x}) dV_p^i \quad (4.14)$$

$$C_p^{S-1} = \int_{V_p^i} B_q^{\text{upper}}(\mathbf{x})' \beta^S B_q^{\text{upper}}(\mathbf{x}) dV_p^i \quad (4.15)$$

Solving for the cantilevered bimorph in question, the amplitude conversion matrices are specifically

$$B_r(\mathbf{x}) = \begin{bmatrix} z \frac{\partial^2}{\partial x^2} \\ -v_{12} z \frac{\partial^2}{\partial x^2} \\ -v_{13} z \frac{\partial^2}{\partial x^2} \\ 0 \\ 0 \\ 0 \end{bmatrix} \left\{ \Phi(\mathbf{x}) \right\} \quad (4.16)$$

$$\mathbf{B}_q^{upper}(\mathbf{x}) = \begin{bmatrix} 0 & 0 \\ 0 & 0 \\ \frac{1}{wL} & 0 \end{bmatrix} \quad (4.17)$$

$$\mathbf{K}_p^D = \frac{\hat{c}^D I_p}{l_p^4} (1 + 3\tau + 3\tau^2) \int_0^{l_p} [\Phi''(x)] [\Phi''(x)]^T dx \quad (4.18)$$

$$\Theta = \frac{\bar{h} t_p^2}{8l_p^3} (2\tau + 1) \left\{ [\Phi']_{l_p} - [\Phi']_0 \right\} \quad (4.19)$$

$$\mathbf{C}_p^s = \frac{\beta_{33}^s t_p}{wL^2} \begin{bmatrix} 1 & 0 \\ 0 & 1 \end{bmatrix} \quad (4.20)$$

where \hat{c}^D and \tilde{h} can be calculated from the piezoelectric constitutive equations in Equation (4.5)

$$\hat{c}^D = c_{11}^D - 2\nu_{12}c_{12}^D - 2\nu_{13}c_{13}^D + \nu_{12}^2c_{22}^D + \nu_{12}\nu_{13}c_{23}^D + \nu_{13}^2c_{33}^D \quad (4.21)$$

$$\tilde{h} = h_{13} - \nu_{12}h_{23} - \nu_{13}h_{33} \quad (4.22)$$

The new absorber equations can be written by adding the piezoelectric terms into Equation (2.26) and Equation (2.27). The equations of motion now contain an additional equation for the piezoelectricity which is coupled to the original equation of motion for the system.

$$\mathbf{M}_s \ddot{r} + \mathbf{D}_s \dot{r} + \mathbf{K}_s^D r - \Theta q = 0 \quad (4.23)$$

$$-\Theta^T r + (\mathbf{C}_p^S)^{-1} q = v \quad (4.24)$$

where v is the voltage.

The electromechanical equation can be rearranged to solve for charge

$$q = C_p^S v + C_p^S \Theta^T r \quad (4.25)$$

and then substituted back into Equation (4.23) to obtain a single set of coupled second order equations.

$$\mathbf{M}_s \ddot{\mathbf{r}} + \mathbf{D}_s \dot{\mathbf{r}} + \mathbf{K}^E \mathbf{r} - \Theta C_p^S v = 0 \quad (4.26)$$

where

$$\mathbf{K}^E = \mathbf{K}_s^D - \Theta C_p^S \Theta^T \quad (4.27)$$

4.4 State Space Formulation

To obtain the closed loop model of the system with controls included, the system is transformed to state space form. Representing the system in state space form obscures some of the insight into how the control system directly affects the physical system, however it makes modeling systems with multiple inputs and outputs simpler.

Beginning with Equation (4.26) and solving for the acceleration of the structure

$$\ddot{\mathbf{r}}(t) = -\mathbf{M}_s^{-1} \mathbf{K}^E \mathbf{r}(t) - \mathbf{M}_s^{-1} \mathbf{D}_s \dot{\mathbf{r}}(t) \mathbf{M}_s^{-1} \mathbf{B}_f \mathbf{f}(t) + \mathbf{M}_s^{-1} C_p^S \Theta^T \mathbf{B}_v \mathbf{v}(t) \quad (4.28)$$

Using $\mathbf{z}(t)$ as the state variable, the transformation is defined as

$$\begin{aligned} \mathbf{z}_1(t) &= \mathbf{r}(t) \\ \mathbf{z}_2(t) &= \dot{\mathbf{r}}(t) \end{aligned} \quad (4.29)$$

substituting Equation (4.29) into Equation (4.26) gives

$$\dot{\mathbf{z}}_2(t) = -M_s^{-1}K^E \mathbf{z}_1(t) - M_s^{-1}D_s \mathbf{z}_2(t) + M_s^{-1}B_f \mathbf{f}(t) + M_s^{-1}C_p^S \Theta' B_v \mathbf{v}(t) \quad (4.30)$$

Equation (4.30) with the definition $\dot{\mathbf{z}}_1(t) = \mathbf{z}_2$ can be written in matrix form as

$$\begin{Bmatrix} \dot{z}_1(t) \\ \dot{z}_2(t) \end{Bmatrix} = \begin{bmatrix} 0 & I \\ -M_s^{-1}K^E & -M_s^{-1}D_s \end{bmatrix} \begin{Bmatrix} z_1(t) \\ z_2(t) \end{Bmatrix} + \begin{Bmatrix} 0 \\ M_s^{-1}B_f \end{Bmatrix} \mathbf{f}(t) + \begin{Bmatrix} 0 \\ M_s^{-1}C_p^S \Theta' B_v \end{Bmatrix} \mathbf{v}(t) \quad (4.31)$$

These equations make up part of the state space representation, where the general form is given as

$$\dot{\mathbf{x}}(t) = A\mathbf{x}(t) + B\mathbf{u}(t) \quad (4.32)$$

$$\mathbf{y}(t) = C\mathbf{x}(t) + D\mathbf{u}(t)$$

where \mathbf{x} is the state vector, \mathbf{y} is the output vector, A is the state matrix, B is the input matrix, C is the output matrix, and D is the feedthrough matrix.

4.5 Pole Placement Control

As demonstrated in Chapter III, we can determine natural frequencies of the absorber that will increase the peak separation in the frequency response of the main beam. Since all the absorbers are independent and of the same geometry, we calculate the gains to adjust the absorber natural frequencies for a single absorber and apply them to every absorber individually. Pole placement is used to find the gains necessary to attain the correct natural frequency for the active absorber system. This control law was chosen due to its ability to select eigenvalues for the absorbers to obtain the desired frequency response of the system.

4.5.1 Absorber Control

Beginning with Equation (4.31), the absorber equation can be simplified to use only the mass and the stiffness terms since we are concerned with adjusting the natural frequency of the absorber system. The damping is reintroduced in the full modeling of the structure. Additionally, we are considering the free response of the absorbers and therefore the forcing term can be neglected. The updated equation is

$$\begin{Bmatrix} \dot{z}_1(t) \\ \dot{z}_2(t) \end{Bmatrix} = \begin{bmatrix} 0 & \mathbf{I} \\ -\mathbf{M}_s^{-1}\mathbf{K}^E & 0 \end{bmatrix} \begin{Bmatrix} z_1(t) \\ z_2(t) \end{Bmatrix} + \begin{Bmatrix} 0 \\ \mathbf{M}_s^{-1}\mathbf{C}_p^S\Theta'B_v \end{Bmatrix} v(t) \quad (4.33)$$

Assuming that the only control in the system is in the form of the piezoelectric voltage applied to the absorber, the control system equation is written as

$$v = -g'z(t) \quad (4.34)$$

where g is a $1 \times n$ matrix (where n is the length of z) of the control gains of the system which relate the input of the system to the output.

For this system, we are interested in finding the gains that will match the eigenvalues of the absorber to a desired frequency in order to increase the peak separation for the frequency response of the entire metastructure system. Equation (4.34) can be substituted back into Equation (4.33) to get

$$\dot{z}(t) = (\mathbf{A} - \mathbf{B}_c\mathbf{g}')z(t) \quad (4.35)$$

where \mathbf{B}_c is the input matrix of the closed loop system.

Traditionally in pole placement, the gains are calculated by solving the characteristic equation

of the closed loop system for the closed loop eigenvalues

$$\lambda_{cl}(S) = |SI - A + B_c g'| \quad (4.36)$$

and equating them to the eigenvalues of the desired characteristic equation [41].

$$\lambda_d(S) = |SI - A| \quad (4.37)$$

where λ_{cl} and λ_d are the closed loop and desired eigenvalues of the system respectively.

4.5.2 Full Metastructure Model

Now that the gain for a single absorber has been obtained, the full system can be constructed by placing the gain matrix inside the full state space system for the metastructure which can then be used to obtain the frequency response. Returning to a model similar to the one used in Section 2.3, the updated mass, stiffness, and damping equations for both the beam and absorber can be written as

$$\begin{bmatrix} \mathbf{M}^\alpha & \mathbf{M}^{\alpha\beta} \\ \mathbf{M}^{\beta\alpha} & \mathbf{M}^\beta \end{bmatrix} \begin{Bmatrix} \ddot{\mathbf{a}} \\ \ddot{\mathbf{y}} \end{Bmatrix} + \begin{bmatrix} \mathbf{D}^\alpha & \mathbf{0} \\ \mathbf{0} & \mathbf{D}^\beta \end{bmatrix} \begin{Bmatrix} \dot{\mathbf{a}} \\ \dot{\mathbf{y}} \end{Bmatrix} + \begin{bmatrix} \mathbf{K}^\alpha & \mathbf{0} \\ \mathbf{0} & \mathbf{K}^\beta \end{bmatrix} \begin{Bmatrix} \mathbf{a} \\ \mathbf{y} \end{Bmatrix} = \begin{bmatrix} \mathbf{F}_1 \\ \mathbf{F}_2 \end{bmatrix} \quad (4.38)$$

where now the mass terms for the absorber include the mass of the piezoelectric and the substrate and the stiffness terms for the absorber include both the stiffness of the substrate and the piezoelectric as well as the coupling and control gain values.

The force on the system is caused by the base excitation of the structure. \mathbf{F}_1 and \mathbf{F}_2 are the inertial forces acting on the total system mass and each absorber mass respectively.

$$\mathbf{F}_1 = \left[\int_0^L m U_r dx + \sum_{j=1}^{N_\beta} M_j^\beta U_r(\beta_j) \right]_{N_\beta \times 1} \quad (4.39)$$

$$\mathbf{F}_2 = \left[M_j^\beta \right]_{N_\beta \times 1} \quad (4.40)$$

To conveniently solve the system for both the beam and the absorber motion, the equations of motion are put into state space form.

Following the general state space equation given in Equation (4.32), the state variables for this system are defined as

$$\begin{bmatrix} \mathbf{x}_1 & \mathbf{x}_2 & \mathbf{x}_3 & \mathbf{x}_4 \end{bmatrix}^T = \begin{bmatrix} \mathbf{a} & \mathbf{y} & \dot{\mathbf{a}} & \dot{\mathbf{y}} \end{bmatrix}^T \quad (4.41)$$

where \mathbf{a} are the modal displacements of the main beam and \mathbf{y} are the displacements of the absorbers.

The state matrix is now

$$\mathbf{A} = \begin{bmatrix} 0 & \mathbf{I} \\ -\mathbf{M}^{-1}\mathbf{K} & \mathbf{M}^{-1}\mathbf{D} \end{bmatrix} \quad (4.42)$$

4.6 Application to Multi Axis Mechanical Metamaterial

While the work in Chapter III involved adjusting the absorber frequencies at the original design phase for passive control, an active control system on the absorbers can achieve the same results during operation. Beginning with the analytical model created in Chapter II, piezoelectric coupling can be added to the absorbers to adjust their natural frequencies using active control to obtain a larger peak separation in the response of the main structure. This is similar to the design updating completed in Chapter III, however this work retrofits an active control system on the existing design from Chapter II instead of changing it at the initial design stages.

For the longitudinal maximum peak separation found in Chapter III, the absorber natural fre-

quency should be around 444 Hz. Because the Young's modulus piezoelectric modulus is almost 31 times larger than the VeroWhite modulus, the addition of a piezoelectric bimorph with a thickness of 127 microns per piezo would raise the natural frequency of the absorbers considerably. For this reason, the thickness of the absorber was adjusted from 6.5 mm to approximately 3.5 mm to maintain the desired absorber frequency. Adjusting the absorber to this natural frequency allows a comparison to experimental data.

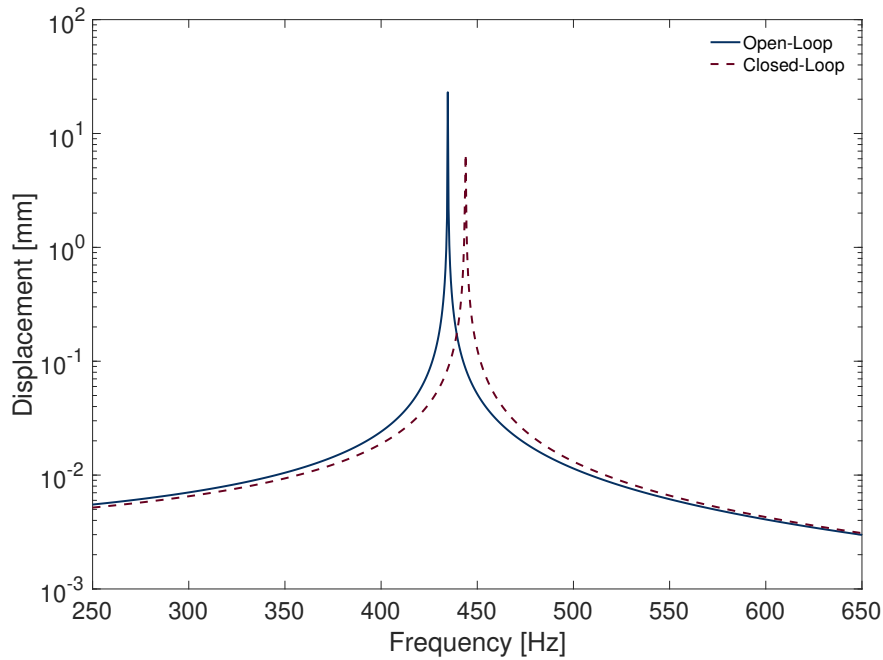


Figure 4.3: Natural frequency of absorber with open and closed loop control

Figure 4.3 presents the absorber natural frequency excited in the thick direction for open loop and closed loop control. The open loop frequency is 434.7 Hz while the desired closed loop frequency was set to 443.9 Hz. As can be seen in the plot, the closed loop system can calculate the necessary gains to shift the natural frequency to the desired closed loop pole.

Results for the longitudinal main beam tip displacement are presented in Figure 4.4. The active control plot is similar to the passive control found in Figure 3.13 demonstrating that both passive design changes and active control additions to the absorbers can achieve similar frequency responses for the main beam. An updated model of the blocked frequency response using the experimental results is also plotted to demonstrate the peak separation that can be created using

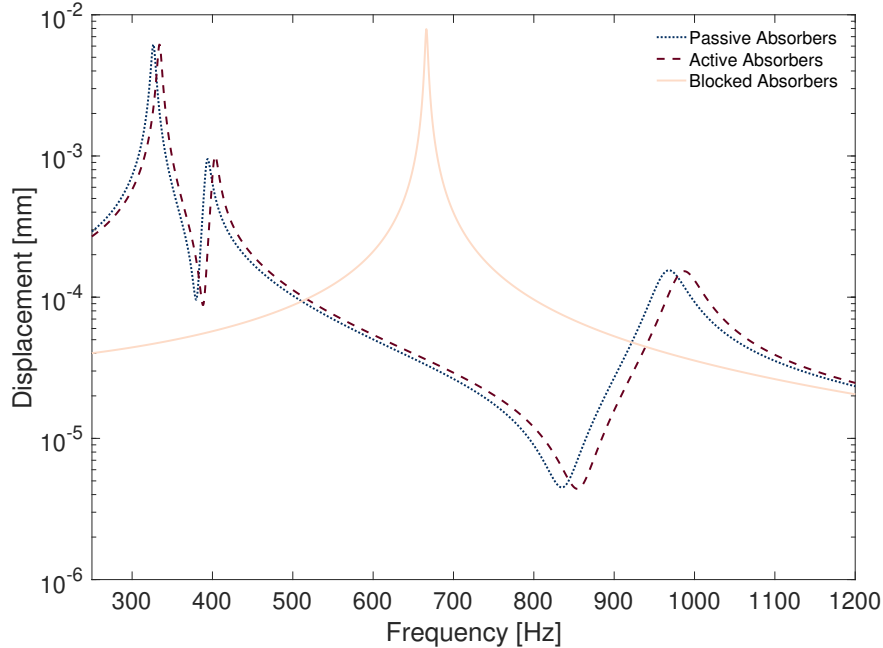


Figure 4.4: Frequency response of longitudinally excited system

active control on the absorbers. When comparing the main beam natural frequency responses for the blocked case and the active control case, it can be seen that the active control system can effectively avoid the undesired blocked natural frequency. In comparison to the original passive absorber frequency response, the active control system can achieve an improvement in natural frequencies of the main beam system peak separation of 11.4 Hz.

Because the absorbers vibrate more to impede the main beam from vibrating, it is necessary to verify the stress in the piezoelectric does not induce material failure. The stress in the piezoelectric actuators is plotted at each absorber array location in Figure 4.5. The ultimate tensile strength of the piezoelectric material was quoted to be 17.24 MPa from the manufacturer and is shown in the graph as the horizontal dashed line. A study performed by Anton et al. [58] showed that the bending strength of PZT-5A was closer to 140 MPa which is shown by the horizontal solid line.

As can be seen from the plot, all of absorbers have a higher stress in the piezoelectric if the originally quoted ultimate tensile strength is used, and absorber arrays six, seven, and eight have a higher stress when the experimental bending strength is used. Because the main structure vibrates more at the free end than the base, the absorbers must vibrate at higher amplitudes to reduce the

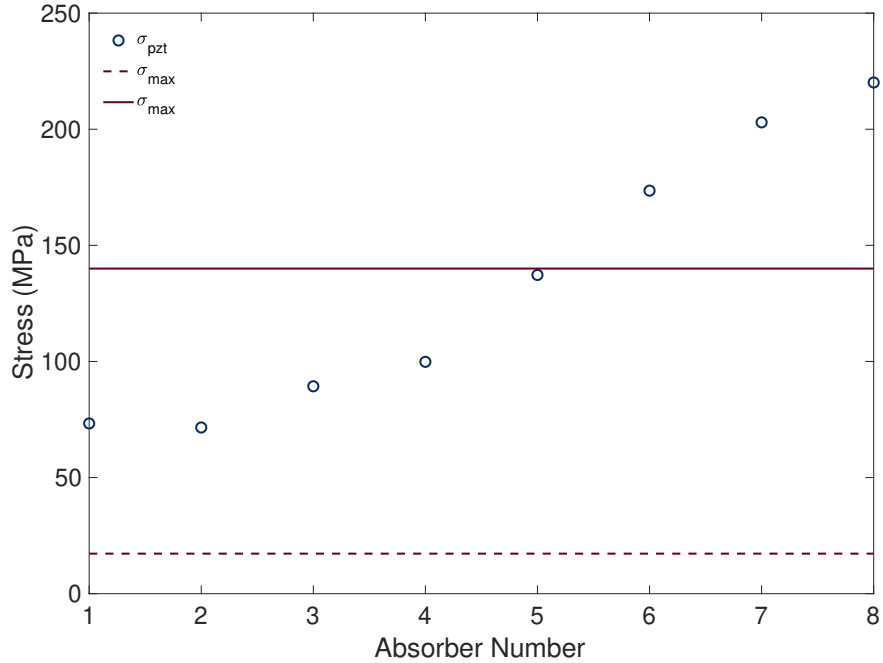


Figure 4.5: Absorber array number vs. maximum stress in absorber piezoelectric

vibration from the main beam. When considering excitation in either the transverse or torsional directions, the absorbers are vibrating in the thin orientation, and would therefore bend with an even larger displacement due to the thinness of the substrate in that direction. Additionally, to match the absorber natural frequency to the main beam, the adjustment to the thickness of the absorbers to account for the added stiffness of the piezoelectric would leave the absorber beam unable to support the tip mass without piezoelectric attached. For this reason, retrofitting a control system to this specific design is not recommended for excitation in any direction.

These results bring up important considerations when deciding whether to implement a control system. Adding a controller increases complexity of design and implementation. The design of the distributed absorber system must account for the added stiffness in the natural frequency to ensure that the absorbers will adequately match the main beam structure. Material stresses must be calculated to avoid electrical and mechanical failure during operations. Additional considerations include the need for a microcontroller and a method to supply power to the control system when active control is implemented.

Although the control system was infeasible for the current multi axis metamaterial design, the

idea should not be discounted for all mechanical metamaterials. If a design used a stiffer material, a metal for instance, there would be less of a mismatch between the substrate and piezoelectric stiffnesses. Furthermore, the absorber material would support the piezoelectric more adequately and the system would be able to withstand higher stresses.

Using a larger system with larger absorbers and therefore more space to attach the actuators can help. The current system needed sizable tip masses on the ends of the absorber cantilever beams to lower the natural frequency of the absorber in a restricted design footprint. A larger system could also allow more freedom to tune the absorber geometries instead of relying on the tip mass for adjustments, thereby reducing the size of the tip mass needed to achieve a certain frequency and in turn decreasing the stress in the absorber materials inflicted by the considerable mass loading on the end.

4.7 Summary

This chapter investigated the addition of a control system to the multi axis mechanical metamaterial previously introduced. While the previous chapters considered the initial design as well as peak separation improvements in the design phase, this chapter examines altering the absorber natural frequencies using a control system after the design has been completed.

First, the addition of piezoelectric material on the system absorbers was modeled using a state space method and a pole placement control law was introduced and implemented. Target poles were determined based on the analysis in Chapter III where the absorber mass and stiffness were varied to determine the maximum peak separation in the frequency response. The optimal absorber natural frequency from the longitudinal design was used to calculate the desired absorber natural frequencies for the longitudinal controller. Due to the much higher stiffness of the piezoelectric material, the absorber thickness was decreased to ensure the absorbers would be able to adequately interface with the main system.

Once the new lumped absorber parameters were determined, the longitudinal analysis was

conducted, and the frequency response of the combined structures were examined to determine the effectiveness of adding a controller to the system. While gains that achieved the desired eigenvalues for the control system could be calculated, it was found that the stresses in the piezoelectric materials would reach values above the bending strength for the piezoelectric material which would cause material failure upon operation. Similar issues occur for the other two excitation directions and therefore, adding a control system to this design is not recommended.

These results highlight crucial considerations when deciding whether to implement an active control system. Adding a controller increases complexity of design and implementation. The design of the distributed absorber system must account for the added stiffness in the natural frequency to ensure that the absorbers will adequately match the main beam structure. Material stresses must be calculated to avoid electrical and mechanical failure during operations.

Although a possible control system was not achievable for the existing multi axis metamaterial, adding a control system to larger structures or structures made of stiffer materials may still be achievable. Active controls on metastructures would allow for adjustment of the absorber frequency and the subsequent structural frequency response during operation.

CHAPTER V

Conclusions and Future Work

5.1 Dissertation Summary

This dissertation focuses on analytical and experimental aspects of mechanical metamaterials for design and implementation. The following contains a summary of Chapters II through IV and highlights of the primary findings and contributions of each chapter.

5.1.1 Chapter II

This chapter focuses on the design of mechanical metastructures for passive vibration suppression. To eliminate the often overwhelming effect of viscous damping, materials with low damping are considered with a further discussion of these impacts in Chapter III. Two approaches to the design of the inserts for mechanical metamaterials are considered. The first is to investigate and model a zigzag shaped insert to improve the absorber design space and the second is to examine an insert absorber capable of absorbing vibrations in multi directional excitation. Lastly, since many of these metastructures are created using additive manufacturing, a discussion of the limitations of current additive manufacturing capabilities is included.

First, a finite element and analytical design for a zigzag absorber with highly tunable natural frequencies is presented and experimentally validated. This absorber design is then incorporated into a low damping aluminum metastructure and analytical and finite element frequency response results are presented to demonstrate the peak separation capabilities of the structure with absorbers

at the natural frequencies of the main beam.

The next section creates an absorber insert that is capable of attenuating vibrations in three directions. This type of insert is included as a set of absorber arrays at cut outs in a main beam and experimental validation of the finite model are presented. An analytical method to model the absorbers and the full system is then presented and compared to the finite element model and experimental results. Both the longitudinal and transverse finite element and analytical models were able to predict the structural natural frequencies with a maximum error of around 12%. The analytical model could predict the natural frequency of the torsional model with an error of close to 22% while the finite element model had an error of 0.52%. This suggests that some additional dynamics may need to be considered for the torsional model. One possibility in the discrepancy is due to warping of the cross section in the absorber cutout locations.

A discussion of current additive manufacturing capabilities and limitations is also included. With the increase in additive manufacturing technology, the ability to experimentally test metastructures has rapidly increased. Issues with creating a homogeneous material and defects in printing are two major obstacles to integrating these structures in existing applications, however the current experiments demonstrate the value in these mechanical metamaterials that will only increase with further additive manufacturing advances.

5.1.2 Chapter III

An experimental impetus for examining the material choice in metastructure design was presented. This fueled a further look into basic design considerations and methods to determine tradeoffs in design choices. A basic two degree of freedom system was examined as well as a multi axis mechanical metamaterial.

With recent interest in metastructures, papers have presented results of complicated geometric designs and optimization without much regard to material selection. One specific chiral lattice metastructure design was fabricated out of TangoPlus and steel annular resonators and tested using hammer impact excitation. A mass conserved structure with a solid TangoPlus core was created

and the frequency response of the solid structure was compared with that of the chiral lattice. Findings from this experiment demonstrate that the solid TangoPlus core attenuated global vibrations over a broadband range of frequencies more quickly than the geometrically designed system, therefore proving the need for taking the material into consideration before embarking on a time expensive geometric optimization.

To simplify the preliminary analysis, a two degree of freedom metastructure was analyzed to determine where the damping or the geometric design in the form of changing stiffness played a more important role in the structural response. Results from this indicated that the damping on the main structure will outperform the geometrically designed absorber system except near locations where the absorber is tuned to the natural frequency of the main system.

To aid with structural design, first the dynamic stiffness was presented as a way to separate the modal parameters and visualize their individual influence on the structural response. This allows a quick graphical means to determine which modal parameter has more influence on the structural design at a given frequency. Next, a type of complex plane plot termed the Vincent plot was introduced. This method plots the displacement of the main beam in the complex plane when the mass and stiffnesses of the absorber system are varied for a single frequency. The closer to the origin the data is, the lower the displacement is. From looking at these plots, the impact of specific design choices can be seen as well as whether improvements can be made on the current design.

A multi axis mechanical metamaterial capable of attenuating vibration in three degrees of excitation was considered as a real-world extension of the two degree of freedom preliminary analysis. This more complicated system includes a vibrating main beam with cutouts for arrays of absorbers. Similar findings as the two degree of freedom system were reached and the frequency response plot upheld the conclusions that the absorbers outperform main beam damping only near the main system natural frequencies. This led to the further design conclusion that when a specific frequency is to be avoided, it is more beneficial from a displacement reduction standpoint to tune absorbers to this frequency instead of system damping. Alternatively, if the system excitation is broadband, increased damping provides a lower global displacement over a broader frequency

range and, therefore, increasing material damping outperforms absorber tuning.

Finally, for a situation where absorbers are desired, both the dynamic stiffness and the Vincent plots were applied to the multi axis mechanical metamaterial in the longitudinal and transverse directions. It was found that the longitudinal design is close to optimal for obtaining the minimum displacement at the longitudinal natural frequency, while the transverse design could be altered to provide lower displacement. Additional calculations were conducted to provide designs for both directions of excitation that would provide a larger peak separation particularly in the transverse direction.

5.1.3 Chapter IV

A fully coupled electromechanical distributed parameter model of the absorber system on the multi axis mechanical metamaterial was presented for use in controlling the absorber natural frequencies. While the previous chapters considered the initial design as well as peak separation improvements in the design phase, this chapter examines retrofitting the current multi axis mechanical metamaterial design with a control system on the absorber array.

The electromechanical coupling terms of the bimorph controller were derived from constitutive relationships for PZT-5A piezoelectric material. The electromechanical equations combined with the assumed modes method for a cantilever beam with a tip mass was used to find the new absorber frequencies for both thick and thin absorber vibration. A pole placement control law was introduced, and the coupled electromechanical equations were used to calculate the controller gain for a single absorber. The target poles were determined based on the analysis in Chapter III where the absorber stiffness was varied to determine the maximum peak separation in the frequency response.

Once these gains were found, the absorber system was reduced to a system of equivalent lumped masses and stiffnesses and integrated into the full beam system. The new natural frequencies and frequency response functions of the controlled system were calculated using the Rayleigh-Ritz analytical method. Although gains that achieved the desired eigenvalues for the control system were calculated, it was found that the stresses in the piezoelectric materials would

reach values above the bending strength for the piezoelectric material. Operating above the bending strength for the material would cause material failure upon operation. Similar issues occur for the other two excitation directions and therefore, adding a control system to this design is not recommended.

These results highlight crucial considerations when deciding whether to implement a control system. Adding a controller increases complexity of design and implementation. The design of the distributed absorber system must account for the added stiffness in the natural frequency to ensure that the absorbers will adequately match the main beam structure. Considering the stress in the structural components is vital as too high of stress can lead to electrical and mechanical failure during operation.

Although a possible control system was not achievable for the existing multi axis metamaterial, adding a control system to larger structures or structures made of stiffer materials may still be achievable. Active controls on metastructures would allow for adjustment of the absorber frequency and the subsequent structural frequency response during operation.

5.2 Key Contributions of the Dissertation

The following list is a summary of the major contributions that the research presented in this dissertation provides for the field of design and implementation of mechanical metamaterials for vibration suppression.

- An analytical Rayleigh-Ritz model was created for a zigzag absorber with highly tunable natural frequencies. The results of these models demonstrate that it is possible to create an absorber system for a metastructure that can fit in a small geometric footprint to match with the frequency of a larger load bearing beam. This beam further strengthens the foundation of metastructure theory by demonstrating the benefits of absorbers without additional added damping on a more complex system.
- The first multi axis mechanical metamaterial design capable of attenuating vibration in three

directions of excitation was proposed and successfully achieved. The structure was first designed using the finite element method. It was fabricated using additive manufacturing and experimentally verified under swept sine excitation in the longitudinal, transverse, and torsional directions.

- An analytical method of designing the multi axis mechanical metamaterial structure was derived using a distributed parameter method for the absorber vibration and then lumping them to create a Rayleigh-Ritz model for the coupled beam and absorber system. This method can capture the system behavior without needing the full finite element model. The method was verified using both finite element and experimental data.
- This work was the first to determine a dividing line between material damping and vibration absorption in mechanical metamaterial design. Previous work had considered complex geometric designs to attenuate vibration without consideration for the material damping in the system. By using the criteria provided in this chapter, a decision can be made on the most effective system design based on excitation constraints.
- A visual method to determine whether improvements can be made to the absorber design was introduced in the form of a complex plane Vincent plot. The use of both the Vincent plot and the dynamic stiffness plots have been expanded to use with the multi axis mechanical metamaterial. These plots can be used for visual determination whether the optimal design has been reached for a given frequency and which structural parameter will have the most influence on the system.
- The peak separation capabilities of the multi axis mechanical metamaterial were considered for augmentation through a control system located on the distributed absorber system. An electromechanical model of including a piezoelectric bimorph to sense and actuate the absorber system was derived. A pole placement control system was introduced to adjust the natural frequencies of the absorbers. While a control system was not recommended to be used in this design case due to the high stresses in the piezoelectric material during exci-

tation, a base method for active control of the absorbers of a metastructure with regards to peak separation was created. Additional insight on control use in mechanical metamaterials is discussed, including recommendations on when an active control system should be considered.

5.3 Recommendations for Future Work

This work has demonstrated both the capabilities of the absorber with highly tunable natural frequencies and the multi axis mechanical metamaterial. A logical progression from this thesis would be to create a new design for the absorbers on the multi axis metastructure to allow for greater tunability in the natural frequencies of the absorbers. The existing zigzag design would work well when using the same configuration for all absorbers in the torsional and transverse directions, however the longitudinal direction would either need a different absorber design or the zigzag would need to be rotated 90 degrees from the absorbers in the other two excitation directions. One possibility would be to alternate the direction of the absorber for each array of absorbers in the beam cutouts.

If this work is to be implemented into an existing structure, an in-depth examination of the fatigue life of absorbers as well as the structure would be necessary. To attenuate the vibrations from the main beam requires that the displacement of the absorbers is increased which would consequently decrease the operation life of the absorber array. Other calculations, such as the load bearing capabilities of the main beam, would also be beneficial if the mechanical metamaterial is to be incorporated into an existing structure.

The current design of the absorbers does not protect them from impact, so an updated design could include a method of shielding the absorbers from impact either due to debris or mishandling. Furthermore, the material chosen is that of an additively manufactured photopolymer and the strength properties are not as high as for other materials, such as metal. With advances in additive manufacturing, metal printing is being rapidly improved. Another advantage to printing these

types of structures out of metal is that they are less susceptible to temperature changes unlike the existing design, which is printed out of a viscoelastic material.

The control system presented in this work was designed with a chosen piezoelectric sheet. These materials are traditionally very brittle, and another design choice may create a more flexible structure capable of large out of plane strains. Alternatively, future active mechanical metamaterials could use a stiffer material, a metal for instance, where there is not as much of a mismatch between the substrate and piezoelectric stiffnesses. Furthermore, a stiffer absorber material would support the piezoelectric more adequately and the system would be able to withstand higher stresses. Other designs could use a larger system with larger absorbers and therefore more space to attach the actuators. The current system needed sizable tip masses on the ends of the absorber cantilever beams to lower the natural frequency of the absorber in a restricted design footprint. A larger system could also allow more freedom to tune the absorber geometries instead of relying on the tip mass for adjustments, thereby reducing the size of the tip mass needed to achieve a certain frequency and in turn decreasing the stress in the absorber materials inflicted by the considerable mass loading on the end.

Finally, the choice of control law is pole placement, however a control law such as a linear quadratic regulator, or LQR could be used. LQR is a control law that still places poles within the frequency domain, but it uses a cost function with competing objectives such as maximum displacement or voltage to find the optimal pole placement.

BIBLIOGRAPHY

- [1] Hobeck, J. D., Laurent, C. M. V., and Inman, D. J., “3D printing of metastructures for passive broadband vibration suppression,” *20th International Conference on Composite Materials*, 2015.
- [2] Kshetrimayum, R., “A brief intro to metamaterials,” *IEEE Potentials*, Vol. 23, No. 5, Jan. 2005, pp. 44–46.
- [3] Engheta, N. and Ziolkowski, R. W., *Metamaterials: Physics and Engineering Explorations*, Wiley & Sons, 2006.
- [4] Veselago, V. G., “The Electrodynamics of Substances with Simultaneously Negative Values of ϵ and μ ,” *Soviet Physics Uspekhi*, Vol. 10, No. 4, April 1968, pp. 509–514.
- [5] Smith, D. R., Padilla, W. J., Vier, D. C., Nemat-Nasser, S. C., and Schultz, S., “Composite Medium with Simultaneously Negative Permeability and Permittivity,” *Physical Review Letters*, Vol. 84, No. 18, May 2000, pp. 4184–4187.
- [6] Zouhdi, S., *Metamaterials and plasmonics : fundamentals, modelling, applications*, Springer In cooperation with NATO Public Diplomacy Division, Dordrecht, 2009.
- [7] Guenneau, S., Movchan, A., Pétursson, G., and Ramakrishna, S. A., “Acoustic metamaterials for sound focusing and confinement,” *New Journal of Physics*, Vol. 9, No. 11, Nov. 2007, pp. 399–399.
- [8] Martínez-Sala, R., Sancho, J., Sánchez, J. V., Gómez, V., Llinares, J., and Meseguer, F., “Sound attenuation by sculpture,” *Nature*, Vol. 378, No. 6554, Nov. 1995, pp. 241–241.
- [9] Liu, Z., “Locally Resonant Sonic Materials,” *Science*, Vol. 289, No. 5485, Sept. 2000, pp. 1734–1736.
- [10] Pai, P. F., “Metamaterial-based Broadband Elastic Wave Absorber,” *Journal of Intelligent Material Systems and Structures*, Vol. 21, No. 5, Jan. 2010, pp. 517–528.
- [11] Sun, H., Du, X., and Pai, P., “Theory of Metamaterial Beams for Broadband Vibration Absorption,” *Journal of Intelligent Material Systems and Structures*, Vol. 21, No. 11, June 2010, pp. 1085–1101.
- [12] Pai, P. F. and Sundaesan, M. J., “Actual working mechanisms of smart metamaterial structures,” *Health Monitoring of Structural and Biological Systems 2013*, SPIE, April 2013.

- [13] Zheng, X., Lee, H., Weisgraber, T. H., Shusteff, M., DeOtte, J., Duoss, E. B., Kuntz, J. D., Biener, M. M., Ge, Q., Jackson, J. A., Kucheyev, S. O., Fang, N. X., and Spadaccini, C. M., “Ultralight, ultrastiff mechanical metamaterials,” *Science*, Vol. 344, No. 6190, June 2014, pp. 1373–1377.
- [14] Zhu, R., Liu, X., Hu, G., Sun, C., and Huang, G., “A chiral elastic metamaterial beam for broadband vibration suppression,” *Journal of Sound and Vibration*, Vol. 333, No. 10, May 2014, pp. 2759–2773.
- [15] Chen, J., Sharma, B., and Sun, C., “Dynamic behaviour of sandwich structure containing spring-mass resonators,” *Composite Structures*, Vol. 93, No. 8, July 2011, pp. 2120–2125.
- [16] Resnick, R., *Physics*, Wiley, New York, 1977.
- [17] Liang, X., Wang, T., Jiang, X., Liu, Z., Ruan, Y., and Deng, Y., “A Numerical Method for Flexural Vibration Band Gaps in A Phononic Crystal Beam with Locally Resonant Oscillators,” *Crystals*, Vol. 9, No. 6, June 2019, pp. 293.
- [18] Hartog, J. P. D., *Mechanical Vibrations*, Crastre Press, March 2011.
- [19] Zuo, L. and Nayfeh, S. A., “Optimization of the Individual Stiffness and Damping Parameters in Multiple-Tuned-Mass-Damper Systems,” *Journal of Vibration and Acoustics*, Vol. 127, No. 1, Feb. 2005, pp. 77–83.
- [20] Sun, J. Q., Jolly, M. R., and Norris, M. A., “Passive, Adaptive and Active Tuned Vibration Absorbers—A Survey,” *Journal of Mechanical Design*, Vol. 117, No. B, June 1995, pp. 234–242.
- [21] Hoang, N. and Warnitchai, P., “Design of multiple tuned mass dampers by using a numerical optimizer,” *Earthquake Engineering & Structural Dynamics*, Vol. 34, No. 2, 2005, pp. 125–144.
- [22] Zuo, L. and Nayfeh, S., “Minimax optimization of multi-degree-of-freedom tuned-mass dampers,” *Journal of Sound and Vibration*, Vol. 272, No. 3-5, May 2004, pp. 893–908.
- [23] Igusa, T. and Xu, K., “Wide-Band Response of Multiple Subsystems with High Modal Density,” *Stochastic Structural Dynamics 1*, Springer Berlin Heidelberg, 1991, pp. 131–145.
- [24] Igusa, T. and Xu, K., “Vibration Control Using Multiple Tuned Mass Dampers,” *Journal of Sound and Vibration*, Vol. 175, No. 4, Aug. 1994, pp. 491–503.
- [25] Yamaguchi, H. and Harnpornchai, N., “Fundamental characteristics of Multiple Tuned Mass Dampers for suppressing harmonically forced oscillations,” *Earthquake Engineering & Structural Dynamics*, Vol. 22, No. 1, Jan. 1993, pp. 51–62.
- [26] Karami, M. A., *Micro-Scale and Nonlinear Vibrational Energy Harvesting*, Ph.D. thesis, Virginia Polytechnic Institute and State University, 2011.

- [27] Essink, B. C., Hobeck, J. D., Owen, R. B., and Inman, D. J., “Magnetoelastic energy harvester for structural health monitoring applications,” *Active and Passive Smart Structures and Integrated Systems 2015*, SPIE, April 2015.
- [28] Santos, A. A. D., Hobeck, J. D., and Inman, D. J., “Orthogonal spiral structures for energy harvesting applications: Theoretical and experimental analysis,” *Journal of Intelligent Material Systems and Structures*, Vol. 29, No. 9, Feb. 2018, pp. 1900–1912.
- [29] Sharpes, N., Abdelkefi, A., Abdelmoula, H., Kumar, P., Adler, J., and Priya, S., “Mode shape combination in a two-dimensional vibration energy harvester through mass loading structural modification,” *Applied Physics Letters*, Vol. 109, No. 3, July 2016, pp. 033901.
- [30] Drouard, S., Hobeck, J. D., and Inman, D. J., “Scientific and Industrial Memory: 3D printed metastructures for passive broadband in torsion and axial vibration suppression,” Tech. rep., ICAM, 2015.
- [31] Reichl, K. K., *Active metastructures for light-weight vibration suppression*, Ph.D. thesis, University of Michigan, 2018.
- [32] Zhou, L. and Ge, Y., “Wind tunnel test for vortex-induced vibration of vehicle-bridge system section model,” *Journal of the Brazilian Society of Mechanical Sciences and Engineering*, Vol. 30, No. 2, June 2008.
- [33] Qiu, Z.-C., Zhang, X.-M., Wu, H.-X., and Zhang, H.-H., “Optimal placement and active vibration control for piezoelectric smart flexible cantilever plate,” *Journal of Sound and Vibration*, Vol. 301, No. 3-5, April 2007, pp. 521–543.
- [34] Sharma, A., Kumar, R., Vaish, R., and Chauhan, V. S., “Lead-free piezoelectric materials’ performance in structural active vibration control,” *Journal of Intelligent Material Systems and Structures*, Vol. 25, No. 13, Nov. 2013, pp. 1596–1604.
- [35] Sharma, A., Kumar, R., Vaish, R., and Chauhan, V. S., “Active vibration control of space antenna reflector over wide temperature range,” *Composite Structures*, Vol. 128, Sept. 2015, pp. 291–304.
- [36] Airoidi, L. and Ruzzene, M., “Design of tunable acoustic metamaterials through periodic arrays of resonant shunted piezos,” *New Journal of Physics*, Vol. 13, No. 11, Nov. 2011, pp. 113010.
- [37] Chen, Y. Y., Huang, G. L., and Sun, C. T., “Band Gap Control in an Active Elastic Metamaterial With Negative Capacitance Piezoelectric Shunting,” *Journal of Vibration and Acoustics*, Vol. 136, No. 6, Sept. 2014.
- [38] Pope, S. A. and Laalej, H., “A multi-layer active elastic metamaterial with tuneable and simultaneously negative mass and stiffness,” *Smart Materials and Structures*, Vol. 23, No. 7, June 2014, pp. 075020.

- [39] Wang, Y.-Z., Li, F.-M., and Wang, Y.-S., “Active feedback control of elastic wave metamaterials,” *Journal of Intelligent Material Systems and Structures*, Vol. 28, No. 15, Jan. 2017, pp. 2110–2116.
- [40] Li, Y., Baker, E., Reissman, T., Sun, C., and Liu, W. K., “Design of mechanical metamaterials for simultaneous vibration isolation and energy harvesting,” *Applied Physics Letters*, Vol. 111, No. 25, Dec. 2017, pp. 251903.
- [41] Leo, D. J., *Engineering Analysis of Smart Material Systems*, Wiley, Sept. 2007.
- [42] Sontag, E., *Mathematical control theory : deterministic finite dimensional systems*, Springer, New York, 1998.
- [43] Bikas, H., Stavropoulos, P., and Chryssolouris, G., “Additive manufacturing methods and modelling approaches: a critical review,” *The International Journal of Advanced Manufacturing Technology*, Vol. 83, No. 1-4, July 2015, pp. 389–405.
- [44] Elmadih, W., Chronopoulos, D., Syam, W. P., Maskery, I., Meng, H., and Leach, R. K., “Three-dimensional resonating metamaterials for low-frequency vibration attenuation,” *Scientific Reports*, Vol. 9, No. 1, Aug. 2019.
- [45] Reichl, K. K. and Inman, D. J., “Dynamic Modulus Properties of Objet Connex 3D Printer Digital Materials,” *Topics in Modal Analysis & Testing, Volume 10*, Springer International Publishing, 2016, pp. 191–198.
- [46] Guo, N. and Leu, M. C., “Additive manufacturing: technology, applications and research needs,” *Frontiers of Mechanical Engineering*, Vol. 8, No. 3, May 2013, pp. 215–243.
- [47] Baravelli, E. and Ruzzene, M., “Internally resonating lattices for bandgap generation and low-frequency vibration control,” *Journal of Sound and Vibration*, Vol. 332, No. 25, Dec. 2013, pp. 6562–6579.
- [48] Abdeljaber, O., Avci, O., and Inman, D. J., “Optimization of chiral lattice based metastructures for broadband vibration suppression using genetic algorithms,” *Journal of Sound and Vibration*, Vol. 369, May 2016, pp. 50–62.
- [49] Mead, D. J., *Passive Vibration Control*, Wiley, Feb. 1999.
- [50] Stone, B., *Chatter and Machine Tools*, Springer, June 2014.
- [51] Ewins, D. J., *Modal Testing: Theory, Practice and Application (Mechanical Engineering Research Studies: Engineering Dynamics Series)*, Wiley, July 2009.
- [52] Vincent, A. H., “A note on the properties of the variation of structural response with respect to a single structural parameter when plotted in the complex plane,” Dynamics Dept. Report GEN/DYN/RES/010R, Westland Helicopter Co., Sept. 1973.
- [53] Done, G. and Hughes, A., “The response of a vibrating structure as a function of structural parameters,” *Journal of Sound and Vibration*, Vol. 38, No. 2, Jan. 1975, pp. 255–266.

- [54] Asami, T., Nishihara, O., and Baz, A., “Analytical Solutions to H_∞ and H_2 Optimization of Dynamic Vibration Absorbers Attached to Damped Linear Systems,” *Transactions of the ASME*, Vol. 124, 2002, pp. 284–295.
- [55] Inman, D. J., *Engineering Vibration (4th Edition)*, Pearson, March 2013.
- [56] Brennan, M. and Dayou, J., “Global Control of Vibration Using a Tunable Vibration Neutralizer,” *Journal of Sound and Vibration*, Vol. 232, No. 3, May 2000, pp. 585–600.
- [57] “Engineering Fundamentals,” www.efunda.com, Accessed: 2019-11-18.
- [58] Anton, S. R., Erturk, A., and Inman, D. J., “Bending strength of piezoelectric ceramics and single crystals for multifunctional load-bearing applications,” *IEEE Transactions on Ultrasonics, Ferroelectrics and Frequency Control*, Vol. 59, No. 6, June 2012, pp. 1085–1092.